Random Matrices and Transfer Matrix Techniques for the Integer Quantum Hall Effect

Dissertation

zur Erlangung des akademischen Grades eines
Doktors der Naturwissenschaften an der
Mathematisch-Naturwissenschaftlichen Fakultät
der Universität Augsburg

vorgelegt von

Frieder Kalisch

Januar 2004

Erstgutachter: Prof. Dr. Klaus Ziegler
Zweitgutachter: Prof. Dr. Thilo Kopp
Tag der mündlichen Prüfung: 30. September 2004

In Christ are hidden all the treasures of wisdom and knowledge.

Colossians 2:3

Contents

Part I

Density of States for Random Matrices

Chapter 1

Introduction to Random Matrix Theory

1.1 Applications of Random Matrix Theory

In this chapter we will give a short overview over the most important items of random matrix theory. For an in depth overview of methods and applications see [1]. Random matrix theory was first introduced by Wigner [2] to describe the chaotic spectra of complex quantum systems like nuclei, heavy atoms and complex molecules. Later, RMT was also applied to very different problems, like disordered systems, chaotic systems with only a few degrees of freedom – for instance microwave cavities, quantum billiards, quantum dots – and the chiral phase transition in QCD.

The most important prediction of RMT is, that level correlations are determined by the basic symmetries of the system only. The details of interaction are not important. At first, three different symmetry classes with Gaussian distributed matrix elements (the so called 'classical ensembles') were considered:

If time-reversal invariance is given, the Hamiltonian can be expressed in terms of a real symmetric matrix. The corresponding ensemble of real symmetric matrices is called Gaussian orthogonal ensemble (goe). If time reversal invariance is broken, e.g. by a strong magnetic field, the matrix elements become complex, which is described by the ensemble of complex hermitian matrices, the Gaussian unitary ensemble (gue). For strong spin-orbit coupling, the Hamiltonian can be expressed by symplectic matrices, and this class of Hamiltonians is described by the Gaussian symplectic ensemble (gse). The word 'Gaussian' in the names of the ensembles corresponds to the Gaussian distribution of the matrix elements. The names orthogonal, unitary and symplectic refer to the symmetry group of the corresponding ensembles.

Two different energy scales are relevant. The bandwidth E_0 (macroscopic scale) and

the average level distance Δ (microscopic scale). In order to consider the limit $N \to \infty$ we have to decide whether we are interested in the microscopic or in the macroscopic scale. On the macroscopic scale the three classical ensembles behave similarly, and the DoS has the shape of a semicircle, $\rho \propto \sqrt{E^2 - E_0^2/4}$. On the microscopic scale we observe level repulsion, which is different for the three ensembles. Consider the two-level correlation function $p(E_1, E_2)$. It turns out, that $p(E_1, E_2)$ is suppressed for $|E_1 - E_2| < \Delta$. For the goe we have $p(E_1, E_2) \propto |E_1 - E_2|$, for the gue there is $p(E_1, E_2) \propto |E_1 - E_2|^2$ and for the gse $p(E_1, E_2) \propto |E_1 - E_2|^4$. The exponent that characterizes the level repulsion is usually called β.

In applications concerning QCD, three additional ensembles are used, the so called chiral ensembles. In addition to the symmetries of the corresponding classical ensemble, matrices M in the chiral ensembles have a 2×2-structure and a chiral symmetry $\sigma_3 M \sigma_3 = -M$, where σ_3 is the Pauli-matrix. In this context nongaussian ensembles are used to study phase transitions like the chiral phase-transition, see e.g. [3].

In most cases the limit $N \to \infty$ is considered, but there are also applications for small finite N, for example the fixed trace ensembles [4].

Calculations for random matrix theory (RMT) are usually done via either of two methods: Orthogonal polynomials or supersymmetry.

The method of orthogonal polynomials is described in great detail by Mehta [5]. The method works by integrating over the symmetry group of the ensemble, which leads to the joint probability distribution $p(\lambda_1, \ldots, \lambda_N)$ of the N eigenvalues λ_i. It is then possible to integrate out the eigenvalues one by one in order to get n-level correlations ($n < N$). While it is possible to calculate level correlations exactly, this method is rather complicated to use and it is not possible to easily transfer the calculations from one ensemble to another with a different symmetry class. It is possible to treat nongaussian ensembles within this framework [6, 7]. However it is necessary, that the properties of the corresponding orthogonal polynomials are well understood.

More versatile is the supersymmetry method introduced by Efetov [8] and Ziegler [9], which is not only applicable to RMT but also to noninteracting disordered systems in general. Usually only the limit of large N is considered within this formalism. In this work we will review supersymmetry and show, that it is capable to capture exact results even for finite N as well as $1/N$-corrections to the large-N limit. We will not only deal with the smooth corrections that are usually given, but we will also calculate oscillations on the microscopic scale.

In order to classify the symmetry of an random matrix ensemble it is not sufficient to only consider the symmetry group of the ensemble. Consider e.g. the GOE and the ensemble of antisymmetric matrices. The symmetry is given by the full orthogonal group for both ensembles. Nevertheless it will turn out, that they have vastly different

properties concerning level density and level repulsion.

Zirnbauer gave a classification in terms of so called Riemannian symmetric spaces [10]. There exist 10 different classes of them. In addition to the three classical and the three chiral ensembles these symmetric classes refer to four symmetry classes that are important in mesoscopic normal-superconducting hybrid structures. Matrices M in these ensembles have particle-hole symmetry, $\sigma_1 M \sigma_1 = -M^T$, and differ in the four possibilities to either have or not have time-reversal symmetry and spin-orbit coupling respectively [11].

Finally we want to mention the relation between RMT and the Calogero-Sutherland models, a class of integrable models whose ground-state wave-function is given by the joint probability density. In this work however we will not make use of this relation.

1.2 Outline of the Following Chapters

In chapter 2 we will give an introduction to Grassmann variables and supersymmetric Gaussian integrals. We will use the results of this chapter to calculate the level density of the GUE in chapter 3. We do this by means of the $\mathbf{Q}$-matrix formalism. In addition to the exact result, this formalism allows us to perform a saddle-point approximation, which yields a $1/N$-expansion for the level density. In a similar way we calculate the level density for the GOE, the GSE, the ensemble of antisymmetric matrices and for class C in chapter 4. Again, $1/N$-expansions will be given in addition to the exact results. The $1/N$-expansion is valid within the whole band, not only at the band-center, which was done previously. For a review of $1/N$-expansion in the vicinity of the band center see [12]

A close view on the results reveals a relation between the level density for finite N and the level repulsion. In chapter 5 we will give a summary of the results.

Chapter 2

The Grassmann Algebra and Supersymmetric Analysis

In this chapter we want to introduce Grassmann-Variables and supersymmetric path-integrals along with some algebraic properties of these constructs. The formalism will be used in chapters 3 and 4. The material presented here is by no means original. Reviews on the subject can be found in [8, 13].

2.1 Real Grassmann Algebra

The real Grassmann Algebra of rank N, $\mathcal{G}_N(\mathbb{R})$, is a real associative algebra with unit element and N generators $\vartheta_1, \ldots, \vartheta_N$. The generators have the unusual property, that they anticommute: $\vartheta_i\vartheta_j = -\vartheta_j\vartheta_i$. In particular there is $\vartheta_i^2 = 0$. The generators are also referred to as Grassmann-variables. Subsequently we drop the index N, because the algebra can be enlarged at any time by adding additional generators. The value of N is therefore not important.

All Elements $g \in \mathcal{G}$ can be written as polynomials of the generators, which are at most linear in each generator. If each monomial of this polynomial consists of a product of an even (odd) number of generators, we call g even or odd respectively. All even elements together form the center of $\mathcal{G}$, i. e. they commute with all other elements of the algebra. Odd elements anticommute with all other odd elements, but they commute with even ones. Each element $g \in \mathcal{G}$ can be decomposed in its real part $g_\mathbb{R} \in \mathbb{R}$, which is just the zeroth-order term of the polynomial, and a nilpotent part g_0: $g = g_\mathbb{R} + g_0$.

Analytic functions on the Grassmann-algebra can be introduced by identifying them with their Taylor-series around the real part of the argument. A lot of properties of such functions can be proven by considering the Taylor-expansion. Convergence of

the Taylor-series is not an issue, because the series is actually a finite sum. Below we will refer to this reasoning as analytic continuation. An element $g \in \mathcal{G}$ with $g_{\mathbb{R}} \neq 0$ for example can be inverted by using the geometric series:

$$g^{-1} = \frac{1}{g_{\mathbb{R}}} \sum_{n=0}^{\infty} \left(\frac{-g_0}{g_{\mathbb{R}}} \right)^n , \tag{2.1a}$$

because

$$(g_{\mathbb{R}} + g_0) \frac{1}{g_{\mathbb{R}}} \sum_{n=0}^{\infty} \left(\frac{-g_0}{g_{\mathbb{R}}} \right)^n = \sum_{n=0}^{\infty} \left(1 + \frac{g_0}{g_{\mathbb{R}}} \right) \left(\frac{-g_0}{g_{\mathbb{R}}} \right)^n = 1 . \tag{2.1b}$$

By using the Taylor-expansion it is also clear, that

$$\exp(\log(g)) = g . \tag{2.2a}$$

But the relation

$$\exp(g + h) = \exp(g) \exp(h) \tag{2.2b}$$

holds only, if the elements g and h commute. E. g. it holds if one of g and h is even, or if g and h are equal up to an even factor. In particular we have $\exp(g) \exp(-g) = 1$.

2.2 Complex Grassmann Algebra

In the Complex numbers there exists the complex conjugation, which we denote by $\overline{}$. In order to have a conjugation in the Grassmann-Algebra, we have to introduce the complex conjugate of each generator. That means $\mathcal{G}_N(\mathbb{C})$ is generated by the $2N$ generators $\vartheta_1, \ldots, \vartheta_N$ and $\overline{\vartheta}_1, \ldots, \overline{\vartheta}_N$. This conjugation should be consistent with the multiplication. In particular $\overline{\vartheta}\vartheta$ should be an analogue of a real number, in the sense that it is invariant under conjugation: $\overline{\overline{\vartheta}\vartheta} = \overline{\vartheta}\vartheta$. In the literature two different notations are used to establish this property. Consider two generators ϑ, ψ of $\mathcal{G}(\mathbb{C})$:

- $\overline{\vartheta\psi} = \overline{\psi}\,\overline{\vartheta}$ and $\overline{\overline{\vartheta}} = \vartheta$; $\overline{\overline{\psi}} = \psi$.
- $\overline{\vartheta\psi} = \overline{\vartheta}\,\overline{\psi}$ and $\overline{\overline{\vartheta}} = -\vartheta$; $\overline{\overline{\psi}} = \psi$.

Throughout this work we will use the first convention. Note, that $\overline{\vartheta}\vartheta$ is not necessarily a real number and is therefore not some sort of absolute value. An important fact about the conjugation is the pairing of the Grassmann-variables (see below).

2.3 Complex Vectorspaces over $\mathcal{G}$

Now we want to construct vectorspaces that contain Grassmann-variables, and we do it as follows. The vectors are split in two components in such a way, that one component consist only of even elements and the other only of odd elements. The vectorspace which consists of k even and l odd elements is called $\mathbb{C}^{k|l}$. In this notation k and l do in general not correspond to the rank of the Grassmann-algebra involved, although we will later on deal mostly with vectorspaces, where l is in fact equal to the rank of $\mathcal{G}$. In the following Roman letters denote even elements and Greek letter denote odd elements. A vector ϕ is thus given by $\phi = (x, \psi)$. The scalar-product is defined in terms of the scalar-product in complex vectorspaces:

$$\langle \phi_1, \phi_2 \rangle := \langle x_1, x_2 \rangle + \langle \psi_1, \psi_2 \rangle = \phi_1^\dagger \phi_2 \,, \tag{2.3}$$

where the hermitian conjugate vector is the transposed conjugate vector as usual. Notice, that the scalar-product is not a norm, because in general, it yields an even element of $\mathcal{G}$ rather than a real number. Therefore, strictly speaking, the vectors as defined here are not elements of a vectorspace but of a $\mathcal{G}$-module. However, for our purpose this difference is of no importance, and we stick to the word vectorspace.

Matrices represent linear mappings and should thus conserve the structure of the vectors. This restricts matrices to the form $\left(\begin{smallmatrix} A & \Theta \\ \Psi & B \end{smallmatrix}\right)$, where A and B are matrices of even elements of $\mathcal{G}$, and Θ and Ψ are matrices of odd elements of $\mathcal{G}$. Matrices can be inverted, if the diagonal blocks A and B are invertible. In order to calculate the inverse explicitly, we apply the geometric series and get

$$\begin{aligned} \begin{pmatrix} 1 & \Theta \\ \Psi & 1 \end{pmatrix}^{-1} &= \sum_{n=0}^{\infty} (-1)^n \begin{pmatrix} 0 & \Theta \\ \Psi & 0 \end{pmatrix}^n \\ &= \sum_{n=0}^{\infty} \begin{pmatrix} (\Theta\Psi)^n & 0 \\ 0 & (\Psi\Theta)^n \end{pmatrix} - \sum_{n=0}^{\infty} \begin{pmatrix} 0 & \Theta(\Psi\Theta)^n \\ \Psi(\Theta\Psi)^n & 0 \end{pmatrix} \\ &= \begin{pmatrix} (1-\Theta\Psi)^{-1} & -\Theta(1-\Psi\Theta)^{-1} \\ -\Psi(1-\Theta\Psi)^{-1} & (1-\Psi\Theta)^{-1} \end{pmatrix} . \end{aligned} \tag{2.4}$$

This implies that

$$\begin{aligned} \begin{pmatrix} A & \Theta \\ \Psi & B \end{pmatrix}^{-1} &= \begin{pmatrix} 1 & A^{-1}\Theta \\ B^{-1}\Psi & 1 \end{pmatrix}^{-1} \begin{pmatrix} A^{-1} & 0 \\ 0 & B^{-1} \end{pmatrix} \\ &= \begin{pmatrix} (A-\Theta B^{-1}\Psi)^{-1} & -A^{-1}\Theta(B-\Psi A^{-1}\Theta)^{-1} \\ -B^{-1}\Psi(A-\Theta B^{-1}\Psi)^{-1} & (B-\Psi A^{-1}\Theta)^{-1} \end{pmatrix} \end{aligned} \tag{2.5}$$

It is also possible to define groups like the linear or the unitary group as well as the corresponding lie-algebras, and study problems like diagonalization of graded matrices [14, 15]. In this work however we confine ourselves to the calculation of the graded trace and determinant in section 2.5

2.4 Real Vectorspaces over $\mathcal{G}$

For real vectorspaces things are a little bit more complicated, mainly due to two reasons. The first one is that the intuitive scalar-product $\phi^T\phi$ is neither symmetric nor skew. The second reason shows up, if we consider the transpose of a matrix. The definition $(M\phi)^T = \phi^T M^T$ leads to

$$\begin{pmatrix} A & \Theta \\ \Psi & B \end{pmatrix}^T = \begin{pmatrix} A^T & \Psi^T \\ -\Theta^T & B^T \end{pmatrix} . \tag{2.6}$$

Therefore we have $M^{T^T} \neq M$.

To fix these inconveniences, we introduce real graded vectorspaces not as spaces over a real Grassmann-Algebra. Instead we define them by means of the complex Grassmann-Algebra. First we define the so called orthosymplectic transpose of a vector in $\mathbb{C}^{2k|2l}$:

$$\begin{pmatrix} x \\ \psi \end{pmatrix}^t = \begin{pmatrix} x_1 \\ x_2 \\ \psi_1 \\ \psi_2 \end{pmatrix}^t := \left(x_2^T, x_1^T, \psi_2^T, -\psi_1^T\right) = \begin{pmatrix} x^T & \psi^T \end{pmatrix} \begin{pmatrix} \sigma_1 & 0 \\ 0 & -\mathrm{i}\sigma_2 \end{pmatrix} = \begin{pmatrix} x^T & \psi^T \end{pmatrix} \Sigma \,, \tag{2.7}$$

where we have introduced the matrix $\Sigma = \left(\begin{smallmatrix} \sigma_1 & 0 \\ 0 & -\mathrm{i}\sigma_2 \end{smallmatrix}\right)$. With this definition of the orthosymplectic transpose, a real vector is then a vector in $\mathbb{C}^{2k|2l}$, with $k|l$ components ϕ and $k|l$ components $\overline{\phi}$, i.e. it can be written as

$$\chi = \begin{pmatrix} x \\ \overline{x} \\ \psi \\ \overline{\psi} \end{pmatrix} \qquad\qquad \chi^t = \left(\overline{x}^T, x^T, \overline{\psi}^T, -\psi^T\right) . \tag{2.8}$$

This definition leads to a real vectorspace with a scalar product $\chi^t\chi$, which is symmetric, and real in the sense, that it fulfills $\overline{\chi^t\chi} = \chi^t\chi$.

The name "orthosymplectic transpose" becomes understandable if we consider the invariance group of the scalar-product. The transformation $\chi \to S\chi$ leads to

$\chi^t \to \chi^t \Sigma^\dagger S^T \Sigma$ and the invariance of the scalar-product requires then $S\Sigma^\dagger S^T = \Sigma^\dagger$. A transformation of the bosonic variables alone is restricted to $S\sigma_1 S^T = \sigma_1$. This is in fact a representation of the orthogonal group, which can be seen by considering $O = \mathrm{e}^{\mathrm{i}\frac{\pi}{4}\sigma_1} S \mathrm{e}^{-\mathrm{i}\frac{\pi}{4}\sigma_1}$. The constraint $S\sigma_2 S^T = \sigma_2$ for transformations of the fermionic variables coincides with the standard definition of the symplectic group. The scalar-product is thus invariant under mixed orthogonal-symplectic transformations.

Note that in the literature the orthosymplectic transpose is sometimes defined somewhat differently [16], so that it leads to a skew symmetric scalar-product.

2.5 Graded Trace and Determinant

We want do define the graded trace like the usual trace, and state, that it is a linear form of square matrices which has the additional property, that $\mathrm{trg}\, M_1 M_2 = \mathrm{trg}\, M_2 M_1$ for two matrices $M_1, M_2 \in \mathbb{C}^{k|l \times k|l}$. We have

$$\begin{aligned} \begin{pmatrix} A_1 & \Theta_1 \\ \Psi_1 & B_1 \end{pmatrix} \begin{pmatrix} A_2 & \Theta_2 \\ \Psi_2 & B_2 \end{pmatrix} &= \begin{pmatrix} A_1 A_2 + \Theta_1 \Psi_2 & A_1 \Theta_2 + \Theta_1 B_2 \\ \Psi_1 A_2 + B_1 \Psi_2 & \Psi_1 \Theta_2 + B_1 B_2 \end{pmatrix} \\ \begin{pmatrix} A_2 & \Theta_2 \\ \Psi_2 & B_2 \end{pmatrix} \begin{pmatrix} A_1 & \Theta_1 \\ \Psi_1 & B_1 \end{pmatrix} &= \begin{pmatrix} A_2 A_1 + \Theta_2 \Psi_1 & A_2 \Theta_1 + \Theta_2 B_1 \\ \Psi_2 A_1 + B_2 \Psi_1 & \Psi_2 \Theta_1 + B_2 B_1 \end{pmatrix} . \end{aligned} \tag{2.9}$$

We fix the normalization $\mathrm{trg}\, \mathbb{1} = k - l$, where $\mathbb{1}$ is the unit-matrix. Therefore the graded trace is uniquely defined to be

$$\mathrm{trg} \begin{pmatrix} A & \Theta \\ \Psi & B \end{pmatrix} = \mathrm{tr}\, A - \mathrm{tr}\, B \tag{2.10}$$

The graded determinant is defined by the relation $\mathrm{detg} \exp M = \exp \mathrm{trg}\, M$, which is also fulfilled for usual complex matrices. Obviously, we have

$$\mathrm{detg} \begin{pmatrix} A & 0 \\ 0 & B \end{pmatrix} = \frac{\det A}{\det B} . \tag{2.11a}$$

Furthermore it is

$$\begin{aligned} \mathrm{detg} \begin{pmatrix} 1 & \Theta \\ \Psi & 1 \end{pmatrix} &= \exp \mathrm{trg} \log \begin{pmatrix} 1 & \Theta \\ \Psi & 1 \end{pmatrix} = \exp \left(- \mathrm{trg} \sum_{n=1}^{\infty} \frac{(-1)^n}{n} \begin{pmatrix} 0 & \Theta \\ \Psi & 0 \end{pmatrix}^n \right) \\ &= \exp \left(- \mathrm{trg} \sum_{n=1}^{\infty} \frac{1}{2n} \begin{pmatrix} \Theta\Psi & 0 \\ 0 & \Psi\Theta \end{pmatrix}^n \right) = \exp \left(\mathrm{tr} \ln (1 - \Theta\Psi) \right) \\ &= \det (1 - \Theta\Psi) , \end{aligned} \tag{2.11b}$$

or equivalently

$$\operatorname{detg}\begin{pmatrix} 1 & \Theta \\ \Psi & 1 \end{pmatrix} = \exp\left(-\operatorname{tr}\ln(1-\Psi\Theta)\right) = \frac{1}{\det(1-\Psi\Theta)}\,. \tag{2.11c}$$

Now we put these two results together and get

$$\begin{aligned}\operatorname{detg}\begin{pmatrix} A & \Theta \\ \Psi & B \end{pmatrix} &= \frac{\det A}{\det B}\operatorname{detg}\begin{pmatrix} 1 & A^{-1}\Theta \\ B^{-1}\Psi & 1 \end{pmatrix} \\ &= \frac{\det A}{\det B}\det(1-A^{-1}\Theta B^{-1}\Psi) &\text{(2.12a)}\\ &= \frac{\det A}{\det B\det(1-B^{-1}\Psi A^{-1}\Theta)} &\text{(2.12b)}\end{aligned}$$

In contrast to the usual determinant the graded determinant is not defined for all matrices, the matrix must be invertible. But like the usual determinant it possesses the important factorization property, that $\operatorname{detg} M_1 M_2 = \operatorname{detg} M_1 \operatorname{detg} M_2$. Before we prove this, let us state two preliminary equalities. The equality $(1+\Theta\Psi)\Theta = \Theta(1+\Psi\Theta)$ entails

$$\Theta(1+\Psi\Theta)^{-1} = (1+\Theta\Psi)^{-1}\Theta\,, \tag{2.13}$$

and we have

$$(1+\Psi\Theta)^{-1} = 1-(1+\Psi\Theta)^{-1}\Psi\Theta\,. \tag{2.14}$$

The proof of the theorem now proceeds as follows: As a first step, we note that

$$\operatorname{detg} M\begin{pmatrix} C & 0 \\ 0 & D \end{pmatrix} = \operatorname{detg}\begin{pmatrix} C & 0 \\ 0 & D \end{pmatrix} M = \operatorname{detg} M \operatorname{detg}\begin{pmatrix} C & 0 \\ 0 & D \end{pmatrix} \tag{2.15}$$

for any matrix M and even blocks C and D. This may be verified by using (2.12). For this reason it is now sufficient to prove the theorem for matrices which have diagonal blocks equal to unity:

$$\begin{aligned}&\operatorname{detg}\begin{pmatrix} 1 & \Theta_1 \\ \Psi_1 & 1 \end{pmatrix}\begin{pmatrix} 1 & \Theta_2 \\ \Psi_2 & 1 \end{pmatrix} = \operatorname{detg}\begin{pmatrix} 1+\Theta_1\Psi_2 & \Theta_1+\Theta_2 \\ \Psi_1+\Psi_2 & 1+\Psi_1\Theta_2 \end{pmatrix} \\ &= \frac{\det\left(1+\Theta_1\Psi_2-(\Theta_1+\Theta_2)(1+\Psi_1\Theta_2)^{-1}(\Psi_1+\Psi_2)\right)}{\det(1+\Psi_1\Theta_2)}\end{aligned}$$

At this step we employ the equality of the two results in (2.11) as well as equation (2.13)

$$\begin{aligned}&= \det\big((1+\Theta_2\Psi_1)(1+\Theta_1\Psi_2)-\Theta_2(\Psi_1+\Psi_2) \\ &\qquad\qquad -(1+\Theta_2\Psi_1)\Theta_1(1+\Psi_1\Theta_2)^{-1}(\Psi_1+\Psi_2)\big) \\ &= \det\big(1-\Theta_2\Psi_2-(1+\Theta_2\Psi_1)\Theta_1((1+\Psi_1\Theta_2)^{-1}(\Psi_1+\Psi_2)-\Psi_2)\big)\end{aligned}$$

Equation (2.14) now allows us to factor out $1 - \Theta_2\Psi_2$:

$$\begin{aligned} &= \det\left(1 - \Theta_2\Psi_2 - (1 + \Theta_2\Psi_1)\Theta_1(1 + \Psi_1\Theta_2)^{-1}\Psi_1(1 - \Theta_2\Psi_2)\right) \\ &= \det(1 - \Theta_1\Psi_1)\det(1 - \Theta_2\Psi_2)\,. \end{aligned}$$

In the last step we have again used equation (2.13) and additionally the factorization property of the usual determinant.

2.6 Analysis with Grassmann Variables

In this section we will define integration and differentiation with respect to Grassmann-variables. It is also possible, to define manifolds in some Grassmann-algebra and to integrate over the manifold, see [10] and the references cited therein. We don't need this feature for our purposes and consider only the simple case.

Differentiation and integration with respect to real or complex numbers works as usual. In particular, when integrating an analytic function over some complex path, the integral does not change when we change the path but keep the endpoints. This feature remains, if we move the path into the Grassmann-Algebra.

To prove this, consider a complex path $z(t, \alpha) = z_0(t) + \alpha z_1(t)$, with $t \in [0, 1]$, $z_0' \neq 0$ and $z_1(0) = z_1(1) = 0$. Now the integral $I = \int \mathrm{d}z\, f(z)$ is constant in the vicinity of $\alpha = 0$. Then all derivatives $\partial^n I/\partial\alpha$ vanish and therefore the integral does not change if we consider the integration path $z(t, x)$ for some even element x of the algebra with vanishing complex part. Of course, for some paths it may be necessary to consider paths $z(t, \alpha_1, \ldots, \alpha_n) = z_0(t) + \sum \alpha_i z_i(t)$ and substitute the αs by different elements of the Grassmann-algebra.

Integration and differentiation with respect to a Grassmann-Variable is simple, because all functions of such variables are at most linear. Integration and differentiation are linear operations, and therefore we only need to consider two cases: $f(\vartheta) = 1$ and $f(\vartheta) = \vartheta$.

Differentiation works like taking the derivative of polynomials, and hence

$$\frac{\partial 1}{\partial \vartheta} = 0 \qquad\qquad \frac{\partial \vartheta}{\partial \vartheta} = 1\,. \tag{2.16}$$

Note, that the order of differentiation is important here, because

$$\frac{\partial}{\partial\vartheta_1}\frac{\partial}{\partial\vartheta_2}\vartheta_1\vartheta_2 = -\frac{\partial}{\partial\vartheta_1}\frac{\partial}{\partial\vartheta_2}\vartheta_2\vartheta_1\,. \tag{2.17}$$

By exchanging the indices it follows, that

$$\frac{\partial}{\partial\vartheta_1}\frac{\partial}{\partial\vartheta_2} = -\frac{\partial}{\partial\vartheta_2}\frac{\partial}{\partial\vartheta_1}\,. \tag{2.18}$$

In order to make the definition of the differentiation unique, we have to fix the sign of the equation above. We state that if a differential-operator acts on the number next to it, we get a $+$-sign, or

$$\frac{\partial}{\partial\vartheta_1}\frac{\partial}{\partial\vartheta_2}\vartheta_2\vartheta_1 = 1\ . \tag{2.19}$$

Otherwise we have to change the order, such that each differential-operator acts on the number next to it. This reasoning also shows, that Grassmann-Variables and differential-operators anticommute. The latter are not elements of the Grassmann-algebra however, because they violate associativity:

$$\frac{\partial}{\partial\vartheta}\left(\vartheta^2\right) = 0 \neq \vartheta = \left(\frac{\partial}{\partial\vartheta}\vartheta\right)\vartheta \tag{2.20}$$

As we will see in the next chapter, we introduce the integral with respect to Grassmann-Variables because we want to calculate expectation values. Therefore we think of it as being a definite integral over some integration domain. This in turn means, that integration reduces the grade of the integrand by 1, because the result must not depend on the integration variable anymore. The only way to satisfy this condition is

$$\int\mathrm{d}\vartheta\ 1 = 0 \qquad\qquad \int\mathrm{d}\vartheta\ \vartheta = 1 \tag{2.21}$$

In other words, integration and differentiation for Grassmann-variables work alike. From this equality follows, that change of variables is different from change of variables in real or complex integrals:

$$\prod_i \mathrm{d}\vartheta\ = \det\left(\frac{\partial\vartheta_i}{\partial\psi_j}\right)^{-1}\prod_j \mathrm{d}\psi_j \tag{2.22}$$

for some linear transform of variables $\vartheta_i(\{\psi_j\})$. But as in the case of complex variables, we have $\int\mathrm{d}\vartheta\ f(\vartheta) = \int\mathrm{d}\vartheta\ f(\vartheta+\psi)$ for ψ odd, because in this case

$$f(\vartheta+\psi) = f_0 + f_1(\vartheta+\psi) + f_2(\vartheta+\psi)^2 = f_0 + f_1(\vartheta+\psi)\,. \tag{2.23}$$

Furthermore, there exists a rule that is similar to integrating by parts:

$$\int\mathrm{d}\vartheta\ \frac{\partial f(\psi\vartheta)}{\partial\vartheta}g(\phi\vartheta) = -\int\mathrm{d}\vartheta\ f(\psi\vartheta)\frac{\partial g(\phi\vartheta)}{\partial\vartheta} \tag{2.24}$$

for two analytic functions f and g, where $f(z)$ and $g(z)$ are even elements for complex numbers z, and odd elements ϕ and ψ. This rule can be verified by expanding f and g with respect to ϑ.

2.7 Complex Gaussian Integrals

In this section we want to discuss how to calculate supersymmetric Gaussian integrals. In our case we deal only with integrals over finite-dimensional spaces and therefore we are even able to prove convergence and the results given are exact.

At first consider a matrix $M \in \mathbb{C}^{N\times N}$ and complex integration variables x_i. If M is quasi positive-definite, i. e. all eigenvalues have a positive real part, we can calculate the integral

$$\int_{\mathbb{C}^N} \prod_{i=1}^{N} \frac{\mathrm{d}\overline{x}_i \, \mathrm{d}x_i}{\pi} \mathrm{e}^{-x^\dagger M x} = (\det M)^{-1} \,. \tag{2.25}$$

To see this, we apply a Schur-factorization M, that decomposes M into a unitary and an upper tridiagonal matrix [17]. Now we can calculate the integral step by step and get indeed the inverse determinant. By analytic continuation it follows, that this result holds even if M is not a complex matrix, but consists of even elements of the Grassmann-algebra. Subsequently the measure $\prod_i \frac{\mathrm{d}\overline{x}_i \, \mathrm{d}x_i}{\pi}$ will be abbreviated by $\mathcal{D}[x]$. In the same way, the integral

$$\int \mathcal{D}[\psi] \, \mathrm{e}^{-\psi^\dagger M \psi} = \int \prod_{i=1}^{N} \mathrm{d}\overline{\psi}_i \, \mathrm{d}\psi_i \, \mathrm{e}^{-\psi^\dagger M \psi} = \det M \tag{2.26}$$

can be calculated, where ψ and $\psi^\dagger$ are generators of the Grassmann-algebra. Integrals over Grassmann-variables do always converge, and therefore there is no restriction on the eigenvalues of M in this case. We could have derived this result also somewhat differently, by noting, that we can change the definition of complex conjugation in the Grassmann-algebra. We can therefore apply a nonunitary transform that diagonalizes M. The integral does than factorize and the result is easily obtained.

With help of these results it is possible to calculate the corresponding mixed complex-Grassmann integral. We introduce the notation $\phi = \left(\begin{smallmatrix} x \\ \vartheta \end{smallmatrix}\right)$ and $M = \left(\begin{smallmatrix} A & \Theta \\ \Psi & B \end{smallmatrix}\right)$. By applying the change of variables $x \to x - A^{-1}\Theta\vartheta$ and $x^\dagger \to x^\dagger - \vartheta^\dagger \Psi A^{-1}$ we get

$$\int \mathcal{D}[\phi] \, \mathrm{e}^{-\phi^\dagger M \phi} = (\mathrm{detg}\, M)^{-1} \,, \tag{2.27}$$

if A has eigenvalues with positive real part.

As a main result of this section we will now show how to express propagators with path-integrals. We do so by introducing the generating function

$$\int \mathcal{D}[\phi] \, \mathrm{e}^{-\phi^\dagger M \phi - \eta^\dagger \phi - \phi^\dagger \eta} = \frac{\exp(\eta^\dagger M^{-1} \eta)}{\mathrm{detg}\, M} \,, \tag{2.28}$$

which was obtained with the change of variables $\phi \to \phi + M^{-1}\eta$. By taking the derivative with respect to η_i and $\eta_j^\dagger$ and setting η to zero afterward, we can calculate all components of

$$\int \mathcal{D}[\phi]\, \phi\phi^\dagger \mathrm{e}^{-\phi^\dagger M \phi} = M^{-1} \operatorname{detg} M^{-1}\,, \tag{2.29}$$

The expression $\phi\phi^\dagger$ has to be understood as an outer product. For the application to noninteracting disordered systems, we set $M = -\mathrm{i}(E - H + \mathrm{i}0) \otimes \mathbb{1}_{ss}$ ($\mathbb{1}_{ss}$ is the unit-matrix in superspace). The determinant detg M is then equal to 1 and M^{-1} is the propagator, which we aim to calculate, with an additional factor of i. The additional factor $-\mathrm{i}$ in front of the Hamiltonian is needed to ensure convergence of the integral.

2.8 Real Gaussian Integrals

Real Gaussian integrals are somewhat more complicated than complex ones, because we have to consider symmetry constraints. Consider the quadratic form $x^T M x$. without loosing generality, M may be chosen to be symmetric. If M is also real and positive definite, the integral over real variables x_i is

$$\int \mathcal{D}[x]\, \mathrm{e}^{-x^T M x} = (\det M)^{-1/2}\,, \tag{2.30}$$

which can be obtained by diagonalizing M first. The measure in the real case is given by $\mathcal{D}[x] = \prod_i x_i/\sqrt{\pi}$. It follows by analytic continuation, that this result holds also if M is complex symmetric. Additionally, M has to be quasi positive-definite in order to ensure convergence of the integral.

In the corresponding Grassmann-integral, M can be chosen to be antisymmetric. If it is also real, all eigenvalues are imaginary and appear in pairs $\mathrm{i}\lambda$, $-\mathrm{i}\lambda$. Thus, by suitable orthogonal transforms, M can be transformed to block diagonal form

$$M' = \begin{pmatrix} 0 & \lambda_1 & & & \\ -\lambda_1 & 0 & & & \\ & & 0 & \lambda_2 & \\ & & -\lambda_2 & 0 & \\ & & & & \ddots \end{pmatrix}. \tag{2.31}$$

Of course, some eigenvalues may be zero. There is always one zero eigenvalue if the dimension of M is odd. Now the path-integral is easily calculated and we get

$$\int \mathcal{D}[\psi]\, \mathrm{e}^{-\psi^T M \psi} := \int \prod_i \psi_i \mathrm{e}^{-\psi^T M \psi} \sqrt{\det 2M}\,, \tag{2.32}$$

where the measure is given by $\mathcal{D}[\psi] = \prod_i \mathrm{d}\psi_i$. Notice the factor of two in the root, that enters through the doubling of each eigenvalue. This result extends again to the case of complex antisymmetric matrices, as can be shown by analytic continuation. We want to stress the fact, that the determinant is always zero, if the dimension of M is odd. Therefore real Grassmann-integrals are interesting only for even dimensions.

Now consider a quadratic form which involves both, real and Grassmann-variables. Symmetry ensures, that it can be written as

$$\phi^T M \phi = \begin{pmatrix} x^T & \psi^T \end{pmatrix} \begin{pmatrix} A & \Theta^T \\ -\Theta & B \end{pmatrix} \begin{pmatrix} x \\ \psi \end{pmatrix}, \tag{2.33}$$

where A is symmetric and B is antisymmetric as discussed above. Furthermore we assume $M \in \mathbb{R}^{k|l \times k|l}$. The change of variables $x \to x + A^{-1}\Theta^T\psi$ then reduces this integral to the product of a real and a Grassmann one and the result is

$$\int \mathcal{D}[\phi]\, \mathrm{e}^{-\phi^T M \phi} = 2^{l/2} \sqrt{\operatorname{detg} M}^{-1}. \tag{2.34}$$

Of course, this result remains true, if we write everything in terms of the orthosymplectic transpose introduced in section 2.4, however with the slight change

$$\int \mathcal{D}[\chi]\, \mathrm{e}^{-\frac{1}{2}\chi^t M \chi} = \sqrt{\operatorname{detg} M}^{-1}. \tag{2.35}$$

In this formulation the matrix M has to be symmetric in the sense that $M^t = M$. This can be expressed as

$$M = \begin{pmatrix} A_1 & A_2 & \Theta_1 & -\Theta_2 \\ A_3 & A_1^T & \Theta_3 & -\Theta_4 \\ \Theta_4^T & \Theta_2^T & B_1 & B_2 \\ \Theta_3^T & \Theta_1^T & B_3 & B_1^T \end{pmatrix}, \tag{2.36}$$

where A_2 and A_3 are symmetric and B_2 and B_3 are antisymmetric.

It is also possible to derive a formula for the inverse of a matrix, namely

$$M^{-1} = \sqrt{\operatorname{detg} M} \int \mathcal{D}[\chi]\, \chi\chi^t \mathrm{e}^{-\frac{1}{2}\chi^t M \chi} \tag{2.37}$$

for a symmetric matrix M. But due to the inconvenient symmetry constraints, this formula is not as useful as equation (2.29). Note however, that the complex integral is a special case of (2.37). If M has a block-structure

$$\begin{pmatrix} A_1 & 0 & \Theta_1 & 0 \\ 0 & A_1^T & 0 & -\Theta_4 \\ \Theta_4^T & 0 & B_1 & 0 \\ 0 & \Theta_1^T & 0 & B_1^T \end{pmatrix}, \tag{2.38}$$

the real integral is in fact a complex one because there are no terms proportional to $x_i x_j$ or $\psi_i \psi_j$ in the exponent.

Chapter 3

The Unitary Ensemble

In this chapter we will show how to calculate the density of states (DoS) for the so called Gaussian unitary ensemble. This chapter is a tutorial for the application of supersymmetry and the $\mathbf{Q}$-matrix formalism. The main result, the exact DoS, was already given by Mehta [5]. The $\mathbf{Q}$-matrix formalism was first developed by Wegner [18].

The Model is given by a ensemble of hermitian $N \times N$ matrices H with entries H_{ij}. The probability-distribution of the entries is given by the Gaussian distribution $\langle H_{ij} \rangle = 0$, $\langle H_{ij} H_{kl} \rangle = \frac{1}{2} \delta_{il} \delta_{jk}$, which can also be written as

$$p\left(\{H_{ij}\}\right) \prod_{i,j} \mathrm{d}H_{ij} \; = \mathrm{e}^{-\operatorname{tr} H^2} \prod_{i,j} \frac{\mathrm{d}H_{ij}}{\sqrt{\pi}} \,. \tag{3.1}$$

This probability-distribution is invariant under unitary transformations of H, hence the name of the ensemble.

3.1 Exact Density of States

We calculate the averaged DoS by means of the propagator:

$$\langle n(E) \rangle = \frac{1}{\pi N} \operatorname{Im} \langle (H - E - \mathrm{i}0)^{-1} \rangle \,, \tag{3.2}$$

where $\langle\rangle$ denotes the average over the ensemble. Normalization is chosen in such a way that $\langle n(E) \rangle \mathrm{d}E$ is the probability to have an eigenvalue in an interval of width $\mathrm{d}E$ at energy E. Following the formulas given in the last chapter, the averaged DoS is then given by

$$\langle n(z) \rangle = \frac{1}{\pi N} \operatorname{Re} \int \mathcal{D}[\phi, H] \, x_i^\dagger x_i \mathrm{e}^{-S_H} \,, \tag{3.3}$$

with the action

$$S_H = \mathrm{i}\phi_i^\dagger(H_{ij} - z\delta_{ij})\phi_j + H_{ij}H_{ji}\,. \tag{3.4}$$

In this notation each ϕ_i is a supersymmetric vector with one complex and one Grassmann component. $\operatorname{Im} z > 0$ is required to ensure convergence. This requirement corresponds to the retarded Greens-function. Integrating over H changes the action to

$$S_4 = -\mathrm{i}z\phi_i^\dagger\phi_i + \frac{1}{4}\operatorname{trg}(\phi_i\phi_i^\dagger)^2\,, \tag{3.5}$$

where $\phi_i\phi_i^\dagger$ denotes the outer product in superspace and summation convention is assumed. In the next step we decouple the fourth-order interaction with a matrix

$$\mathbf{Q} = \begin{pmatrix} q & \bar{\vartheta} \\ \vartheta & \mathrm{i}p \end{pmatrix}\,, \tag{3.6}$$

where q and p are complex and ϑ and $\overline{\vartheta}$ are Grassmann-variables. We achieve the decoupling by inserting a "one" into the integral: $1 = \int \mathcal{D}[\mathbf{Q}]\,\mathrm{e}^{-\operatorname{trg}(\mathbf{Q}+\frac{\mathrm{i}}{2}\phi_i\phi_i^\dagger)^2}$, with $\mathcal{D}[\mathbf{Q}] = \frac{\mathrm{d}p\,\mathrm{d}q}{\pi}\frac{\mathrm{d}\bar{\vartheta}\,\mathrm{d}\vartheta}{2}$. We get as a new action

$$S_\mathbf{Q} = \mathrm{i}\phi_i^\dagger(\mathbf{Q} - z)\phi_i + \operatorname{trg}\mathbf{Q}^2\,. \tag{3.7}$$

This action factorizes the ϕ-integral. By introducing the $\mathbf{Q}$-matrix we have therefore reduced the large number of integrations to a small one, which, even more, does not depend on N. In order to evaluate the DoS

$$\langle n(z)\rangle = \frac{1}{\pi N}\operatorname{Re}\int\mathcal{D}[\mathbf{Q},\phi]\,x_i^\dagger x_i\mathrm{e}^{-S_\mathbf{Q}} = \frac{-1}{\pi N}\operatorname{Im}\int\mathcal{D}[\mathbf{Q},\phi]\,(-\mathrm{i})\overline{x}_i x_i\mathrm{e}^{-S_\mathbf{Q}}\,, \tag{3.8}$$

we perform an integration by parts with respect to the q-integration

$$\int\mathrm{d}q\,\bar{x}_i x_i\mathrm{e}^{-\mathrm{i}\bar{x}_i x_i q - q^2} = 2\mathrm{i}\int q\mathrm{e}^{-\mathrm{i}\bar{x}_i x_i q - q^2}\,, \tag{3.9}$$

which leads to

$$\langle n(z)\rangle = \frac{-2}{\pi N}\operatorname{Im}\int\mathcal{D}[\mathbf{Q},\phi]\,q\mathrm{e}^{-S_\mathbf{Q}}\,. \tag{3.10}$$

Now it is simple to integrate out the ϕ-fields as well as the Grassmann-part of $\mathbf{Q}$:

$$\langle n(z)\rangle = \frac{-2}{\pi N}\operatorname{Im}\int\mathcal{D}[\mathbf{Q}]\,\frac{q\mathrm{e}^{-\operatorname{trg}\mathbf{Q}^2}}{\operatorname{detg}(\mathbf{Q}-z)^N} \tag{3.11}$$

$$= \frac{-2}{\pi N}\operatorname{Im}\int\frac{\mathrm{d}p\,\mathrm{d}q}{\pi}q\mathrm{e}^{-p^2-q^2}\frac{(\mathrm{i}p-z)^N}{(q-z)^N}\left(1 - \frac{N}{2(q-z)(\mathrm{i}p-z)}\right)\,. \tag{3.12}$$

We may now proceed in two ways. Either we attempt to calculate the DoS exactly for finite N, or we do an expansion for large N. The large-N expansion will be presented in the next chapter. In order to calculate the density of states exactly for finite N, we have to put z onto the real axis: $z \to E + \mathrm{i}0 \in \mathbb{R}$. In this limit the integral (3.12) can be carried out and we end up with the result

$$\langle n(E) \rangle = \frac{\mathrm{e}^{-E^2}}{2^N N! \sqrt{\pi}} \left(H_N^2(E) - H_{N+1}(E) H_{N-1}(E) \right) . \tag{3.13}$$

Here $H_N(x)$ denotes the Nth Hermite-polynomial, which is by definition given by

$$H_N(x) := (-1)^N \mathrm{e}^{x^2} \frac{\partial^N}{\partial x^N} \mathrm{e}^{-x^2} . \tag{3.14}$$

For the details of the calculation we point the reader to appendix A.1. Even though we have now calculated the DoS exactly, a large-N expansion is still useful, because the large-N behavior of the Hermite-polynomials is not obvious. This expansion can either be done by inseting the known asymptotes of the Hermite-polynomials or by considering a saddle-point approximation of (3.12).

3.2 Saddle Point Integration

We now want to calculate the leading order and first correction of the large-N expansion of the given exact integral for the density of states by means of a so called saddle-point integration. Before we proceed with the calculation of the DoS, let us sketch the method briefly. A more detailed introduction can be found in [19]. Consider the integral

$$(*) = \int \mathrm{d}x \, \mathrm{e}^{-NS(x)} f(x) . \tag{3.15}$$

For large N this integral is dominated by the minima of S. For simplicity, let's assume, that S has only one extremum, which is the minimum. This minimum, which is located at $x = x_0$, is determined by the equation $S'(x) = 0$. We rewrite the integral by the change of variables $x \to x_0 + x/\sqrt{N\Delta}$ with the abbreviation $\Delta = S''(x_0)/2$.

This yields

$$(*) = \mathrm{e}^{-NS(x_0)} \int \mathrm{d}x \, \frac{\mathrm{e}^{-x^2}}{\sqrt{N\Delta}} \mathrm{e}^{-Ng(x/\sqrt{N\Delta})} f(x_0 + x/\sqrt{N\Delta}) . \tag{3.16}$$

Here we have decomposed S into $S(x+x_0) = S(x_0) + \frac{\Delta}{2} x^2 + g(x)$. We have $g(x) \propto x^3$ for small x. For $N\Delta \gg 1$, the integrand is therefore very well approximated by a Gaussian, and the corrections can be evaluated by applying a $1/N$-expansion to the slowly varying

contribution $f_s = \mathrm{e}^{-Ng(x/\sqrt{N\Delta})} f(x_0 + x/\sqrt{N\Delta})$. Note, that if the expansion of $f_s(1/N)$ has only a finite radius of convergence, the $1/N$-expansion of the whole integral is an asymptotic series rather than a convergent one.

In the general case, x_0 may be complex rather than real. We then have to remove the path of integration suitably into the complex plane. In this procedure we have to take care of the singularities in the integrand. Furthermore holomorphic functions do not have extrema, and therefore the solution of $S'(x) = 0$ determines a saddle-point rather than a maximum or minimum. Quadratic saddle-points have one stable and one unstable direction, where the e^{-S} falls off or rises fastest. The saddle-point approximation is well-defined, when the integration path traverses it in the stable direction. In this case, the integrand is a Gaussian with only small deviations. The saddle-point approximation is therefore also called "method of steepest descent". The stable direction is determined by the second derivatives, also called the stability matrix.

3.3 $1/N$ Expansion for the DoS

In order to separate the integral for the DoS into a fast varying and a slow varying one, it is necessary to switch to the macroscopic energy scale. We employ $E = x\sqrt{2N}$, and rescale also $p \to p\sqrt{2N}$ and $q \to q\sqrt{2N}$. This leads to the integral

$$\langle n(x) \rangle = \frac{-4}{\pi} \operatorname{Im} \int \frac{\mathrm{d}p\,\mathrm{d}q}{\pi/(2N)} \mathrm{e}^{-NS(p,q,x)} q \left(1 - \frac{1}{4(q-x)(\mathrm{i}p - x)}\right) \tag{3.17}$$

with the action

$$S(p,q,x) = 2p^2 - \ln(\mathrm{i}p - x) + 2q^2 + \ln(q - x)\,. \tag{3.18}$$

The saddle-point is now determined by the system of equations

$$0 = \frac{\partial S}{\partial p} = 4p - \frac{\mathrm{i}}{\mathrm{i}p - x}\,, \qquad 0 = \frac{\partial S}{\partial q} = 4q + \frac{1}{q - x}\,, \tag{3.19}$$

which has the four solutions

$$q_\pm = \frac{1}{2}\left(x \pm \mathrm{i}\sqrt{1 - x^2}\right)\,, \qquad p_\pm = -\mathrm{i}q_\pm\,. \tag{3.20}$$

The stability matrix reads

$$\begin{aligned} \left.\frac{\partial^2 S}{2\partial q^2}\right|_{q=q_\pm} &= 2(1 - 4q_\pm^2) = \mp 8\mathrm{i}\sqrt{1-x^2}\, q_\pm =: \Delta_\pm\,, \\ \left.\frac{\partial^2 S}{2\partial p^2}\right|_{p=p_\pm} &= \Delta_\pm\,. \end{aligned} \tag{3.21}$$

The non-diagonal entry $\frac{\partial^2 S}{\partial p \partial q}$ vanishes and is therefore not listed. This is due to the fact, that the action is a sum of two parts, where each part depends only on one of p and q.

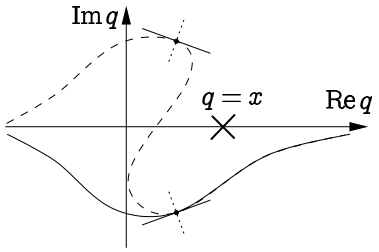

Figure 3.1: The saddle-points of q and possible integration paths. Solid lines denote the stable directions and dotted lines the unstable directions. It is not possible to touch both saddle-points unless you also cross a region where the integrand is large. The cross marks the singularity of the integrand.

In figures 3.1 and 3.2 the location of the saddle-points are sketched along with their stable directions and possible integration-paths. The integral (3.17) converges only for $\mathrm{Im}\, x > 0$ because we used the retarded Greens-function to calculate the DoS. This means, that the integration-path of q must pass below the singularity at $q = x$. This forces us to use the saddle-point q_- of the q-integration. A path of integration which also crosses q_+ leads through the region between the two saddle-points, where the integrand of (3.17) is large. This is no well-controlled procedure. Therefore the correct choice for the path of integration is the solid line in figure 3.1. In contrast it is possible to use an integration-path, that passes both saddle-points of p. This is shown in figure 3.2

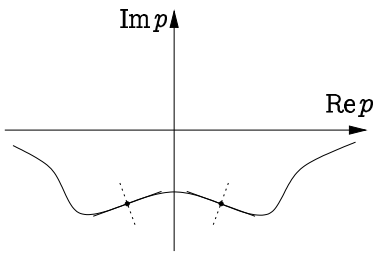

Figure 3.2: The saddle-points of the p-Integration. It is possible to chose a path of integration that reaches both saddle-points.

At first we consider the saddle-point (q_-, p_-). It is appropriate to change the vari-

ables

$$q \to q_- + \frac{\delta q}{\sqrt{N\Delta_-}}\,, \qquad\qquad p \to p_- + \frac{\delta p}{\sqrt{N\Delta_\pm}}\,. \tag{3.22}$$

The width of the Gaussian is now fixed to one and consequently it is strait forward to expand around the saddle-point. As a result we get the well known semi-circle behavior for the DoS [5].

The second saddle-point is more delicate, since the action $S_0 := -\mathrm{i}S(q_-, p_+)$ is nonzero. This leads then to an overall N-dependent prefactor $\mathrm{e}^{\mathrm{i}NS_0}$, which is of modulus 1. Otherwise the calculation proceeds as for the first saddle-point. Notice, that the factor $(1 - \frac{1}{4(q-x)(\mathrm{i}p-x)})$ is zero at the saddle-point (p_-, q_+), and thus this saddle-point does not contribute to the DoS at $N = \infty$, i. e. it does not change the semi-circle law. It does however add corrections to it. The final result, combining the results for both saddle-points, is

$$\langle n(x)\rangle = n_0(x) - \frac{1}{N}\frac{2\cos\left(NS_0(x)\right)}{\pi^3 n_0^2(x)} + \mathcal{O}\left(\frac{1}{N^2}\right) \tag{3.23}$$

with

$$\begin{aligned} n_0(x) &:= \frac{2}{\pi}\sqrt{1-x^2}\,, \\ S_0(x) &:= -\mathrm{i}S(p_+, q_-) = 2x\sqrt{1-x^2} + 2\arcsin x + \pi \end{aligned} \tag{3.24}$$

$S_0(x)$ seems to be a complicated function at first glance, but it turns out to be closely related to the semicircle DoS,

$$S_0(x) = 2\pi \int_{-1}^{x} \mathrm{d}t\, n_0(t)\,. \tag{3.25}$$

The $1/N$-correction diverges at the band edge. This stems from the fact, that at this point the relation $N\Delta \gg 1$ which we assume in the $1/N$-expansion does not hold. This in turn occurs, because the two saddle-points coalesce into one. To perform a valid $1/N$-expansion in the vicinity of the band-edge, it is necessary, to consider a third order saddle-point. This third order saddle-point will lead to exponents $N^{-n/3}$, where n is some integer. Using the asymptotes of the Hermite-polynomials, it is known, that the DoS can be written in terms of Airy-functions [5]. Although we expect this calculation not to be very complicated, we will not do it here, because it is not of major interest in the context of this work.

A plot of the exact density of states and the approximated one is shown in figure 3.3. The approximation is remarkably well within the band, even for small N.

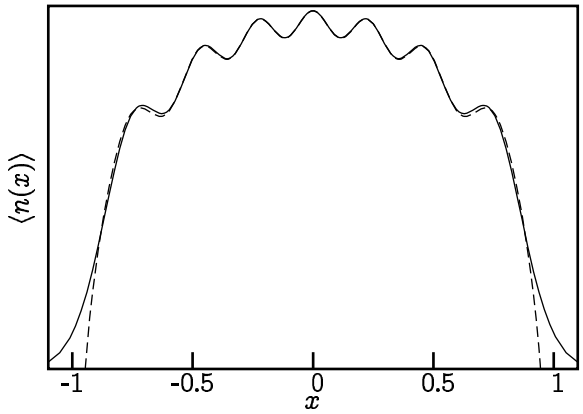

Figure 3.3: The exact density of states and approximation for $N = 7$.

Equations (3.24) and (3.25) ensure, that there are N maxima of the DoS. Furthermore, the frequency of the oscillations is proportional to the averaged density of states in the limit $N \to \infty$. We therefore conclude, that the most probable distribution of eigenvalues is the one, where there is one state at each maximum of the DoS. This feature is in principle known from the joint probability distribution, which is minimal, if the Eigenvalues are the zeros of some Hermite-polynomial. We conjecture, that the wiggles are due to level repulsion. We will discuss this point later in more detail.

3.4 Two Point Correlation Functions

As a final remark we want to state that it is possible to also calculate two-point correlation functions in the same way. But due to the two propagators in

$$K(x, y) = \langle G(x)G(y) \rangle \,, \tag{3.26}$$

we need two sets of supersymmetric vectors:

$$K_{i,j}(x, y) = -\int \mathcal{D}[\phi_1, \phi_2, H]\; \phi_{1,i}\phi^\dagger_{1,k}\phi_{2,k}\phi^\dagger_{2,j} \mathrm{e}^{-S} \,, \tag{3.27}$$

with

$$S = \mathrm{i}\phi^\dagger_1(H - x)\phi_1 + \mathrm{i}\phi^\dagger_2(H - y)\phi_2 + \mathrm{tr}\, H^2 \,. \tag{3.28}$$

This duplication of variables renders the derived $\mathbf{Q}$-matrix representation more complicated. In general, a nonlinear sigma-model emerges, see e. g. [8]. Calculating higher correlation functions is even more complicated. Subsequently we will not calculate any higher correlation functions explicitly, but stick to the DoS.

Chapter 4

Other Gaussian Ensembles

4.1 Introduction

In this chapter we will calculate the DoS for four additional matrix ensembles. These are the orthogonal ensemble (goe), the ensemble of real antisymmetric matrices, the symplectic ensemble (gse) and the ensemble of quaternion matrices that change sign under conjugation. The last ensemble is also known as class C. The Ensemble of antisymmetric matrices is also called class D for even dimension.

In sections 4.2 to 4.5 which are rather formal, we will calculate the exact DoS. This leads to rather cumbersome expressions and therefor we will compare the DoS to the large N results in section 4.6.

4.2 Orthogonal Ensemble

The goe consist of symmetric $N \times N$ matrices H whose entries are Gaussian distributed. The averaged DoS can be expressed in the same way we did it in the last chapter. We employ the action

$$\begin{aligned} S_H &= \mathrm{i}\phi_i^\dagger (H_{ij} - z\delta_{ij})\phi_j + \frac{1}{2} H_{ij}H_{ji} \\ &= \frac{\mathrm{i}}{2}\chi_i^t \left(H_{ij} - z\delta_{ij}\right)\chi_j + \frac{1}{2} H_{ij}H_{ji}\,. \end{aligned} \tag{4.1}$$

The factor $1/2$ in front of $H_{ij}H_{ji}$ has been introduced for reasons of convenience. z has again positive imaginary part and H is a real symmetric matrix. We have used the real vector $\chi_i^t = \left(x_i^\dagger, x_i^T, \psi_i^\dagger, -\psi_i^T\right)$, which was introduced in chapter 2, to symmetrize the action with respect to H. It is now strait forward to integrate over H, which leads to the action

$$S_4 = -\frac{\mathrm{i}}{2} z\chi_i^t\chi_i + \frac{1}{8}\operatorname{trg}\left(\chi_i\chi_i^t\right)^2\,. \tag{4.2}$$

We decouple the interaction term with the $\mathbf{Q}$-matrix

$$\mathbf{Q} = \begin{pmatrix} q_1 & \bar{q}_2 & \bar{\vartheta}_1 & -\vartheta_2 \\ q_2 & q_1 & \bar{\vartheta}_2 & -\vartheta_1 \\ \vartheta_1 & \vartheta_2 & \mathrm{i}p & 0 \\ \bar{\vartheta}_2 & \bar{\vartheta}_1 & 0 & \mathrm{i}p \end{pmatrix} \tag{4.3}$$

and end up with the factorized action

$$S_{\mathbf{Q}} = \frac{\mathrm{i}}{2}\chi_i^t(\mathbf{Q} - z)\chi_i + \frac{1}{2}\operatorname{trg}\mathbf{Q}^2 \,. \tag{4.4}$$

After integration over the χ-fields the DoS is given by

$$\langle n(z)\rangle = \frac{-2}{\pi N}\operatorname{Im}\int \mathcal{D}[\mathbf{Q}]\,\frac{q\,\mathrm{e}^{-\operatorname{trg}\mathbf{Q}^2}}{\operatorname{detg}(\mathbf{Q}-z)^{N/2}} \tag{4.5}$$

To further evaluate this integral we have to calculate

$$\operatorname{detg}\mathbf{Q} = \frac{Q}{(\mathrm{i}p)^2}\exp\left(-\frac{2}{Q(\mathrm{i}p)}(q_1\Theta_1 - q_2\Theta_2 - \bar{q}_2\bar{\Theta}_2) - \frac{2\Theta_2\bar{\Theta}_2}{Q(\mathrm{i}p)^2}\right)\,, \tag{4.6}$$

where $Q = q_1^2 - q_2\bar{q}_2$, $\Theta_1 = \bar{\vartheta}_1\vartheta_1 + \bar{\vartheta}_2\vartheta_2$, $\Theta_2 = \bar{\vartheta}_1\vartheta_2$. Integrating over the Grassmann variables now yields

$$\begin{aligned}\langle n(z)\rangle = \frac{-2}{\pi N}\operatorname{Im}\int_{\mathbb{R}^2}\frac{\mathrm{d}p\,\mathrm{d}q}{\pi}\int_0^\infty \mathrm{d}r\;\mathrm{e}^{-p^2-q^2-r}\frac{q(\mathrm{i}p-z)^N}{((q-z)^2-r)^{N/2}} \\ \times\left(1 - \frac{N(q-z)}{(\mathrm{i}p-z)((q-z)^2-r)} + \frac{(N-1)N}{4(\mathrm{i}p-z)^2((q-z)^2-r)}\right)\,,\end{aligned} \tag{4.7}$$

where the branch cut of the root lies on the positive real axis.

This integral must be calculated separately for N even and N odd due to the factor $((q-z)^2-r)^{-N/2}$. In the former case it evaluates to Hermite-polynomials, while in the latter integrals over the error-function come into play. We give here the result for $N = 2\nu$ even:

$$\begin{aligned}\langle n(E)\rangle = \frac{-\mathrm{e}^{-E^2}}{4^\nu\nu!\sqrt{\pi}}\Bigg[H_{2\nu}(E)\left(\sum_{k=1}^{\nu-1}\frac{k!}{(2k)!}H_{2k}(E) + \sqrt{\frac{\pi}{8}}E\mathrm{e}^{\frac{E^2}{2}}\operatorname{erf}\frac{E}{\sqrt{2}} - \frac{1}{2}\right) \\ - 2H_{2\nu-1}(E)\left(\sum_{k=0}^{\nu-1}\frac{k!}{(2k)!}H_{2k+1}(E) - \sqrt{\frac{\pi}{2}}(1-E^2)\mathrm{e}^{\frac{E^2}{2}}\operatorname{erf}\frac{E}{\sqrt{2}} + E\right) \\ + 2(2\nu-1)H_{2\nu-2}(E)\left(\sum_{k=1}^{\nu}\frac{k!}{(2k)!}H_{2k}(E) + \sqrt{\frac{\pi}{2}}E\mathrm{e}^{\frac{E^2}{2}}\operatorname{erf}\frac{E}{\sqrt{2}} - 1\right)\Bigg]\end{aligned}$$

$$= \frac{\mathrm{e}^{-E^2}}{4^\nu\sqrt{\pi}}\left[\frac{H_{2\nu-1}(E)^2 - H_{2\nu}(E)H_{2\nu-2}(E)}{N\,(2\nu-2)!}\right. \\ \left. - \frac{H_{2\nu-1}(E)}{\nu!}\left(\sum_{k=1}^{\nu-1}\frac{2k!}{(2k)!}H_{2k-1}(E) - \sqrt{\frac{\pi}{8}}\mathrm{e}^{\frac{E^2}{2}}\operatorname{erf}\frac{E}{\sqrt{2}}\right)\right] \tag{4.8}$$

In the last step we have used the recursion relation for Hermite-polynomials. The integrals needed can be found in appendix A.1.

Later on we will discuss the large-N expansion of equation (4.7). The macroscopic scaling employed is given by $x = E/\sqrt{2N}$. This leads to the integral expression

$$\langle n(x)\rangle = \frac{-4}{\pi N}\operatorname{Im}\int_{\mathbb{R}^2}\frac{\mathrm{d}p\,\mathrm{d}q}{\pi/(2N)}\int_0^\infty 2N\mathrm{d}r\; q\,\mathrm{e}^{-NS} \\ \times\left(1 - \frac{q-x}{2(\mathrm{i}p-x)((q-x)^2-r)} + \frac{1-1/N}{16(\mathrm{i}p-x)^2((q-x)^2-r)}\right), \tag{4.9a}$$

with

$$S = 2p^2 + 2q^2 + 2r + \frac{1}{2}\ln((q-x)^2-r) - \ln(\mathrm{i}p - r)\,. \tag{4.9b}$$

4.3 Symplectic Ensemble

Symplectic matrices possess a 2×2 block structure with the constraint $\sigma_2 H\sigma_2 = H^T$. Additionally, we require H to be hermitian, $H^\dagger = H$. Due to these constraints H can be written as $H = \left(\begin{smallmatrix} A & B \\ B^\dagger & A^T\end{smallmatrix}\right)$, where A and B are $N\times N$ matrices and A is hermitian and B is complex and antisymmetric. The entries of H are again Gaussian distributed. We introduce two flavors of bosonic and fermionic variables x_1, x_2 and ψ_1, ψ_2 respectively, along with the notation $\phi_{1/2} = \left(\begin{smallmatrix} x_{1/2} \\ \psi_{1/2}\end{smallmatrix}\right)$, which leads to the action

$$\begin{aligned} S_H &= I\begin{pmatrix}\phi_1^\dagger & \phi_2^\dagger\end{pmatrix}\begin{pmatrix}A-z & B \\ B^\dagger & A^T - z\end{pmatrix}\begin{pmatrix}\phi_1 \\ \phi_2\end{pmatrix} + \operatorname{tr}\left(A^2 + BB^\dagger\right) \\ &= \frac{\mathrm{i}}{2}\begin{pmatrix}\chi_1^t & \chi_2^t\end{pmatrix}\begin{pmatrix}A-z & B\Sigma_3 \\ B^\dagger\Sigma_3 & A^T - z\end{pmatrix}\begin{pmatrix}\chi_1 \\ \chi_2\end{pmatrix} + \operatorname{tr}\left(A^2 + BB^\dagger\right), \end{aligned} \tag{4.10}$$

where we have introduced the new symbols

$$\chi_1^t = \begin{pmatrix}x_1^\dagger & x_2^T & \psi_1^\dagger & -\psi_2^T\end{pmatrix} \qquad \chi_2^t = \begin{pmatrix}x_2^\dagger & x_1^T & \psi_2^\dagger & -\psi_1^T\end{pmatrix}. \tag{4.11}$$

The matrix Σ_3 is a Pauli matrix which acts on the space of the two flavors of variables. We have employed the convenient features $\chi_1^t\chi_1 = \chi_2^t\chi_2$ and $\chi_1^t\Sigma_3\chi_2 = -\chi_2^t\Sigma_3\chi_1$.

These features enable us to to easily integrate over the random matrix ensemble, which leads to the action

$$S_4 = -\mathrm{i}z\chi_1^t\chi_1 + \frac{1}{8}\operatorname{trg}\left(\chi_1\chi_1^t + \Sigma_3\chi_2\chi_2^t\Sigma_3\right)^2 . \tag{4.12}$$

We decouple the quartic term with the $\mathbf{Q}$-matrix

$$\mathbf{Q} = \begin{pmatrix} q & 0 & \bar{\vartheta}_1 & \bar{\vartheta}_2 \\ 0 & q & -\vartheta_2 & -\vartheta_1 \\ \vartheta_1 & \bar{\vartheta}_2 & \mathrm{i}p_1 & \mathrm{i}\bar{p}_2 \\ \vartheta_2 & \bar{\vartheta}_1 & \mathrm{i}p_2 & \mathrm{i}p_1 \end{pmatrix} \tag{4.13}$$

and get the factorized action

$$S_{\mathbf{Q}} = \mathrm{i}\chi_1^t(\mathbf{Q} - z)\chi_1 + \frac{1}{2}\operatorname{trg}\mathbf{Q}^2 . \tag{4.14}$$

In contrast to the orthogonal ensemble, this action corresponds to a complex path-integral with respect to the χ-variables. We integrate over the χ-variables and the Grassmann-part of $\mathbf{Q}$ by help of

$$\operatorname{detg}\mathbf{Q}^{-1} = \frac{P}{q^2}\exp\left(\frac{2}{Pq}(\mathrm{i}p_1\Theta_1 - \mathrm{i}p_2\Theta_2 - \mathrm{i}\bar{p}_2\bar{\Theta}_2) - \frac{2\Theta_2\bar{\Theta}_2}{Pq^2}\right) , \tag{4.15}$$

where $P = (\mathrm{i}p_1)^2 - (\mathrm{i}p_2)(\mathrm{i}\bar{p}_2)$, $\Theta_1 = \bar{\vartheta}_1\vartheta_1 + \bar{\vartheta}_2\vartheta_2$, $\Theta_2 = \bar{\vartheta}_2\vartheta_1$. We end up with the integral

$$\begin{aligned} \langle n(z)\rangle &= \frac{-1}{\pi N}\operatorname{Im}\int\mathcal{D}[\mathbf{Q}]\,\frac{\mathrm{e}^{-\frac{1}{2}\operatorname{trg}\mathbf{Q}^2}}{\operatorname{detg}(\mathbf{Q}-z)^N} \\ &= \frac{-1}{\pi N}\operatorname{Im}\int_{\mathbb{R}^2}\frac{\mathrm{d}p\,\mathrm{d}q}{\pi}\int_0^\infty \mathrm{d}r\; q\mathrm{e}^{-p^2-q^2-r}\frac{((\mathrm{i}p-z)^2+r)^N}{(q-z)^{2N}} \\ &\qquad \times\left(1 - \frac{2N(\mathrm{i}p-z)}{(q-z)(\mathrm{i}p-z)^2+r)} + \frac{(2N+1)N}{2(q-z)^2((\mathrm{i}p-z)^2+r)}\right) . \end{aligned} \tag{4.16}$$

In the limit $z \to E + \mathrm{i}0$ this integral evaluates to Hermite-polynomials:

$$\begin{aligned} \langle n(E)\rangle &= \frac{N!\mathrm{e}^{-E^2}}{(2N)!\sqrt{\pi}}\left(H_{2N}(E)\sum_{k=0}^{N}\frac{H_{2k}(E)}{4^k k!} - \frac{H_{2N+1}(E)}{2N}\sum_{k=0}^{N-1}\frac{H_{2k+1}(E)}{4^k k!}\right. \\ &\qquad\left. + \frac{H_{2N+2}(E)}{4N}\sum_{k=0}^{N-1}\frac{H_{2k}(E)}{4^k k!}\right) \\ &= \frac{\mathrm{e}^{-E^2}}{(2N)!\sqrt{\pi}}\left(\frac{H_{2N}(E)^2 - H_{2N+1}(E)H_{2N-1}(E)}{4^N} - \frac{N!}{2N}H_{2N}(E)\sum_{k=0}^{N-1}\frac{H_{2k}(E)}{4^k k!}\right) . \end{aligned} \tag{4.17}$$

In the last step we have employed the recursion-relation for Hermite-polynomials. The details of the integration are presented in appendix A.1.

For the saddle-point approximation we rewrite equation (4.16) in the macroscopic scaling $x = E/\sqrt{4N}$, which leads to

$$\begin{aligned}\langle n(x)\rangle = \frac{-4}{\pi}\operatorname{Im}\int\limits_{\mathbb{R}^2}\frac{\mathrm{d}p\,\mathrm{d}q}{\pi/(4N)}\int\limits_0^\infty 4N\mathrm{d}r\; q\,\mathrm{e}^{-2NS} \\ \times\left(1-\frac{\mathrm{i}p-x}{2(q-x)(\mathrm{i}p-x)^2+r)}+\frac{2+1/N}{32(q-x)^2((\mathrm{i}p-x)^2+r)}\right),\end{aligned} \tag{4.18a}$$

with

$$S = 2p^2+2q^2+2r+\ln(q-x)-\frac{1}{2}\ln((\mathrm{i}p-x)^2+r)\,. \tag{4.18b}$$

4.4 Antisymmetric Matrices

In this section we consider antisymmetric matrices with Gaussian distributed matrix elements. Let H be real. Then the action, that leads to the correct DoS is

$$S_H = \mathrm{i}\phi^\dagger\left(\mathrm{i}H - z\right)\phi - \frac{1}{2}\operatorname{tr}H^2 \tag{4.19}$$

$$= \frac{\mathrm{i}}{2}\chi_i^t\left(\mathrm{i}H_{ij}\Sigma_3 - z\delta_{ij}\right)\chi_j - \frac{1}{2}\operatorname{tr}H^2\,. \tag{4.20}$$

Here we have used the real vector χ associated with the complex vector ϕ as we did for the orthogonal ensemble. Averaging yields the effective action

$$S_4 = -\frac{\mathrm{i}}{2}z\chi^t\chi + \frac{1}{8}\operatorname{trg}\left(\chi_i\chi_i^t\Sigma_3\right)^2\,, \tag{4.21}$$

which can be decoupled by

$$\mathbf{Q} = \begin{pmatrix} q_1 & \bar{q}_2 & -\vartheta_1 & -\vartheta_2 \\ q_2 & -q_1 & \bar{\vartheta}_2 & \bar{\vartheta}_1 \\ \bar{\vartheta}_1 & \vartheta_2 & \mathrm{i}p & 0 \\ \bar{\vartheta}_2 & \vartheta_1 & 0 & -\mathrm{i}p \end{pmatrix} \tag{4.22}$$

to get the factorized action

$$S_{\mathbf{Q}} = \frac{\mathrm{i}}{2}\chi_i^t(\Sigma_3\mathbf{Q}-z)\chi_i + \frac{1}{2}\operatorname{trg}\mathbf{Q}^2\,. \tag{4.23}$$

It is not possible to integrate over the χ-variables directly, because the complex part of $\Sigma_3\mathbf{Q}$ has non-real eigenvalues. Therefore we need to move the integration path into the complex plane to ensure convergence. For $\operatorname{Re} z > 0$ e. g. the choice

$$\begin{aligned} \chi &\to \mathrm{e}^{\mathrm{i}\pi/8}\chi \\ q_1 &\to \mathrm{e}^{-\mathrm{i}\pi/4}q_1 + \varepsilon\mathrm{e}^{\mathrm{i}\pi/4}\tanh(q_1/\varepsilon) \\ \rho = \sqrt{q_2\bar{q}_2} &\to \mathrm{e}^{\mathrm{i}\pi/4}\rho + \varepsilon\mathrm{e}^{-\mathrm{i}\pi/4}\tanh(\rho/\varepsilon) \end{aligned} \tag{4.24}$$

with $0 < \varepsilon < (\operatorname{Im} z + \operatorname{Re} z)/\sqrt{2}$ works. In the following we call the new integration domain Ω. Integrating over χ leads to the determinant

$$\operatorname{detg} \sigma_3\mathbf{Q} = \frac{Q}{(\mathrm{i}p)^2}\exp\left(-\frac{2}{Q(\mathrm{i}p)}(q_1\Theta_1 - q_2\Theta_2 + \bar{q}_2\bar{\Theta}_2) - \frac{2\Theta_2\bar{\Theta}_2}{Q(\mathrm{i}p)^2}\right) \tag{4.25}$$

with $Q = q_1^2 + q_2\bar{q}_2$, $\Theta_1 = \bar{\vartheta}_1\vartheta_1 - \bar{\vartheta}_2\vartheta_2$, $\Theta_2 = \vartheta_1\vartheta_2$, and after integration over the remaining Grassmann-variables we obtain

$$\begin{aligned} \langle n(z)\rangle &= \frac{-2}{\pi N}\operatorname{Im}\int\mathcal{D}[\mathbf{Q}]\,\frac{\mathrm{e}^{-\frac{1}{2}\operatorname{trg}\mathbf{Q}^2}}{\operatorname{detg}(\Sigma_3\mathbf{Q} - z)^{N/2}} \\ &= \frac{-2}{\pi N}\operatorname{Im}\int_\Omega\frac{\mathrm{d}p\;\mathrm{d}q}{\pi}\mathrm{d}r\;\frac{q\,\mathrm{e}^{-p^2-q^2-r}(\mathrm{i}p - z)^N}{((q-z)^2 + r)^{N/2}}\left(1 - \frac{N(N-1)}{4((q-z)^2 + r)(\mathrm{i}p - z)^2}\right), \end{aligned} \tag{4.26}$$

where we substituted $r = q_2\overline{q}_2$. The root has its branch cut on the negative imaginary axis. We need to consider this integral separately for N even and N odd. For $N = 2\nu$ even, the DoS reads

$$\begin{aligned} \langle n(E)\rangle &= \frac{(-1)^{\nu-1}\mathrm{e}^{-E^2}}{4^\nu\nu!\sqrt{\pi}}\left[H_{2\nu}(E)\left(\sum_{k=0}^{\nu-1}\frac{(-1)^k k!}{(2k)!}H_{2k}(E) + \frac{1}{2E^2}\right)\right. \\ &\qquad\left. + 2(2\nu-1)H_{2\nu-2}\left(\sum_{k=0}^{\nu}\frac{(-1)^k k!}{(2k)!}H_{2k}(E) + \frac{1}{2E^2}\right)\right] \\ &= \frac{-\mathrm{e}^{-E^2}}{4^\nu\sqrt{\pi}}\left[\frac{H_{2\nu}(E)H_{2\nu-2}(E)}{\nu\,(2\nu-2)!} + \frac{2E}{\nu!}H_{2\nu-1}(E)\left(\sum_{k=0}^{\nu-1}\frac{(-1)^{k+\nu}k!}{(2k)!}H_{2k}(E) + \frac{1}{2E^2}\right)\right]. \end{aligned} \tag{4.27}$$

For the last step we have used again the recursion-relation for Hermite-polynomials.

The macroscopic scaling $x = E/\sqrt{2N}$ allows us to write equation (4.26) in a form

suitable for the saddle-point approximation:

$$\langle n(x)\rangle = \frac{-4}{\pi}\,\mathrm{Im}\int_\Omega \frac{\mathrm{d}p\;\mathrm{d}q}{\pi/(2N)} 2N \mathrm{d}r\; q\,\mathrm{e}^{-NS}\left(1-\frac{1-1/N}{16((q-x)^2+r)(\mathrm{i}p-x)^2}\right)\,. \tag{4.28}$$

$$S = 2p^2+2q^2+2r+\frac{1}{2}\ln((q-x)^2+r)-\ln(\mathrm{i}p-x) \tag{4.29}$$

4.5 Class C

Class C consists of quaternion matrices that change sign under conjugation. When written as complex matrices they have therefore imaginary eigenvalues. As a consequence we can characterize matrices of class C as hermitian matrices (up to a factor of i) with the additional constraint $\sigma_2 H \sigma_2 = -H^T$. These matrices can be written as $H = \left(\begin{smallmatrix} A & B \\ B^\dagger & -A^T \end{smallmatrix}\right)$, where A is hermitian and B is complex-symmetric. Following the notation for the symplectic ensemble, the action is given by

$$S_H = \frac{\mathrm{i}}{2}\begin{pmatrix}\chi_1^t & \chi_2^t\end{pmatrix}\begin{pmatrix} A\Sigma_3 - z & B \\ B^\dagger & -A^T\Sigma_3 - z\end{pmatrix}\begin{pmatrix}\chi_1 \\ \chi_2\end{pmatrix} + \mathrm{tr}\left(A^2+BB^\dagger\right)\,. \tag{4.30}$$

This leads to the effective action

$$S_4 = \mathrm{trg}(\chi_1\chi_1^t\Sigma_3 + \Sigma_3\chi_2\chi_2^t)^2\,, \tag{4.31}$$

which may be decoupled by

$$\mathbf{Q} = \begin{pmatrix} q & 0 & -\vartheta_1 & \bar\vartheta_2 \\ 0 & -q & -\vartheta_2 & \bar\vartheta_1 \\ \bar\vartheta_1 & \bar\vartheta_2 & \mathrm{i}p_1 & \mathrm{i}\bar p_2 \\ \vartheta_2 & \vartheta_1 & \mathrm{i}p_2 & -\mathrm{i}p_1 \end{pmatrix} \tag{4.32}$$

to get the factorized action

$$S_{\mathbf{Q}} = \mathrm{i}\chi_1^t(\Sigma_3\mathbf{Q}-z)\chi_1 + \frac{1}{2}\,\mathrm{trg}\,\mathbf{Q}^2\,. \tag{4.33}$$

Using

$$\mathrm{detg}\,\Sigma_3\mathbf{Q}^{-1} = \frac{P}{q^2}\exp\left(\frac{2}{Pq}(\mathrm{i}p_1\Theta_1+\mathrm{i}p_2\Theta_2-\mathrm{i}\bar p_2\bar\Theta_2) - \frac{2\Theta_2\bar\Theta_2}{Pq^2}\right) \tag{4.34}$$

with $P = (\mathrm{i}p_1)^2 + (\mathrm{i}p_2)(\mathrm{i}\bar{p}_2)$, $\Theta_1 = \bar{\vartheta}_1\vartheta_1 - \bar{\vartheta}_2\vartheta_2$, $\Theta_2 = \bar{\vartheta}_1\bar{\vartheta}_2$, we end up with the expression

$$\begin{aligned}\langle n(z)\rangle &= \frac{-1}{\pi N}\operatorname{Im}\int\mathcal{D}[\mathbf{Q}]\,\frac{\mathrm{e}^{-\frac{1}{2}\operatorname{trg}\mathbf{Q}^2}}{\operatorname{detg}(\Sigma_3\mathbf{Q}-z)^N}\\ &= \frac{-1}{\pi N}\operatorname{Im}\int_{\mathbb{R}^2}\frac{\mathrm{d}p\,\mathrm{d}q}{\pi}\int_0^\infty \mathrm{d}r\,\mathrm{e}^{p^2-q^2-r}\,q\frac{((\mathrm{i}p-z)^2-r)^N}{(q-z)^{2N}}\left(1-\frac{N(2N+1)}{2((\mathrm{i}p-z)^2-r)(q-z)^2}\right)\end{aligned} \tag{4.35}$$

for the averaged DoS. In the limit $z \to E + \mathrm{i}0$ also this integral can be computed exactly:

$$\begin{aligned}\langle n(E)\rangle &= \frac{(-1)^N N!\mathrm{e}^{-E^2}}{(2N)!\sqrt{\pi}}\left(H_{2N}(E)\sum_{k=0}^{N}\frac{(-1)^k}{k!4^k}H_{2k}(E) + \frac{H_{2N+2}(E)}{4N}\sum_{k=0}^{N-1}\frac{(-1)^k}{k!4^k}H_{2k}(E)\right)\\ &= \frac{\mathrm{e}^{-E^2}}{2\sqrt{\pi}}\left(\frac{H_{2N}(E)H_{2N+1}(E) - H_{2N+2}(E)H_{2N-1}(E)}{4^N E(2N)!}\right)\end{aligned} \tag{4.36}$$

In the last step we have rewritten the Hermite-polynomials in terms of Laguerre-polynomials. This allowed us to make use of a finite sum of Laguerre-polynomials. Theses properties of the orthogonal polynomials together with the integrals needed can be found in appendix A.1.

In order to apply a $1/N$-expansion for equation (4.35), it is necessary to switch to the macroscopic scaling $x = E/\sqrt{4N}$:

$$\langle n(x)\rangle = \frac{-4}{\pi}\operatorname{Im}\int_{\mathbb{R}^2}\frac{\mathrm{d}p\,\mathrm{d}q}{\pi/(4N)}\int_0^\infty 4N\mathrm{d}r\,q\,\mathrm{e}^{-2NS}\left(1-\frac{2+1/N}{32((\mathrm{i}p-x)^2-r)(q-x)^2}\right), \tag{4.37a}$$

$$S = 2p^2 + 2q^2 + 2r + \ln(q-x) - \frac{1}{2}\ln((\mathrm{i}p-x)^2 - r)\,. \tag{4.37b}$$

4.6 Large N expansion

In this section we attempt to give a saddle-point approximation to the exact results of the DoS of the four ensembles. We start from the integral representations (4.9a), (4.18a), (4.28) and (4.37a). Due to the additional integration variable r, the saddle-point structure is more complicated than in the unitary case. First off, we have to consider the boundary point $r = 0$. For $r = 0$, the action of all four ensembles coincides with the action in the unitary case. The discussion of the saddle-points for the gue does therefore apply as well to the four ensembles considered here.

However, there are possibly further saddle-points for $r \neq 0$ given by the set of equations

$$\frac{\partial S}{\partial p} = 0 \,, \qquad \frac{\partial S}{\partial q} = 0 \,, \qquad \frac{\partial S}{\partial r} = 0 \,. \tag{4.38}$$

These equations have different solutions for the four ensembles. The solutions for goe and gse are

Ensemble	p	q	r
goe	$-\frac{\mathrm{i}}{2}\left(x \pm \mathrm{i}\sqrt{1-x^2}\right)$	$\frac{x}{2}$	$-\frac{1}{4}(1-x^2) < 0$
gse	$-\mathrm{i}\frac{x}{2}$	$\frac{1}{2}(x \pm \mathrm{i}\sqrt{1-x^2})$	$\frac{1}{4}(1-x^2)$

For the goe, this additional saddle-point can not be reached, as r is positive by definition. The additional saddle-point can however be reached for the gse and has therefore to be considered separately.

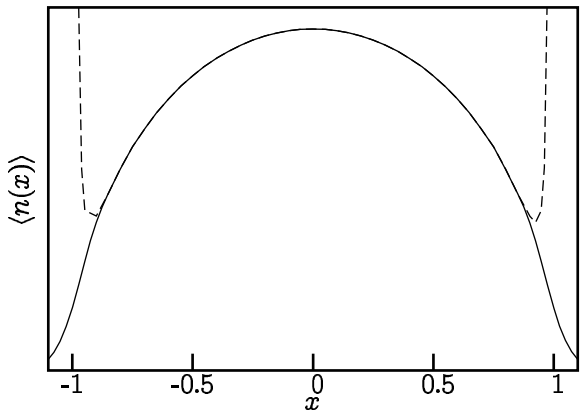

Figure 4.1: Exact DoS and saddle-point approximation of orthogonal ensemble for $N = 20$.

The DoS for the goe reads up to order $1/N^2$

$$\langle n(x)\rangle = n_0(x) - \frac{1}{N}\frac{1}{\pi^2 n_0(x)} + \frac{1}{N^2}\frac{6+8x^2}{\pi^6 n_0^5(x)} - \frac{1}{N^2}\frac{4\cos\left(NS_0(x) - \arcsin(x)\right)}{\pi^6 n_0^5(x)} \,, \tag{4.39}$$

with $S_0(x)$ as given in 3.23. The exact result along with the saddle-point approximation is shown in figure 4.1. The wiggles that were present in the gue are invisible here. This is because the wiggles are of order $1/N^2$ with a very small prefactor.

For the gse the DoS is up to order $1/N$ given by

$$\langle n(x)\rangle = n_0(x) - \frac{1}{\sqrt{N}}\frac{\cos\left(NS_0(x) + \frac{1}{2}\arcsin(x)\right)}{\pi\sqrt{n_0(x)}} + \frac{1}{N}\frac{1}{2\pi^2 n_0(x)} \,. \tag{4.40}$$

The exact result and the saddle-point approximation are plotted in figure 4.2. Here the wiggles are of order $1/\sqrt{N}$ and are therefore much more pronounced than in the gue.

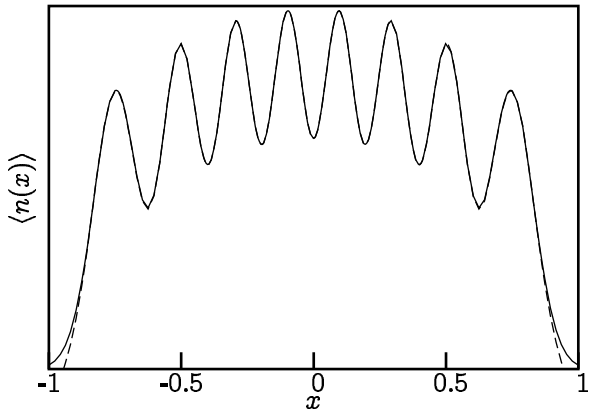

Figure 4.2: Exact DoS and Saddle-Point approximation of symplectic ensemble for $N = 8$.

We find this result striking, because level repulsion in the gue is stronger than in the goe and weaker than in the gse. Obviously there is a close relation between level repulsion and the oscillatory part of the DoS. Let α be the exponent that characterizes the decay of the oscillatory part of the DoS for large N, and β the exponent that characterizes the level repulsion. Then α and β are related by $\alpha = 2/\beta$ for the three classical ensembles, which is depicted in table 4.1.

	goe	gue	gse
α	2	1	1/2
β	1	2	4

Table 4.1: Relation between level repulsion and oscillatory part of the DoS. α characterizes the decay of the oscillatory part of the DoS and β the level repulsion.

Let us now turn to the nonstandard ensembles. For the antisymmetric matrices and class C, solutions of the saddle-point equations exist only for $x = 0$, and they read

antisymmetric	$p = \pm\frac{1}{2}$	$r = -\frac{1}{4} - q^2$
Class C	$q = \frac{\mathrm{i}}{2}$	$r = \frac{1}{4} - p^2$

Obviously, the point $x = 0$ is special in these ensembles, because the spectrum is symmetric. As we can see, at this point there exists a saddle-point manifold for each of the two ensembles. We think however, that these manifolds do not contribute to the

DoS, because we may choose the integration-path to cross the manifold in only one point, namely $r = 0$, $q = \pm\mathrm{i}$ or $p = \pm\mathrm{i}$ respectively. This claim is supported by the fact, that the manifold extends to infinity, but it does so in the direction $r \propto \mathrm{i}$ and $q^2 \propto \mathrm{i}$, $q \propto \mathrm{i}$ respectively for large p, q, r. Integrating over the manifold therefore destroys convergence of the integrals (4.28) and (4.37a). The saddle-point manifold is therefore transversal to the integration path. This claim will also be supported by comparison of the saddle-point approximation to the exact results. It could be proven, by showing that the result does not change, if we integrate over some part of the saddle-point manifold. We do not attempt to do this calculation within this work, because a more detailed investigation of this problem has already been done by Ivanov [12].

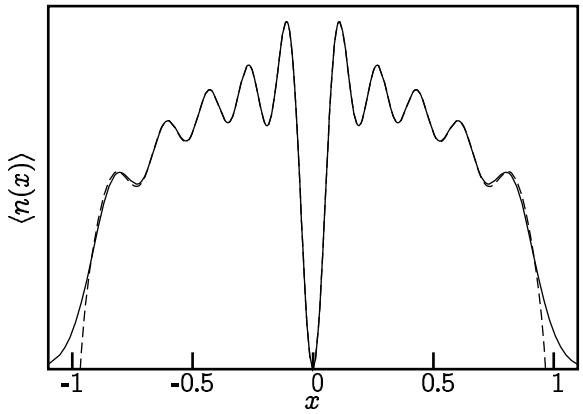

Figure 4.3: Exact DoS and Saddle-Point approximation of class C for $N = 5$.

A straight forward calculation of the DoS for $x \neq 0$ yields for class C up to order $1/N$

$$\langle n(x)\rangle = n_0(x) + \frac{1}{N}\frac{1}{2\pi^2 n_0(x)} - \frac{1}{N}\frac{\sin\left(2NS_0(x) + \arcsin(x)\right)}{\pi^3 x n_0^2(x)}\,. \tag{4.41}$$

The exact DoS and the saddle-point approximation are shown in figure 4.3.

The DoS of the antisymmetric matrices is up to order $1/N$ given by

$$\langle n(x)\rangle = n_0(x) - \frac{1}{N}\frac{1}{\pi^2 n_0(x)} + \frac{1}{N}\frac{2\sin\left(NS_0(x) - \arcsin(x)\right)}{\pi^3 x n_0^2(x)}\,, \tag{4.42}$$

which is shown along with the exact DoS in figure 4.4. It is striking, how well the saddle-point approximation reproduces the exact result within the band and even right at the band center. In the limit $N \to \infty$ the semicircle law of the DoS is recovered for both ensembles. Even though $\langle n(0)\rangle \neq n_0(0)$ for all finite N, the deviation has vanishing statistical weight for large N.

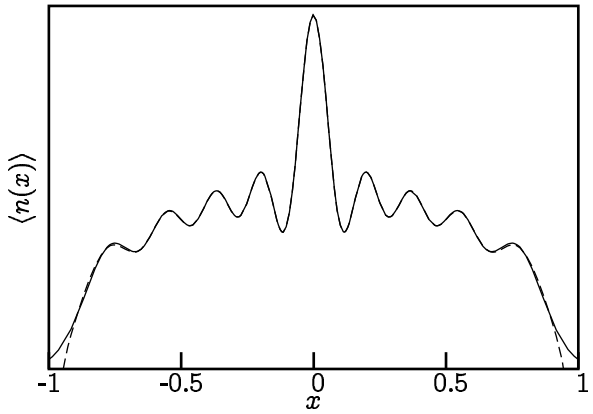

Figure 4.4: Exact DoS and Saddle-Point approximation of class D for $N = 10$.

In both ensembles, class C and the antisymmetric matrices, the oscillatory part decreases $\propto 1/N$ except at the band center. The level repulsion in these ensembles is therefore similar to the unitary case. For class C this is true even right at the band center, which can be seen using a formula derived by Zirnbauer [11].

For $x \neq 0$ and $N \to \infty$ the universality of level repulsion is therefore the same for these ensembles and the unitary ensemble. It depends highly on the physical application, whether the deviation from unitary universality plays any role and is measurable at all.

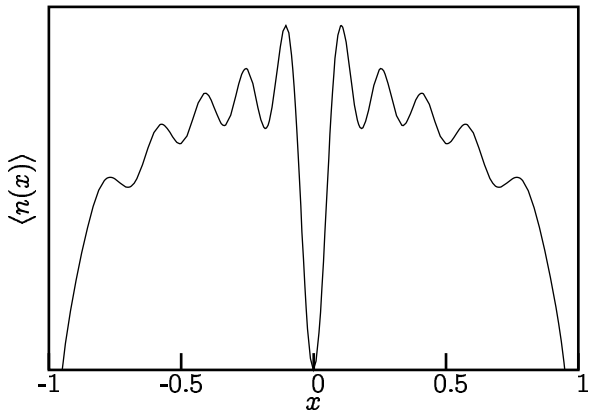

Figure 4.5: Saddle-point approximation of antisymmetric matrices for $N = 11$. The Saddle-point approximation does not capture the δ-function at $x = 0$.

In figure 4.5 the DoS for the antisymmetric ensemble with $N = 11$ is shown. The DoS for the antisymmetric matrices looks rather different for N even and N odd. The reason lies in the fact, that for N odd, there is always one eigenvalue equal to zero.

Due to level repulsion, the DoS is therefore suppressed in the vicinity of $x = 0$. This confirms, that the level repulsion is characterized by $\beta = 2$ for antisymmetric matrices.

As a conclusion of this section we want to stress the fact, that the universality class of a random matrix ensemble does not solely depend on the symmetry-group of its probability distribution. The classification by "Riemannian symmetric spaces" is much more accurate.

Chapter 5

Conclusions

In the mostly technical first part of this thesis we gave an introduction to supersymmetry and saddle-point approximation. We applied these techniques to random matrix theory.

The averaged DoS for five Gaussian Ensembles, namely the GUE, GOE, GSE, Gaussian antisymmetric matrices and class C were calculated exactly for finite N and within a $1/N$-approximation, where N is the dimension of the matrices. The $1/N$-expansion is valid within the whole band. This extends previous work, where the DoS was calculated within $1/N$-expansion in the vicinity of the band-center, $E = 0$. See [12] for an overview. The $1/N$ corrections to the semicircle-behavior of the DoS in the limit $N \to \infty$ diverge right at the band-edge, because there a third order saddle-point gives the relevant contributions.

By inspecting the results of the three classical ensembles, we found a relation between the behavior of the 1-point function (DoS) and the two-point function (level repulsion). More specifically, the DoS consists of a smooth part, and a oscillatory part that varies on the scale of the mean level spacing. The oscillatory part falls off like $1/N^{\alpha}$. This exponent α is related to the exponent β that characterizes the level repulsion by $\alpha = 2/\beta$.

This is a very remarkable result. β is universal quantity that discerns the three classical ensembles. Our analysis reveals, that not only two-level correlations but also the DoS shows characteristic differences between the different ensembles, while the DoS was up to now considered to be a quantity that behaves similarly for all Gaussian ensembles.

The averaged DoS for class C and the antisymmetric ensemble differs from the three classical ensembles in that it is strongly enhanced (antisymmetric, N even) or depleted (class C; antisymmetric, N odd) at $E = 0$. However this deviation from the semicircle DoS carries no statistical weight in the limit $N \to \infty$. In this limit the

semicircle DoS is therefore recovered, although convergence is not uniform as it was in the three classical ensembles. Application of the relation between DoS and level repulsion yields, that the level repulsion is similar to the unitary ensemble. Note, that while the relation between α and β is not applicable right at the band-center where the oscillatory part of the DoS does not vanish, the level repulsion is still the same as in the GUE.

We propose to extend these calculation to random-matrix ensembles with other symmetries, to non-Gaussian ensembles and to disordered systems in general, in order to test the robustness of the relation between the averaged level density and the level repulsion.

Part II

Application of Transfer Matrix Techniques

Chapter 6

Introduction to the Integer Quantum-Hall-Effect and Dirac Fermions

6.1 The Integer Quantum Hall Effect

In 1879 Edward Hall discovered the effect now named after him: In a thin conducting film in a strong magnetic field B, a current I induces a voltage perpendicular to it. This so called Hall voltage is given by $V_H = BI/nec$, where n is the electron density in the conducting film, e is the electron charge and c the velocity of light. It took over 100 years, till 1980 to find a corresponding quantum effect [20], because the integer quantum Hall effect requires semiconducting samples with very high mobilities of about $10^4 - 10^5 cm^2 Vs$ (compared to $35\text{cm}^2/\text{Vs}$ for copper [21]).

In the quantum Hall regime the Hall conductivity does not increase linearly anymore. It shows plateaus instead, see figure 6.1. The Hall conductivity on the plateaus does not depend on the specific sample and is given by $\sigma_H = l\sigma_0$, where $\sigma_0 = e^2/h \approx 25.8k\Omega$ and l is a small integer in the integer quantum Hall effect. For even higher mobilities the fractional Hall effect is observed [24], and l can take special fractional values. In this thesis we will not talk about the fractional effect and subsequently the term quantum Hall effect refers to the integer quantum Hall effect. The most astonishing feature of the quantum Hall effect is, that its universal conductance is constant to about 3×10^{-8}. This is an improvement in comparison to wire-wound resistors, which drift by about 5×10^{-8} per year [23].

Theoretically, several different approaches have been pursued. An extensive overview can be found in [22] and [25]. Here we will only mention the most important results.

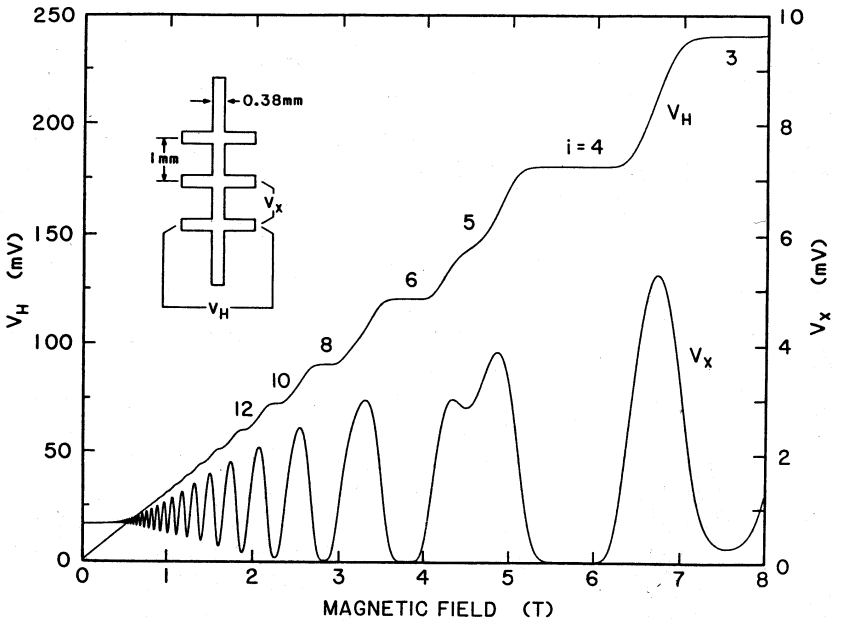

Figure 6.1: Chart recordings of V_H and V_x vs. B for a GaAs-AlGaAs heterostructure cooled to 1.2K. The source-drain current is 25.5μA and $n = 5.6 \times 10^{11}$electrons/cm^2. Taken from [22], see also [23]

Topological arguments have been given by Laughlin [26], Thouless [27] (see also [28]) and others, that the Hall conductivity is quantized, if the states at the Fermi energy are localized. Field theory leads to a nonlinear σ-model with a topological ϑ term [29, 30]. Numerical studies of the of the Hamiltonian projected onto the lowest Landau level [31, 32] give a localization exponent $\nu \approx 2.4$, which is consistent with experimental data [33, 34]. For slowly varying disorder, the quantum Hall effect can be expressed in terms of quantum percolation. Chalker and Coddington found numerically a localization exponent in the same range given above [35]. We will discuss the existence of edge modes within this model in chapter 8. Unfortunately, field theory is not able to reproduce the localization exponent found numerically. The only analytical result that gives a localization exponent in the same range was given by Mil'nikov and Sokolov who consider quantum percolation [36]. However, it is not entirely clear, whether their approach describes percolation correctly, because they employ the approximation, that only a single path dominates the longitudinal conductivity.

Another approach consists in writing down a model that captures the important properties already in the clean limit. Disorder is then added in order to get the correct scaling behavior. Among these models random Dirac fermions [37] are most popular. We will deal with Dirac fermions in the remainder of this work in more detail, and therefore give a more detailed introduction into Dirac fermions in the next section.

6.2 Dirac Fermions as a model for the Quantum Hall Effect

Dirac-fermions were introduced as a model for the IQHE by Ludwig et al. [37]. In their paper, Dirac-fermions are derived as the low-energy sector of a π-flux model with an alternating potential and diagonal hopping in addition to nearest-neighbor hopping.

In the clean limit, the model is given by the Hamiltonian

$$H = \left(-\mathrm{i}\sigma_1\partial_1 - \mathrm{i}\sigma_2\partial_2\right)/2 + m\sigma_3 \,. \tag{6.1}$$

In the continuum limit ∂_i denote the derivatives, while on a square lattice ∂_1 is nearest-neighbor hopping given by $(\partial_1\psi)_{i,j} = \frac{1}{2}\left(\psi_{i+1,j} - \psi_{i-1,j}\right)$ and ∂_2 acts on the second index accordingly. After Fourier-transformation the Hamiltonian on the lattice reads

$$H_{kk'} = \left(\sigma_1 \sin k_1 + \sigma_2 \sin k_2 + m\sigma_3\right)\delta_{kk'} \,. \tag{6.2}$$

The σ_i are the Pauli-matrices. Further on we will also use the symbol σ_0 for the unit-matrix in the Dirac-space.

It turns out, that the lattice model exhibits additional symmetries in comparison to the continuous one. On the lattice, pure Dirac-fermions possess a $SU(2)$-symmetry with the three generators $s_1 = \mathrm{i}\sigma_1 S_2$, $s_2 = \mathrm{i}\sigma_2 S_1$, and $s_3 = \mathrm{i}\sigma_3 S$, where we have introduced the alternating-sign functions S_1, S_2 and $S = S_1 S_2$ on the two-dimensional lattice. S_1 varies along the '1'-direction ($(S_1)_{i,j} = (-1)^i$) and S_2 along the '2'-direction ($(S_2)_{i,j} = (-1)^j$). This $SU(2)$-symmetry splits the lattice into two sublattices, such that the functions on each sublattice belong to the eigenvalue 1 and -1 of s_3 respectively.

Both models also have some symmetries in common. For $m = 0$ the spectrum is symmetric because of $\sigma_3 H \sigma_3 = -H$, and we have time-reversal symmetry: $\sigma_2 H \sigma_2 = H^T$. These two discrete symmetries lead to a particle-hole symmetry $\sigma_1 H \sigma_1 = -H^T$, which is not broken by the mass term in contrast to the both symmetries mentioned before.

Of course there are also the usual spatial symmetries in the clean limit, i. e. rotational (by 90° and translational invariance w.r.t the lattice and parity. Note that rotation and spatial mirroring have to be accompanied by suitable transformations of the Pauli-matrices.

It is possible to break the spatial symmetry without touching the internal symmetry, by considering a real random hopping. Random phase hopping (RPH) also breaks particle-hole and time-reversal symmetry.

It is also common to introduce some local disorder terms. A random potential $E(r)\sigma_0$ breaks the symmetry of the spectrum as well as particle-hole symmetry, but

has no influence on time-reversal and the $SU(2)$-symmetry. A Dirac-mass term $m(r)\sigma_3$ reduces the $SU(2)$ symmetry group to $U(1)$. This $U(1)$ symmetry is not a simple phase-factor, but rather a factor $e^{\mathrm{i}\phi\sigma_3}$. Note, that this reduction of symmetry also occurs for a constant non-zero Dirac-mass. In the clean limit, the transition point $m = 0$ is therefore related to an enhanced symmetry on the lattice, but not in the continuum. We have mentioned before, that the $U(1)$-symmetry divides the system into two subsystems, with two Hamiltonians h and h'. I turns out, that for random mass $h = -h'$ is a tight-binding model with π-flux with a random potential. For random energy, we get two identical copies of the π-flux model ($h = h'$). Therefore random Dirac-mass and random energy are equivalent in the lattice formulation, while they are different in the continuum.

Local chiral disorder $a_1(r)\sigma_1 + a_2(r)\sigma_2$ breaks the $SU(2)$-symmetry completely as well as particle-hole and time-reversal invariance. It still does preserve the symmetry of the spectrum $\sigma_3 H \sigma_3 = -H$. This type of disorder does not exist in the continuum. There, chiral disorder is always a random vector potential. Local chiral disorder however is different from random phases of the hopping elements. We will be discuss this issue in chapter 10.

The continuous symmetry is a major difference between the lattice model and the continuous one. This larger symmetry is accompanied by four nodes of the discrete model in comparison to one node in the continuous model. In fact, the multitude of nodes is a direct consequence of the additional symmetry. The generators s_1 and s_2, which are also symmetry-operators themselves, map the nodes onto each other, because i k-space the alternating-sign S_i can be regarded as a unitary transform that shifts the Brillouin-zone by π in the i-direction.

Up to now, we have not discussed, how Dirac-fermions are related to the Quantum-Hall effect. To this end, we will give a short summary of some of the results given in [37] for the clean limit of the model.

The dispersion is given by

$$E = \pm\sqrt{\sin^2 k_1 + \sin^2 k_2 + m^2}\,. \tag{6.3}$$

Therefore, there exists a gap of width $2m$, which is closed only at the transition-point $m = 0$. The important features of the Hall transition are therefore located at $E = 0$, and we will assume $m = 0$ in the following except where stated otherwise.

Obviously, the longitudinal conductivity σ_{xx} vanishes for $m \neq 0$, and even though the DoS vanishes also for $m = 0$, we have in this case

$$\sigma_{xx} = \frac{e^2}{h}\frac{\pi}{8}\,. \tag{6.4}$$

The Hall-conductivity σ_{xy} is nontrivial, and we have

$$\sigma_{xy} = \frac{e^2}{2h} \operatorname{sgn} m \,. \tag{6.5}$$

We therefore have a behavior that is reminiscent to the quantum Hall transition: At $m = 0$, the Hall conductivity undergoes a jump of e^2/h and the longitudinal conductivity is finite. For $m \neq 0$, σ_{xy} is constant, and σ_{xx} vanishes, as we would expect on the plateaus. The main question now is, whether it is possible to add some disorder, that leads to the scaling behavior of the longitudinal and Hall conductivities that is needed for a correct description of the quantum Hall effect.

In the continuum, a random vector-potential does not localize the state at $E = 0$. However, the DoS vanishes for any nonzero constant mass due to $H^2 = k^2 + m^2$. It does therefore not lead to a scaling behavior of either the longitudinal or the Hall conductivity. A random mass term in the continuum is said to be a marginally irrelevant operator in the continuum due to its relation to the random bond Ising model [38, 39, 40]. On the other hand there exists a proof that random Dirac-mass generates a nonvanishing DoS for the lattice model given in 6.2 [16]. We will discuss this issue in chapter 9

6.3 Outline of the following chapters

In chapter 7 we will present two numerical methods, the iterative Greens function method and transfer matrix method, that are the main tools used in the other chapters. A close inspection of the transfer-matrix method applied to models with bond disorder leads to a proof of delocalization for these systems in the thermodynamic limit. For mesoscopic systems the details are important.

We will use the two methods mentioned above to calculate the DoS for different models with random Dirac mass in chapter 9. We will answer the question in which way these models differ from each other. Additionally we will consider localization properties of one of these models.

In chapter 10 we will consider two models of Dirac-fermions with chiral disorder, random phase hopping (RPH) and local chiral disorder. the DoS of the RPH model is singular for strong disorder at zero energy. However this singularity differs from the one in the continuum model as given in [37]. This model is delocalized at zero energy for all disorder strengths. Local chiral disorder is considered in the strong disorder limit via a hopping expansion. This expansion yields a vanishing DoS at zero energy. Furthermore we consider localization properties of this model via transfer matrix calculations and find that it is localized for all disorder strengths, even though the localization length is

exponentially large. Local chiral disorder and RPH behave therefore quite differently, even though they are both realizations of chiral disorder and thus seem to be related.

In chapter 8 we will reconsider the network model of Chalker and Coddington [35]. This model describes localization properties of the Quantum Hall effect. We find additionally, that it exhibits delocalized edge states that lead to the quantized Hall conductivity.

Chapter 7

Iterative Methods for Correlation Functions

In the subsequent chapters we calculate the DoS and localization length of different disordered systems numerically. One possible method to choose is exact diagonalization. On the other hand we are not interested in the full spectrum and/or all eigenstates, but only in the properties of the system in the vicinity of a fixed energy. It turns out, that iterative methods are more efficient in the cases we are interested in. In order to estimate the benefits, it is quite instructive, to have a look on the numerical effort required for different methods.

Consider a d-dimensional lattice of linear size L in all directions. A diagonalization or matrix inverse is an $\mathcal{O}(n^3)$ process, where n is the dimension of the considered matrix. Therefore the numerical cost of an exact diagonalization is $\mathcal{O}(L^{3d})$. If we are interested in the spectrum only, open boundary conditions result in a banded matrix of width L^{d-1}. The numerical effort to calculate its spectrum scales like L^{3d-1}. If we cut the lattice into slices to calculate the DoS iteratively (this is possible for nearest neighbor hopping), the Volume of each slice is L^{d-1}. We need L iterations and for the DoS, the numerical effort per slice is $\mathcal{O}(L^{3(d-1)})$. Therefore we expect this scheme to scale like $\mathcal{O}(L^{3d-2})$, which is much faster than the exact diagonalization. Additionally, we need storage not for the whole matrix but only for one slice at a time. Therefore we also need much less memory than for exact diagonalization.

In this chapter we will present two methods. The first is the iterative Greens-function method [41], which computes the Greens-function and its therefore suited to compute all correlation functions. The second method is the transfer-matrix technique [42], which is a specialized and very fast way to calculate the localization length of a system.

As an application we will discuss in the last section localization properties of systems with bond disorder only. We prove, that these systems are delocalized at zero

energy in the thermodynamic limit without regard of type and strength of the disorder. If the system is finite in some directions, boundary conditions are important.

7.1 Iterative Greens Function Method

Consider a Hamiltonian on an $N^{d-1} \times L$-lattice with open boundary conditions in L-direction. We want to extend the System to an $N^{d-1} \times (L+1)$-lattice. $\hat{G}^L$ and $\hat{H}^L$ denote the propagator and the Hamiltonian on the lattice of length L. Lower indices denote projection onto the corresponding slice. $\hat{G}^L_{k,l}$ e. g. is the part of the propagator $\hat{G}^L$ that connects slices k and l. Each $\hat{G}^L_{k,l}$ is therefore a matrix of dimension $N^{d-1} \times N^{d-1}$. With the definitions $h^L = \hat{H}^L_{L,L}$ and $t^L = \hat{H}^L_{L,L-1} + \hat{H}^L_{L-1,L}$ we can write

$$\hat{H}^L = \hat{H}^{L-1} + h^L + t^L \,. \tag{7.1}$$

We now use the Dyson-equation to get a recursion-relation for the propagator.

$$\hat{G}^L(z) = (z - \hat{H}^L)^{-1} = \left(z - \hat{H}^{L-1} - h^L - t^L \right)^{-1} \tag{7.2}$$

$$= \hat{G}^{L-1}(z) + \hat{G}^{L-1}(z)(h^L + t^L)\hat{G}^L(z) \tag{7.3}$$

We now show how to write this equation in terms of the $\hat{G}_{k,l}$, which is necessary to get the relevant information in the most simple way. At first, we consider the diagonal element

$$g^L(z) := \hat{G}^L_{L,L}(z) = \frac{1}{z} \left(\mathbb{1} + h^L g^L(z) + t^L_{L,L-1} \hat{G}^L_{L-1,L}(z) \right) \,. \tag{7.4}$$

Now let $k, l = 1, \ldots, L-1$. We have

$$\hat{G}^L_{k,L}(z) = \hat{G}^{L-1}_{k,L-1}(z) t^L_{L-1,L} g^L(z) \,, \qquad \hat{G}^L_{L,k} = g^L(z) t^L_{L,L-1} \hat{G}^{L-1}_{L-1,k}(z) \,, \tag{7.5a}$$

and thus

$$g^L(z) = \left(z - h^L - t^L_{L,L-1} g^{L-1}(z) t^L_{L-1,L} \right)^{-1} \,. \tag{7.5b}$$

Additionally we have

$$\hat{G}^L_{k,l} = \hat{G}^{L-1}_{k,l}(z) + \hat{G}^{L-1}_{k,L-1} t^L_{L-1,L} g^L(z) t^L_{L,L-1} \hat{G}^{L-1}_{L-1,l} \,. \tag{7.5c}$$

These recursion relations enable us to calculate all correlation functions exactly. In the following we will derive the recursion relations for the density of states. Other correlation functions can be computed similarly since they can be written in terms of the Greens-function. We need to calculate

$$\begin{aligned} \operatorname{tr} \hat{G}^L(z) &= \operatorname{tr} \left(g^L(z) + \sum_{k=1}^{L-1} \hat{G}^L_{k,k}(z) \right) \\ &= \operatorname{tr} \hat{G}^{L-1} + \operatorname{tr} g^L(z) \left(1 + t^L_{L,L-1} \sum_{k=1}^{L-1} \hat{G}^{L-1}_{L-1,k}(z) \hat{G}^{L-1}_{k,L-1}(z) t^L_{L-1,L} \right) \,. \end{aligned} \tag{7.6}$$

With help of the definition and recursion relation

$$b^L(z) := \sum_{k=1}^{L} \hat{G}^L_{L,k}(z)\hat{G}^L_{k,L}(z) = g^L(z)\left(\mathbb{1} + t^L_{L,L-1}b^{L-1}(z)t^L_{L-1,L}\right) g^L(z) \tag{7.7a}$$

this leads to

$$\rho(z) = \frac{1}{\pi V}\,\mathrm{Im}\,\mathrm{tr}\sum_L g^L(z)\left(1 + t^L_{L,L-1}b^{L-1}(z)t^L_{L-1,L}\right)\ . \tag{7.7b}$$

Due to the definition of the Greens-function, the recursion has the starting point $g^0 = b^0 = 0$. It is computationally much cheaper to sum up (7.7) than to do a full diagonalization, as the matrices involved are much smaller. If we want to calculate the DoS in a whole energy range, it may still be better to do full diagonalization though, because the iterative method works only for a fixed energy.

7.2 The transfer matrix method

Now we want to discuss how to calculate the localization length for a very long bar or strip efficiently. Within this section we assume periodic lateral boundary conditions to avoid boundary-effects like edge-states. The cross section of the bar is a (d-1)-dimensional cube of linear size N.

The localization length ξ is then given by

$$\frac{1}{\xi} = -\lim_{|r-r'|\to\infty} \frac{\langle \ln |G_{r,r'}| \rangle}{|r-r'|}\ , \tag{7.8}$$

where $G_{r,r'}$ is the matrix-element of the propagator that connects sites r and r'. The transfer-matrix method however yields

$$\frac{1}{\xi'} = -\lim_{L\to\infty} \frac{\langle \ln \|\hat{G}_{0,L}\|^2 \rangle}{2L}\ , \tag{7.9}$$

where $\|\bullet\|^2$ denotes the matrix scalar-product $\|M\|^2 = \mathrm{tr}\, MM^\dagger$ and $G_{L,L'}$ connects slices L and L' of the bar. For very long strips or bars ($L \gg \xi$) these two definitions are in fact equivalent. To see this, we assume that r lies on the zeroth slice and r' on the Lth one, so that $G_{r,r'}$ is just a matrix element of $\hat{G}_{0,L}$. Now ξ' is bounded by ξ from above, because

$$-\frac{\langle \ln \|\hat{G}_{0,L}\|^2 \rangle}{2L} = -\frac{\ln \sum_{r,r'} |G_{r,r'}|^2}{2L} \geq -\frac{\langle \ln |G_{r,r'}| \rangle}{|r-r'|}\ . \tag{7.10}$$

for any r, r' on the corresponding slices (note that both sides are positive for $L \gg \xi$). On the other hand ξ' is bounded by ξ from below, because for large bar-lengths the sum $\|\hat{G}_{0,L}\|^2 = \sum_{r,r'} |G_{r,r'}|^2$ is dominated by pairs r, r' where r and r' are almost aligned in the direction of the bar. For fixed r, the diameter D of the relevant region is given by $(\sqrt{L^2 + D^2} - L)/\xi = \text{const}$ or $D \propto \sqrt{\xi L}$. Therefore we have $\|\hat{G}_{0,L}\|^2 \propto |G_{r,r'}|^2 (N\sqrt{\xi L})^{d-1}$ and

$$-\frac{\langle \ln \|\hat{G}_{0,L}\|^2 \rangle}{2L} \leq -\frac{\langle \ln |G_{r,r'}| \rangle}{|r - r'|} + \frac{d-1}{2L} \ln\left(N\sqrt{\xi L}\right) + \frac{c}{L}\,, \tag{7.11}$$

for some constant c and if r and r' are aligned exactly in the direction of the bar. In the limit $L \to \infty$ it follows that $\xi' = \xi$. Subsequently we will omit the averaging over disorder, because the localization length is a self-averaging quantity (see below).

Now it is in principle possible, to evaluate

$$\frac{1}{\xi} = \lim_{L\to\infty} \frac{1}{2L} \ln \left\| \hat{G}^L_{0,L}(z) \right\|^2 \tag{7.12}$$

with the iterative Green's-function method. To do this, we need a matrix inversion and a matrix-product in each step of the recursion. On the other hand, the transfer-matrix method [42] needs a matrix inversion less often and is therefore numerically advantageous. This makes it one of the main methods for numerical studies of localization [43].

To derive it, we start with the definition of the propagator, $(z-H)G = \mathbb{1}$, projected onto slices l and l'. In a notation slightly different from that in the last section, this reads

$$z G_{l,l'} - t_{l+1} G_{l+1,l'} - t_l^\dagger G_{l-1,l'} - h_l G_{l,l'} = \delta_{l,l'} \tag{7.13}$$

This equation can be viewed as a recursion relation, which is best written in matrix form

$$\begin{aligned} \begin{pmatrix} t_0^{-1} t_{l+1} G_{l+1,l'} \\ G_{l,l'} \end{pmatrix} &= \begin{pmatrix} (z - h_l)\, t_l^{-1} & -t_0^{-1} t_l^\dagger \\ t_0 t_l^{-1} & 0 \end{pmatrix} \begin{pmatrix} t_0^{-1} t_l G_{l,l'} \\ G_{l-1,l'} \end{pmatrix} - \begin{pmatrix} t_0^{-1} \delta_{l,l'} \\ 0 \end{pmatrix} \\ &=: \hat{T}_l \begin{pmatrix} t_0^{-1} t_l G_{l,l'} \\ G_{l-1,l'} \end{pmatrix} - \begin{pmatrix} t_0^{-1} \delta_{l,l'} \\ 0 \end{pmatrix} . \end{aligned} \tag{7.14}$$

$\hat{T}_l$ is called the transfer matrix, because it transfers the system one lattice distance along the bar. t_0 is introduced as an arbitrary but fixed energy scale in order to make the transfer matrix dimensionless. Of course, the localization properties are independent of t_0. As we are interested in the nondiagonal part of the Greens function only ($l \neq l'$), the transfer $\hat{T}$ matrix contains all relevant information about localization

properties. This holds despite the fact that the transfer-matrix method is not capable of reproducing the full propagator (and calculating, say, the DoS), because it is hard to account for boundary conditions at the end of the bar and at $l = l'$ within this method.

The matrix $\Lambda_L = \sqrt[2L]{\hat{T}_1^\dagger \cdot \ldots \cdot \hat{T}_L^\dagger \cdot \hat{T}_L \cdot \ldots \cdot \hat{T}_1}$ obeys the multiplicative ergodic theorem of Oseledec [44], which states, that there exists a limiting matrix

$$\Lambda = \lim_{L \to \infty} \Lambda_L \tag{7.15}$$

which is unique for almost all realizations of the disorder. The eigenvalues of $\ln \Lambda$ are called Lyapunov-exponents. They determine length-scales, on which the corresponding components of the propagator decay exponentially. The largest of these length-scales is the localization length. In order to find the localization-length, we therefore need to calculate the Lyapunov-exponent with the smallest absolute value. We have already stated that the localization length is self-averaging. This follows from the fact that Λ is independent of the realization of disorder.

Notice, that we can not calculate the localization length numerically by directly evaluating (7.15) due to rounding errors. These rounding-errors however can be circumvented by repeated reorthogonalization of the matrix $\mathcal{T}_L = \hat{T}_L \cdot \ldots \cdot \hat{T}_1$ by means of a so called QR-decomposition [17]. The QR-decomposition is a factorization into a unitary matrix Q and a upper triagonal matrix R. This factorization is numerically advantageous, because the product of two upper tridiagonal matrices is again tridiagonal, and the diagonal elements of the product are given by the product of the diagonal elements of the two factors. The logarithms of the diagonal elements determine the Lyapunov exponents, because the eigenvalues of $\mathcal{T}_L$ are distinct by orders of magnitude [47]. As we calculate only matrix factorizations rather than matrix inverses, we can directly set $z = E - \mathrm{i}\varepsilon$ onto the real axis and need not to be careful about taking this limit.

The transfer matrix possesses a special symmetry, namely

$$\tau_2 \hat{T}_l^\dagger \tau_2 = \hat{T}_l^{-1} \,, \tag{7.16}$$

with the Pauli-matrix τ_2 in the 2×2-space introduced by the construction of the transfer-matrix. This relation means, that the Lyapunov-exponents appear in pairs, where one exponent is the negative of the other. Note, that this situation covers both, a random potential as well as a random hopping.

How can we understand the pairing of the Lyapunov-exponents? Assume that the bar extends infinitely, so that we do not need to consider the boundary conditions at both ends of the bar. The propagator then decays for large $|l - l'|$. However l' does

not enter (7.14) as long as $l \neq l'$. Thus the recursion does not distinguish whether $l < l'$ and the propagator increases, or $l > l'$ and the propagator decreases. Therefore both Lyapunov exponents appear in the transfer matrix. This reflects the fact that the system does essentially not change if we rotate the bar by 180° and consider the application of the transfer-matrix in the opposite direction.

In addition to the localization length the whole set of Lyapunov exponents allows us to calculate the conductivity of a finite system. The conductivity of a strip of length L is given by the transmission matrix [45, 46] and reads

$$\sigma = 4\frac{e^2}{h}\,\mathrm{tr}(\Lambda_L^L + \Lambda_L^{-L})^{-2}\,. \tag{7.17}$$

For completeness we should mention, that in the literature the transfer-matrix method is usually introduced in terms of a recursion relation for the wave-function

$$\begin{pmatrix} t_0^{-1} t_{l+1}\psi_{l+1} \\ \psi_l \end{pmatrix} = \hat{T}_l \begin{pmatrix} t_0^{-1} t_l \psi_l \\ \psi_{l-1} \end{pmatrix}\,. \tag{7.18}$$

Of course the two approaches are equivalent, because they contain the same transfer-matrix. We will use the latter approach subsequently, because it its somewhat easier to grasp.

7.3 Bond Disordered Systems at zero Energy

One parameter scaling for localization [48] predicts, that noninteracting disordered systems are alway localized in one dimension. Two dimensions is the marginal case, but localization is there encountered usually as well , with the exception of the quantum Hall effect and systems with strong spin-orbit interaction [49].

As a further exception it has long been known, that in one dimension the Anderson-model with bond-disorder is delocalized at zero energy [52]. In two dimensions, the same behavior was found numerically [53, 54, 50, 51], and analytically for weak disorder [55, 56]. In three dimensions the Anderson model with bond disorder is known to be delocalized at zero energy for all disorder strengths [57]. In this section we will prove, that bond disordered systems are delocalized at zero energy in any dimension irrespectively of type and strength of the disorder. The result holds also in the presence of a magnetic field. In bars with finite cross-section the boundaries are important and odd/even-effects occur.

More precisely, we will show, that there is a Lyapunov-exponent equal to zero under certain conditions. Using (7.17) this leads to a nonvanishing conductivity through such systems. Unfortunately we can no tell whether the system is truly metallic (which

means that $\sigma(L) \to \infty$ for the conductivity σ of a d-dimensional system of size L^d and large L) or whether it is critical, in which case we have $\sigma(L) \to$ const. This can only be established by knowledge of *all* Lyapunov-exponents. We are free however to chose a suitable kind of periodic boundary conditions (for details see below) lateral to the bar that eliminate these boundaries. Therefore the system is definitely delocalized in the bulk and not only at the boundary.

Our result is somewhat similar to directed localization introduced by Barnes et al. [58]. In both cases the transmission through a disordered quasi 1-dimensional system does not decay exponentially. However the systems considered are different. Barnes et al. consider a model of N modes propagating in one direction and M modes propagating in the opposite direction. Transmission remains finite in the direction where the number of modes is higher. Within this model we still consider the case $N = M$, which is not covered by their result.

Before we start with our proof for the general case, let us have a look at the one-dimensional case. The one-dimensional bond-disordered Hamiltonian is given by

$$\hat{H} = \sum_l t_{l+1} c_l^\dagger c_{l+1} + h.c.\,, \tag{7.19}$$

where t_l is a random variable for which we do not specify the disorder distribution. At zero energy the Schrödinger-equation reads

$$t_{l+1}\psi_{l+1} = t_l^* \psi_{l-1}\,, \tag{7.20}$$

which leads to a recursion relation for the ψ_l. The inverse localization-length is then given by

$$\frac{1}{\xi} = \lim_{L\to\infty} \frac{1}{2L} \ln \left| \frac{\psi_{2L}}{\psi_1} \right| = \lim_{L\to\infty} \frac{1}{2L} \sum_{l=0}^{L-1} \ln \left| \frac{t_{2l}}{t_{2l+1}} \right| = 0 \tag{7.21}$$

Now we consider a bond disordered system with nearest-neighbor hopping on a square lattice in d dimensions. We will find, that such a system is delocalized at zero energy.

The sketch of the proof is as follows: Most systems are isotropic in the sense that it does not matter, whether the transfer-matrix proceeds to the right or to the left. On the other hand, the Lyapunov-exponents change their sign under reversal of direction. Therefore the Lyapunov exponents appear in pairs λ, $-\lambda$. We have already discussed this issue for a special class of systems in equation (7.16). If we construct a transfer-matrix with odd dimension, one Lyapunov-exponent must be zero. It is obvious, that this construction is not feasible within the formalism presented in the last section, because there the transfer-matrix has even dimension, no matter which Hamiltonian

we consider. In one dimension this problem did not occur because the Hamiltonian had no local terms.

As a first step, we rewrite the Hamiltonian in such a way, that the Schrödinger-equation can be written as $\hat{T}_{l+1}\psi_{l+1} = \hat{T}_l^\dagger \psi_{l-1}$ similar to the one-dimensional case. But now ψ_l is a vector, the wave function on the slice given by constant l, and $\hat{T}_l$ some hopping-matrix. This goal can be accomplished, by introducing nonorthogonal lattice-vectors as indicated in figure 7.1. We assume that the lattice is infinite in the $\hat{e}_l$-direction and finite in the remaining directions. The Hamiltonian is now indeed given by

$$\hat{H} = \sum_l (\hat{T}_l + \hat{T}_l^\dagger)\,, \tag{7.22}$$

where $\hat{T}_l$ are the hopping matrices and $\hat{T}_l$ connects the slices l and $l+1$. We assume, that the probability distribution for the $\hat{T}_l$ is the same for all l, which is mandated by homogeneity. The Schrödinger-equation for $E = 0$ on the lth slice is then given by

$$0 = (\hat{H}\psi)_l = \hat{T}_l \psi_{l+1} + \hat{T}_{l-1}^\dagger \psi_{l-1}\,. \tag{7.23}$$

This Schrödinger-equation leads to the iteration $\psi_{l+1} = \hat{T}_l^{-1}\hat{T}_{l-1}^\dagger \psi_{l-1}$. Now consider $\mathcal{T}_L = \hat{T}_{2L}^{-1}\hat{T}_{2L-1}^\dagger \cdot \ldots \cdot \hat{T}_2^{-1}\hat{T}_1^\dagger$ and $\Lambda = \lim_{L\to\infty} \sqrt[4L]{\mathcal{T}_L^\dagger \mathcal{T}_L}$. Again, this limit exists due to the multiplicative ergodic theorem of Oseledec [44].

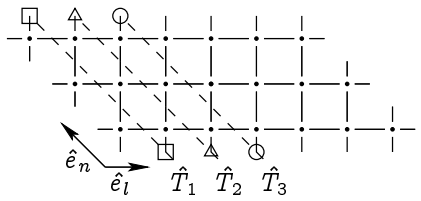

Figure 7.1: Sketch of the lattice employed in the proof of delocalization. The indices i and j are incremented along the directions indicated by the arrows. The transfer-matrix T transfers the system along the direction of $\hat{e}_i$. The symbols at the top and at the bottom of the strip indicate the helical boundary conditions mentioned in the text.

If we traverse the system in the opposite direction, $\mathcal{T}_L$ gets replaced by $\mathcal{T}_L^{-1}$. Furthermore we apply a rotation around the l-axis. This rotation essentially maps $\hat{T} \to \hat{T}^T$. To understand this, we have to take a look at the structure of $\hat{T}$ (see figure 7.2). In our notation, the rotation matrix R rotates $\hat{T}$ by 180°, which is equivalent to $\hat{T}^T$ up to a measure conserving change of the random entries of $\hat{T}$. Using the definition of $\mathcal{T}_L$ and Λ and the multiplicative ergodic theorem, we have therefore

$$R\Lambda^T R = \Lambda'^{-1}\,, \tag{7.24}$$

where

$$\Lambda' = \lim_{L\to\infty} \sqrt[4L]{\mathcal{T}_L \mathcal{T}_L^\dagger}\,. \tag{7.25}$$

Note, that $\mathcal{T}_L^\dagger \mathcal{T}_L$ and $\mathcal{T}_L \mathcal{T}_L^\dagger$ possess the same eigenvalues including degeneracies[1] and therefore Λ, Λ^T and Λ' also have the same eigenvalues.

Figure 7.2: Structure of $\hat{T}$ and R in two dimensions. The lines and dots denote nonzero entries. The nonzero entries of R are equal to 1.

It follows, that the eigenvalues of Λ and Λ^{-1} are the same including the number of degeneracies. Therefore the Lyapunov-Exponents appear in pairs λ, $-\lambda$. But in contrast to the general case of the transfer-matrix, $\hat{T}$ is not restricted to be of even dimension. Due to the pairing of eigenvalues, if $\hat{T}$ has odd dimension, there must be one Lyapunov-exponent equal to zero, so that the system is delocalized. The hopping-matrix has odd dimension if the bar considered has a cross-section with an odd number of sites. This gives rise to an odd/even effect: The system is delocalized for odd cross-sections but not for even ones. When the cross-section tends to infinity, we expect the localization-length to diverge in the case of even cross-section, so that the localization-length is unique and infinite in this limit.

In figure 7.2 we have indicated periodic boundary conditions for $\hat{T}$ by the dot in the lower left corner. These boundary-conditions correspond to so called helical boundary-conditions for the lattice Hamiltonian. The helical boundary conditions are indicated in figure 7.1 by the different links at the upper and lower edges of the strip. They are periodic w.r.t. the nonorthogonal lattice-vectors and thus connect two neighboring slices of the lattice. This choice of boundary conditions removes the boundary in the transversal direction and thus avoids edge-states at the boundary of the bar, which would correspond to a vanishing Lyapunov-exponent, even though the system is localized in the bulk. These edge-states do indeed occur in systems describing the quantum-Hall effect, as we will see in chapter 8. Of course, these arguments also hold in the presence of a uniform or random magnetic field.

[1] This in turn holds, because for some square matrix M the eigenvalues $MM^\dagger$ are the squares of the singular values of M. See e. g. [17].

Special attention deserve systems with spin-orbit coupling without magnetic field. In this case, the dimension of the transfer-matrix is doubled and we would therefore expect, that this system shows localization within our framework. However, as the Hamiltonian and the transfer-matrix are expressed in terms of quaternion matrices[2] in this case, all Lyapunov exponents are doubly degenerate and the system shows delocalization. In contrast to spinless particles however, a magnetic field adds a local term and breaks the symplectic structure. Thus it may lead to localization.

Our proof relied crucially on the fact, that all hopping elements are subject to the same probability distribution. Consider e. g. a one-dimensional system, where the hopping-amplitude is alternating along the system with real values t_1 and t_2. Then we have $\psi_{l+1} = t_1/t_2\psi_{l-1}$ for l even and $\psi_{l+1} = t_2/t_1\psi_{l-1}$ for l odd and therefore we get finite Lyapunov-exponents[3]. Generally speaking, if the probability distribution of $\hat{T}_l^{-1}\hat{T}_{l-1}^{\dagger}$ and $\hat{T}_{l+1}^{-1}\hat{T}_l^{\dagger}$ are different for fixed l, we possibly end up with two different matrices Λ_1 and Λ_2 depending on whether we started with l even or odd. Λ_1 and Λ_2 are then related by $\Lambda_1 = \Lambda_2^{-1}$ and we can draw no conclusions about the Lyapunov-exponents on such a general level.

[2] I.e. matrices of the form $\left(\begin{smallmatrix} a & b^* \\ -b & a^* \end{smallmatrix}\right)$.

[3] In this case we could state this fact also in a different manner: There is no state at $E = 0$ and we get a tunneling-like exponential decay

Chapter 8

The Network Model of Chalker and Coddington

8.1 Introduction to the Model

Introduced by Chalker and Coddington in 1988 [35], this model describes electrons in a random potential in the presence of a strong magnetic field. The random potential is varying on a length-scale much larger than the magnetic length.

In this limit, the motion of the electrons can be split into two components, that take place on very different time scales. On the fast time scale, the electrons move on cyclotron orbits. On the slow time scale, the guiding center of these cyclotron orbits moves along equipotential lines of the random potential.

This setting allows a nice illustration of the system: Consider a landscape that is filled with water. The water-level describes the Fermi-energy. The coastline is most important in this illustration, because it describes the currents flowing in the system. Due to the magnetic field, the direction of the currents is determined by the slope of the landscape: All currents are flowing in such a way, that the water is always on one side, say to the right of the current, and the dry land is always to the left. Of course, if we reverse the magnetic field, all currents also change direction.

Below the transition most of the landscape is dry and there are only some lakes within it. Beyond the transition, most of the landscape is filled with water, only some islands remain. In both cases all coastlines have a finite length. Right at the transition, there are neither islands nor lakes, but the coastline extends throughout the system. The Chalker-Coddington model is therefore often referred to as the percolation picture of the IQHE.

Quantum mechanically the currents are described by a complex variable $\psi(x)$, where $|\psi(x)|^2 = I(x)$ determines the current. The quantum-Hall system is described

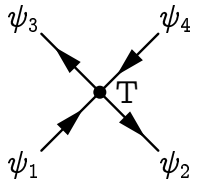

Figure 8.1: Sketch of a node of the network-model. The arrows denote the direction of the currents.

as a network of currents, where the nodes of the network are related to the saddle-points of the potential. We describe one node by a matrix T hat connects the incoming and the outgoing currents, $\binom{\psi_3}{\psi_4} = T \binom{\psi_1}{\psi_2}$. See figure 8.1 for an illustration. Current-conservation at the nodes requires $|\psi_1|^2 + |\psi_4|^2 = |\psi_2|^2 + |\psi_3|^2$. In terms of the vectors $\vec{v} = \binom{\psi_1}{\psi_2}$ and $\vec{w} = \binom{\psi_3}{\psi_4}$ current conservation requires

$$0 = \langle \vec{v}, \sigma_3 \vec{v} \rangle - \langle \vec{w}, \sigma_3 \vec{w} \rangle = \langle \vec{v}, \sigma_3 (\mathbb{1} - \sigma_3 T^\dagger \sigma_3 T) \vec{v} \rangle \,. \tag{8.1}$$

Current conservation therefore translates to the condition $\sigma_3 T^\dagger \sigma_3 = T^{-1}$ on T. Shifting all phases onto the bonds restricts T to

$$T = \begin{pmatrix} \cosh\gamma & \sinh\gamma \\ \sinh\gamma & \cosh\gamma \end{pmatrix} \,. \tag{8.2}$$

For very large and very small values of $\sinh\gamma$, the currents behave classically. For $\sinh\gamma \ll 1$, the currents flow from bond 1 to bond 3 and from bond 4 to bond 2. For $\sinh\gamma \gg 1$, the currents flow from bond 1 to bond 2 and from bond 4 to bond 3. for values of $\sinh\gamma$ about 1, tunneling occurs, and the currents are allowed to take either way.

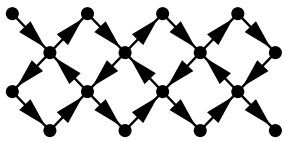

Figure 8.2: Square lattice of the Chalker-Coddington model. The arrows denote the direction of the current on the bond.

If the saddle-points of the potential are all of second order, the currents flow on a square lattice, where the flux through each plaquette is random, because the plaquettes cover different areas. Therefore the currents acquire a random Peierl's phase on the bonds. On such a lattice, there exist two kinds of nodes, which are rotated by 90° relative to each other (see figure 8.2). Rotation by 90 degrees changes $T(\gamma)$ to $T'(\gamma) = T(\gamma')$, where $\sinh\gamma \sinh\gamma' = 1$.

The Chalker-Coddington model is constructed in a way suitable for a transfer-matrix calculation, because the matrices T and T' are already transfer-matrices. In the paper of Chalker and Coddington, γ was taken as a fixed value on all nodes. It is however possible, to consider the situation, where γ is some randomly distributed variable [59]. In both cases delocalization was found at $\sinh\gamma = 1$ with a localization exponent of $\nu \approx 2.4$ (see also [60, 61].

8.2 Edge States in the Chalker-Coddington Model

In this section we want to apply the ideas about delocalization introduced in chapter 7 to the Chalker-Coddington model. Here we do not only have one transfer-matrix, but rather several ones, namely $T(\gamma)$, $T'(\gamma)$, which are block diagonal. The 2×2-blocks of T and T' are shifted by a lattice constant relative to each other. Additionally, there are and random phases $\mathrm{e}^{\mathrm{i}\hat{\phi}}$ in between, where $\hat{\phi}_{ij} = \delta_{ij}\phi_i$ is a diagonal matrix. The transfer matrix which transfers the system by two lattice constants is thus given by $T_l = T_l \mathrm{e}^{\phi_{1,l}} T'_l \mathrm{e}^{\phi_{2,l}}$. We consider now $\mathcal{T}_L = T_l T_{l-1} \dots T_1$ and $\Lambda = \lim_{L\to\infty}(\mathcal{T}_L^\dagger \mathcal{T}_L)^{1/2L}$. Due to $\sigma_3 T^\dagger \sigma_3 = T^{-1}$, we have also $S\mathcal{T}_n^\dagger S = \mathcal{T}_n^{-1}$, where S is an alternating sign, $S_{ij} = (-1)^i \delta_{ij}$. This feature leads to $S\Lambda S = \Lambda^{-1}$. Therefore all Lyapunov-exponent appear in pairs. If T has odd dimension, it follows, that there is one exponent exactly zero. Unlike the delocalization theorem of the last chapter, this result is a special case of the quantum railroad model developed by Barnes et al.[58], which also predicts delocalization. A suitable lattice with an odd-dimension transfer matrix is shown in figure 8.3.

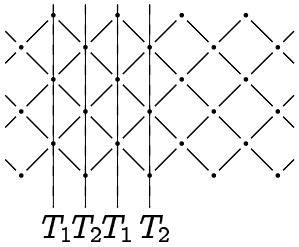

Figure 8.3: Lattice for the Chalker-Coddington Model with edge states. In each column there are five bonds.

In contrast to this reasoning the Chalker-Coddington is known to be localized for $\sinh\gamma \neq 1$ if we apply periodic boundary conditions. In this case however, we have an even number of bonds. We therefore conclude, that the Chalker-Coddington model with odd bond-number exhibits an edge state. As the model is invariant under a change

of $\sinh\gamma \to 1/\sinh\gamma$ and simultaneous rotation by 180 degrees, the edge state changes its position from the left to the right side (or vice versa), at the transition.

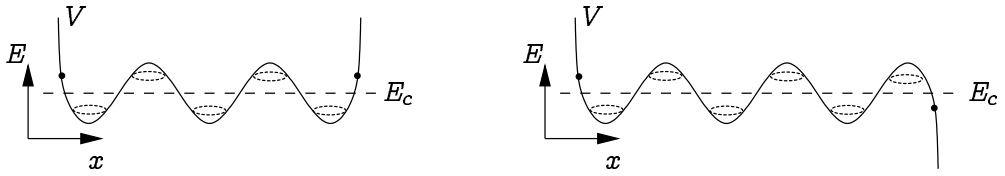

Figure 8.4: Cross-section of a potential that belongs to the Chalker-Coddington model with an even/odd number of bonds. The dashed line denotes the critical Fermi-energy. The ellipses denote the circular currents, that flow below and beyond the transition. Additionally there may be a non-circular current at the edges of the system. These are denoted by black dots.

Before we proceed further let us discuss the physical interpretation of the edge states in more detail. Usually, one expects to have an edge state, that exists only on one side of the Hall-transition and surrounds the whole system. This is not the case with an odd number of bonds, because there an edge states exists on both sides of the transition, and it is located only on one edge of the system. In figure 8.4 potentials that lead to an even and odd number of bonds are sketched. The physical realization of the QHE in FETs corresponds to the even bond-number situation. We do however claim, that the interpretation remains the same in the odd bond-number case, because the electrons are only allowed to move on equipotential lines due to the strong magnetic field.

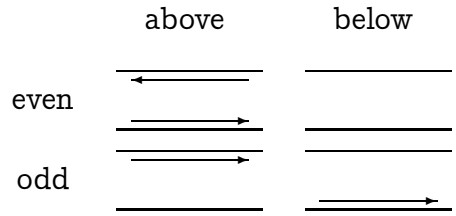

Figure 8.5: A view on the edge-currents of the even/odd bond-number models on both sides of the Hall-transition.

The two situations differ slightly concerning the edge currents. In the even bond-number situation, the edge currents have opposite direction, because the potential has an opposite slope on both sides of the Hall bar. In contrast, in the odd bond-number situation, both edge currents flow in the same direction, see figure 8.5. The jump in the Hall-current at the transition however is the same in both situations.

Of course, these edge-states must also exist in the even-bond number situation on one side of the transition. Based on a remark by Chalker and Coddington [35], we

expect them however not to have a Lyapunov-exponent $\lambda = 0$. Rather, their Lyapunov-exponent should be exponentially small, when the strip-width increases.

We want to confirm the arguments given above numerically, by looking at the corresponding current distribution, which is given by the modulus squared of the orthogonal state-vectors, that appear in the transfer-matrix calculation.

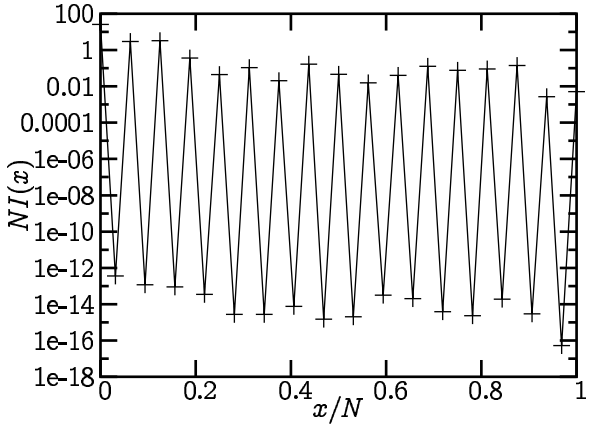

Figure 8.6: Current distribution perpendicular to the bar at a randomly chosen column. The current vanishes on every second bond up to numerical accuracy.

In figure 8.6 a current distribution on a randomly chosen column is shown. The current distribution has the striking feature, that the current is zero up to numerical precision on every second bond. This stems from the fact, that $S\Lambda S = \Lambda^{-1}$. Two current distributions ψ_λ and $\psi_{-\lambda}$ related to the Lyapunov exponents λ and $-\lambda$ respectively are therefore related by $\psi_{-\lambda} = S\psi_\lambda$. In our case, where $\lambda = 0$ and we have no degeneracy for $\lambda = 0$, this relation requires, that ψ is an eigenstate of S: $\psi = \pm S\psi$. Therefore the current vanishes on every second bond.

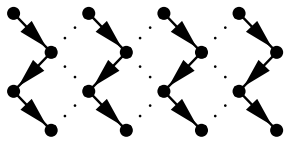

Figure 8.7: Sketch of the current distribution of the $\lambda = 0$ state. The currents vanish on every second site and therefore all currents flow in one direction. The corresponding state is highly anisotropic.

A closer look on figure 8.2 reveals, that this condition is equivalent to the property, that all currents on the lattice flow in one direction, which is depicted in figure 8.7. In contrast, the sum of all currents (including direction of the current) is zero for states with non-vanishing Lyapunov-exponent due to current-conservation. In subsequent

figures showing the current distribution of the edge states, we will omit the bonds with vanishing current.

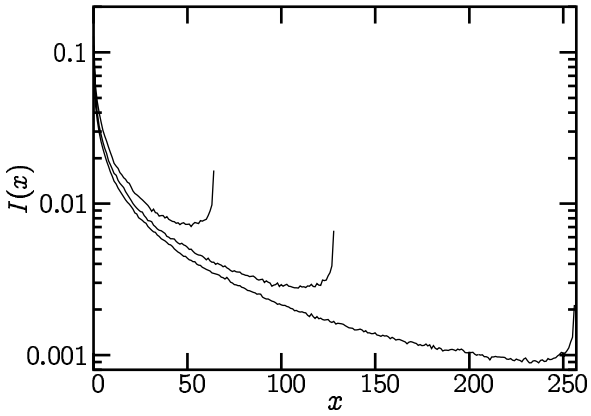

Figure 8.8: Averaged current density for $\sinh\gamma = 0.9$ for 65, 129 and 257 bonds with nonvanishing current.

In figure 8.8 we show the averaged current density of the edge state for $\sinh\gamma = 0.9$. It decreases strongly within the strip. The state extends throughout the system right at the transition, which is shown in figure 8.9. However, the current is still zero on every second bond. The state is therefore highly anisotropic, and does not contribute to the longitudinal conductivity. In contrast, the state with the smallest nonzero Lyapunov exponent is nonzero on each bond, see figure 8.10. Here the net current is zero, as we did expect. Upon switching on an electrical field, this state contributes to the longitudinal conductivity.

This highly anisotropic bulk-mode is a peculiarity of the odd bond-number situation. We have already stated, that for an even bond-number, the edge-states are not related to a vanishing Lyapunov exponent. We expect therefore to get a superposition of the two edge-states at the left and the right edge. Right at the transition, these states do support a nonvanishing current on all bonds and are no longer related to the Hall-conductivity.

We want to stress the fact, that the edge-states do exist even if γ is chosen randomly, or if the distribution of the phases is changed in any way. We would therefore propose to study a somewhat different model, where the phases are kept constant but nonzero and disorder is introduced via a varying γ. This is more along the lines of the model discussed in [62].

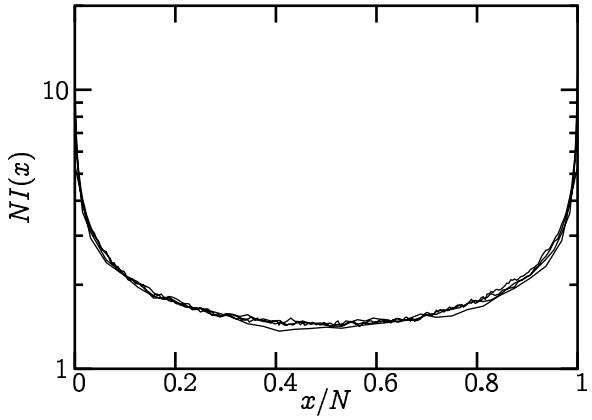

Figure 8.9: Averaged current density at the transition ($\sinh\gamma = 1$ for 65, 129, 257 and 513 bonds. The current density does not change with increasing bond number and is therefore approximately constant in the bulk of the system.

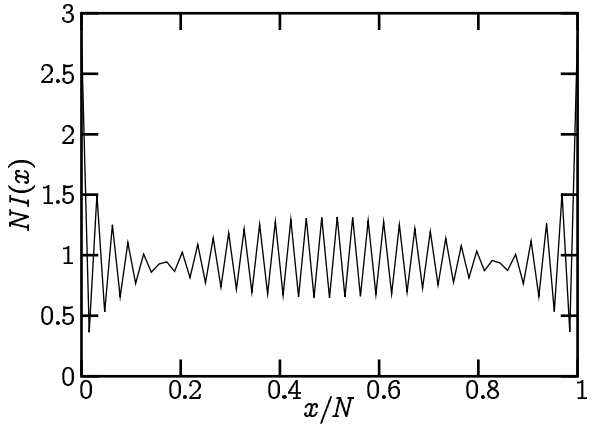

Figure 8.10: Averaged current density for the most extended bulk-state at the transition ($\sinh\gamma = 1$) and for a strip-width of $N = 65$. The current density is nonzero on all bonds. The total current is zero. This state is delocalized in the sense, that $\xi_N \approx 2.5N$.

Chapter 9

Dirac Fermions with Random Mass

Whether or not the random Dirac-mass model is relevant for the IQHE has been under discussion in the community. More specifically, it has been debated, whether the DoS is nonzero at the transition point $M = 0$. In renormalization-group calculations, random Dirac-mass is a marginally irrelevant operator [37, 63] and thus the DoS should vanish. On the other hand it has been proven, that the DoS is strictly positive [64].

In this chapter we want to shed some light onto this issue. At first we notice, that actually several different models were studied in the literature. In the paper of Ludwig et al. [37], a continuous model with only one node is considered, whereas Ziegler discusses a lattice model with nearest-neighbor hopping only, which has four nodes. Our approach in this chapter is similar to that of Hirschfeld [65]. However we think that it is important to consider varying system sizes to capture scaling behavior.

First, we will discuss a N-orbital model and consider the limit of large-N. This has been done in great detail with supersymmetry by Ziegler [66]. For our purposes, it is sufficient and more illuminating to discuss this issue diagrammatically. We will then augment these results with numerical calculations. These will be done for several realizations of Dirac-fermions with 4, 2 an one node and with and without the $SU(1)$-symmetry mentioned in the introduction to the model.

9.1 Perturbation Theory for the DoS

A common approach to disordered systems is the self-consistent Born-approximation. This approximation becomes exact for infinitely many flavors of Dirac-fermions, that are coupled randomly by the disorder. When using supersymmetric methods, this so called $N \to \infty$-limit is somewhat similar to the $N \to \infty$-limit for random matrices. In this limit, it is possible to apply a saddle-point approximation to calculate a $1/N$-expansion. In the limit $N \to \infty$, only the noncrossing diagrams contribute to the DoS.

In this section, we want to show, that it is not sufficient to consider the large N-limit to distinguish between different number of nodes and different types of disorder. In this limit, the Greens-function is given by

$$G_k = G_k^0 + G_k^0 \Sigma_k G_k \tag{9.1a}$$

with

$$\Sigma_k = \frac{1}{2V} \sum_{k'} \langle V_{k-k'} \sigma G_{k'} \sigma V_{k'-k} \rangle \ . \tag{9.1b}$$

V_k is uncorrelated Gaussian disorder, i.e. $\langle V_k \rangle = 0$, $\langle V_k V_{-k'} \rangle = g\delta_{kk'}$. G_k^0 is the unperturbed and G_k the self-consistent Greens-function and σ is either σ_0 (random potential) or σ_3 (random Dirac-mass). the ansatz $G_k^{12} = -G_{-k}^{12}$ and hence

$$\sum_k G_k = \begin{pmatrix} \rho_1 & 0 \\ 0 & \rho_2 \end{pmatrix} \tag{9.2}$$

does not distinguish between these two kinds of disorder and leads to the solution

$$G_k = \frac{1}{(\varepsilon + g\rho_1)(\varepsilon + g\rho_2) + \kappa\overline{\kappa}} \begin{pmatrix} \mathrm{i}(\varepsilon + g\rho_2) & \overline{\kappa} \\ \kappa & \mathrm{i}(\varepsilon + g\rho_1) \end{pmatrix} \tag{9.3}$$

for both, random energy and random Dirac-mass. We denote the k-dependent terms by $\kappa = \sin k_1 + \mathrm{i} \sin k_2$. This leads to the self-consistency equations

$$\rho_{1/2} = \sum_k \frac{\varepsilon + g\rho_{2/1}}{(\varepsilon + g\rho_1)(\varepsilon + g\rho_2) + \kappa\overline{\kappa}} \,, \tag{9.4}$$

which requires $\rho_1 = \rho_2 = \rho$. For $\varepsilon = 0$, ρ is indeed the DoS, and we have

$$\frac{1}{g} = \sum_k \frac{1}{g^2\rho^2 + \kappa\overline{\kappa}} \,. \tag{9.5}$$

This self-consistency equation determines ρ to be exponentially small for small g [66]. We have already said, that this calculation does not distinguish between random energy and random Dirac-mass.This insensitivity to the details of the disorder and the dispersion of the Dirac-fermions is not due to our ansatz (9.2) for the propagator, but rather due to the fact, that all non-crossing diagrams already have this insensitivity. This can be seen from equation (9.1a) and the fact, that G and G^0 have the same structure.

This result is sensible for systems with sublattice symmetry, where random energy and random Dirac-mass are indeed equal. In the continuous theory however, random Dirac-mass and random energy behave differently under renormalization-group flow.

Furthermore, the number of nodes of the dispersion does not change equation 9.5 except for an integer prefactor. It is therefore not sufficient to only consider the $N\to\infty$-limit in order to draw any conclusions about these different systems. We have to calculate finite-N corrections or apply some other renormalization scheme to calculate corrections to this result. In this work we will not do so analytically, but rather perform numerical simulations in order to establish any impact of the number of nodes and the symmetry of the system to the DoS.

As a side-note, we want to mention, that the local chiral disorder $V = \left(\begin{smallmatrix} 0 & v \\ v^\dagger & 0 \end{smallmatrix}\right)$, which we will discuss in the next chapter leads to the same saddle-point in the large-N approximation. Here the the self-consistency equations are slightly different:

$$\rho_{1/2} = \sum_k \frac{1}{\varepsilon + g\rho_{1/2}} (\varepsilon + g\rho_1)(\varepsilon + g\rho_2) + \kappa\overline{\kappa}\,. \tag{9.6}$$

For finite ε this equations have the solution given above. The only difference enters for $\varepsilon \to 0$. In the limit of vanishing ε, the two equations both become

$$\frac{1}{g} = \sum_k \frac{1}{g^2\rho_1\rho_2 + \kappa\overline{\kappa}}\,. \tag{9.7}$$

This equation determines only the product $\rho_1\rho_2$ and not ρ_1 and ρ_2 individually: A saddle-point manifold emerges. As we have seen in the first part of this work, such a manifold is related to very large fluctuations around the saddle-point, and we can not tell anything about the DoS at all.

9.2 Numerical Results for the DoS

In this section the DoS for several variants of Dirac-fermions with random Dirac-mass (RDM) will be calculated. As we are interested in the transition-point, the Dirac-mass is zero on average. Disorder is box distributed in all cases. We will give the different numerical results first and discuss them subsequently.

The system considered first is the original lattice model, where the full $U(1)$-symmetry exist and there are four nodes. All of these four nodes are equivalent in the sense, that the $U(1)$-symmetry shifts the Brillouin-zone by π in either the x- or the y-direction and thus maps the four nodes onto each other. Disorder breaks this symmetry partially, and only nodes that differ by (π, π) are equivalent. The Hamiltonian in k-space is given by

$$H = \sigma_1 \sin k_1 + \sigma_2 \sin k_2 + \sigma_3 M\,, \tag{9.8}$$

where M is the disorder term. The DoS for this system is shown in figure 9.1. In the clean system the exact result $\rho \propto \varepsilon \ln \varepsilon$ is reproduced. If we switch on disorder, the DoS becomes finite for finite system sizes.

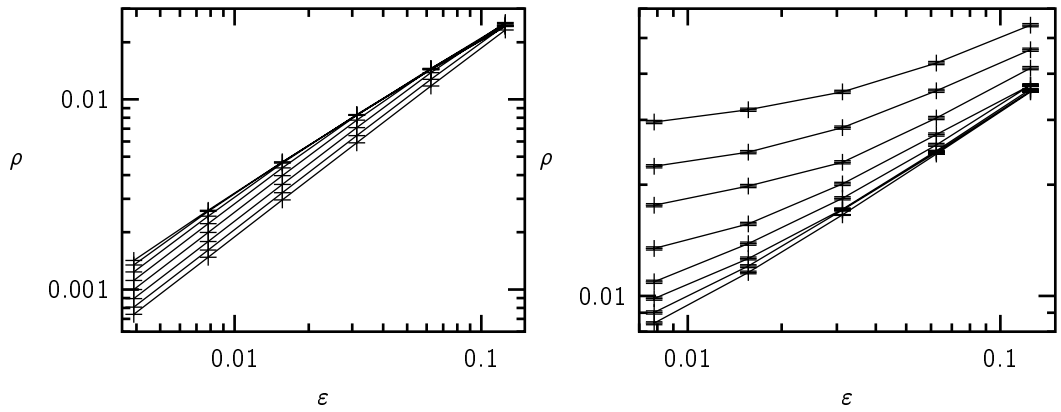

Figure 9.1: Averaged DoS for RDM with 4 nodes and $U(1)$-symmetry. The different lines belong to different system sizes, which range from 4^2 to 512^2 in powers of two. On the left the clean system is shown. The DoS increases for larger system size. On the right, the width of the disorder is 3 in units of the hopping. The DoS decreases for larger system size.

The $U(1)$-symmetry and thus the splitting into two sublattices can be lifted by adding a hopping term, that extends over two lattice constants. In k-space this Hamiltonian is given by

$$H = \sigma_1 \sin k_1 + \sigma_2 \left(\sin k_2 + 1/6 \sin 2k_2\right) + \sigma_3 M \,. \tag{9.9}$$

This Hamiltonian still has four nodes. However the symmetry between these nodes is broken. The DoS is shown in figure 9.2. Note, that this Hamiltonian does also break isotropy of the system. Adding also a term $1/6\sigma_1 \sin 2k_1$ would have complicated the numerical calculations, because the iterative Greens-function method exploits the fact, that we only have nearest neighbor-hopping in the '1'-direction. We have decided to break isotropy in order to consider larger system sizes. We do expect, that breaking isotropy does not change the DoS significantly, as the DoS of the symmetric Hamiltonian and this one are still qualitatively the same.

Alternatively it is possible to retain the $U(1)$-symmetry, while removing two nodes of the system. We do so by adding a hopping-term to the Hamiltonian, that is diagonal in the Dirac-structure and connects most distant points on each plaquette:

$$H = \sigma_1 \sin k_1 + \sigma_2 \sin k_2 + 1/\sqrt{2}\sigma_3 \left(\cos(k_1 + k_2) + 1\right) + \sigma_3 M \tag{9.10}$$

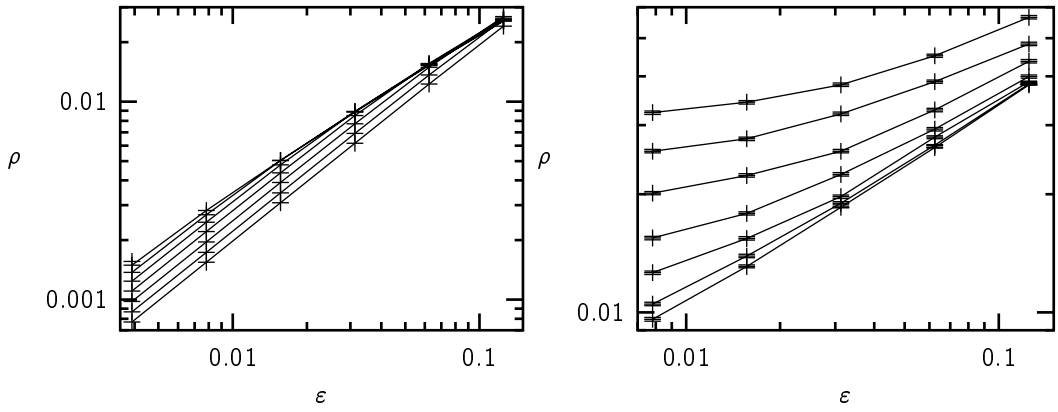

Figure 9.2: Averaged DoS for RDM with 4 nodes and broken $U(1)$-symmetry. The different lines belong to different system sizes, which range from 4^2 to 512^2 in powers of two. On the left the clean system is shown. The DoS increases for larger system size. On the right, the width of the disorder is 3 in units of the hopping. The DoS decreases for larger system size.

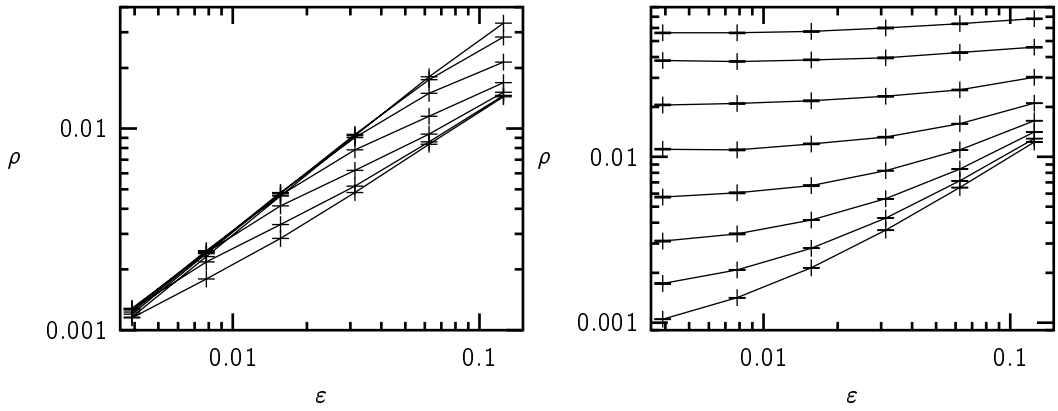

Figure 9.3: Averaged DoS for RDM with 2 nodes and $U(1)$-symmetry. The different lines belong to different system sizes, which range from 8^2 to 512^2 in powers of two. On the left the clean system is shown. On the right, the width of the disorder is 3 in units of the hopping. The DoS decreases for larger system size in both cases.

The DoS is still finite for finite systems, even though it is much smaller compared to the two Hamiltonians above. Breaking the $U(1)$-symmetry while keeping both nodes with the Hamiltonian

$$H = \sigma_1 \sin_k 1 + \sigma_2 \sin k_2 + 1/\sqrt{2}\sigma_3 \left(\cos k_1 - \cos k_2\right) \tag{9.11}$$

drives the DoS to zero even for finite system sizes. This can be seen in figure 9.4.

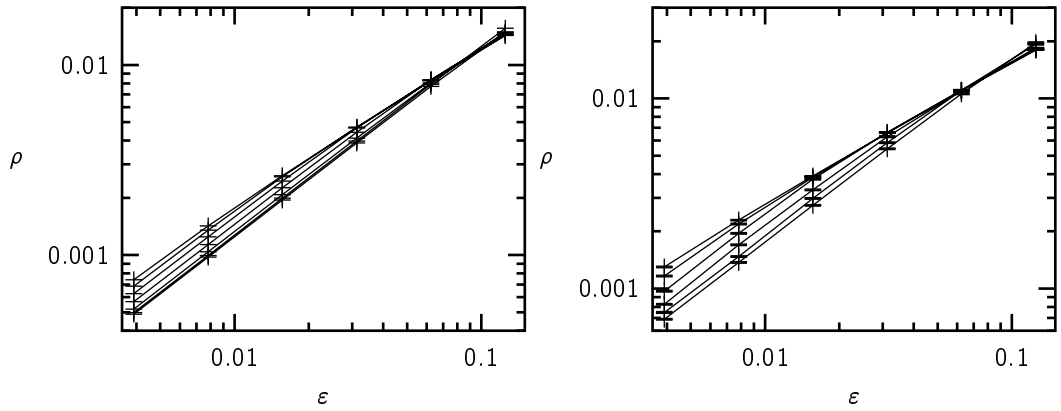

Figure 9.4: Averaged DoS for RDM with 2 nodes and broken $U(1)$-symmetry. The different lines belong to different system sizes, which range from 4^2 to 256^2 in powers of two. On the left the clean system is shown. On the right, the width of the disorder is 3 in units of the hopping. The DoS increases for larger system size in both cases, at least for small ε.

The system can also be reduced to have only one node by adding a suitable nearest-neighbor hopping-term which is diagonal in Dirac-space:

$$H = \sigma_1 \sin k_1 + \sigma_2 \sin k_2 + 1/\sqrt{2}\sigma_3 \left(\cos k_1 + \cos k_2 + 2\right) + \sigma_3 M \tag{9.12}$$

This term also lifts $U(1)$-symmetry because symmetry between different nodes is obviously destroyed. Figure 9.5 shows the DoS, which tends to zero, when the broadening ε vanishes.

After we have shown all results in summary, let us now have a closer look on them. In the clean limit the DoS behaves similarly in all cases. In some cases, the analytically calculable result DoS $\propto \varepsilon \ln \varepsilon$ is reproduced, but in some others further work would be necessary to reveal this behavior. We do not do this here , because we are interested in the disordered case. But notice, that in the clean limit the DoS vanishes in all cases for finite system sizes because there are no eigenvalues equal to zero. For nonvanishing disorder, the DoS behaves very differently depending on the number of nodes in the system.

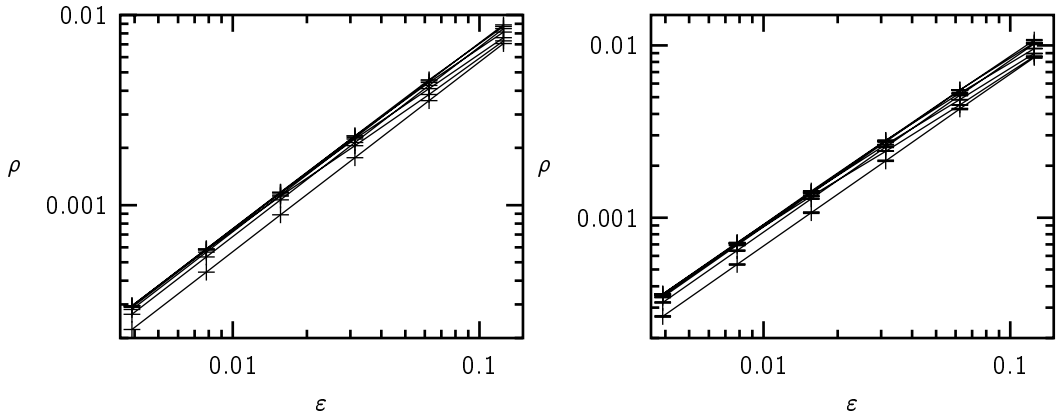

Figure 9.5: Averaged DoS for RDM with 1 node. The different lines belong to different system sizes, which range from 4^2 to 256^2 in powers of two. On the left the clean system is shown. The DoS increases with increasing system size. On the right, the width of the disorder is 3 in units of the hopping. The DoS increases with increasing system size for small ε and decreases for larger ε.

In order to characterize the dependence of the DoS on the system size we consider the scaling ansatz

$$\rho(\varepsilon, L) = L^{-\alpha} f(L\varepsilon) \tag{9.13}$$

for the two systems with four nodes. L denotes the linear size of the lattice. This ansatz yields $\alpha \approx 0.56$ in the sublattice-symmetric case and $\alpha \approx 0.54$ in the nonsymmetric case. See figure 9.6 for the scaling plot of the nonsymmetric system. Of course, this scaling implies, that the DoS vanishes in the thermodynamic limit. However, we do not want to draw any conclusions in this direction, because we think that we would need much larger system sizes to actually see a finite but exponentially small DoS.

This scaling is quite distinct from the scaling with two nodes and sublattice symmetry. In this case, we find scaling with $\rho(\varepsilon, L) = L^{-1} f(L\varepsilon)$. This is shown in figure 9.7. The DoS decreases therefore much faster than in the four-node case.

The systems with broken sublattice symmetry and two respectively one nodes do not show a finite DoS for finite system sizes. The DoS vanishes in the disordered case in a way similar to the clean limit.

Even though we did not attempt to account for the statistical errors of the scaling exponents, it is clear, that the scaling behavior of the DoS depends strongly on the number of nodes. This difference should show up in renormalization calculations. At least for four nodes the DoS depends only weakly on the presence or absence of the sublattice symmetry, which was (wrongly) emphasized by Bouquet et al. [16].

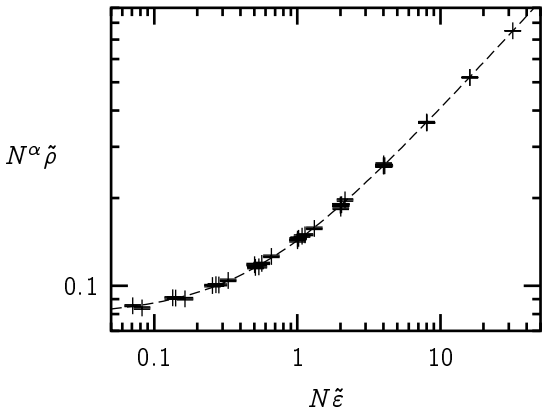

Figure 9.6: Scaling of the DoS for Dirac fermions with four nodes and without sublattice symmetry. The DoS was fitted to $\rho(L,\varepsilon)\cdot L^\alpha(1+a/L^2) = (b+cL\varepsilon(1+d/L^2))^\alpha$ using a widely available software package (gnuplot) [67]. L is the linear size of the lattice.

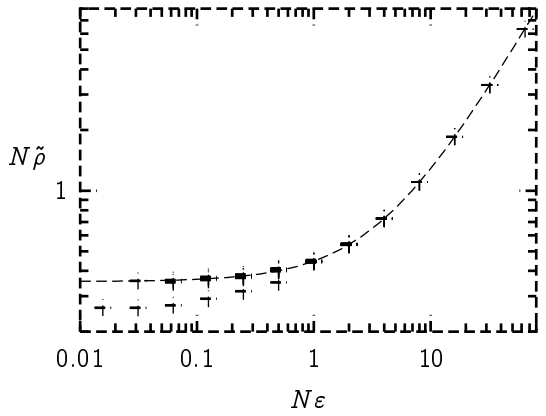

Figure 9.7: Scaling of the DoS for Dirac-fermions with two nodes and with sublattice symmetry. The DoS was fitted to $\rho(L,\varepsilon)(L+a) = b+c/L+dL\varepsilon$. The data that deviates from the scaling function belongs to $L = 4$.

9.3 Localization Properties

If the random-mass model is able to describe a quantum-Hall transition, it must not only possess a finite DoS at zero energy and in the vicinity of the transition point $\langle M \rangle = 0$, but additionally a delocalized state has to exist at zero energy.

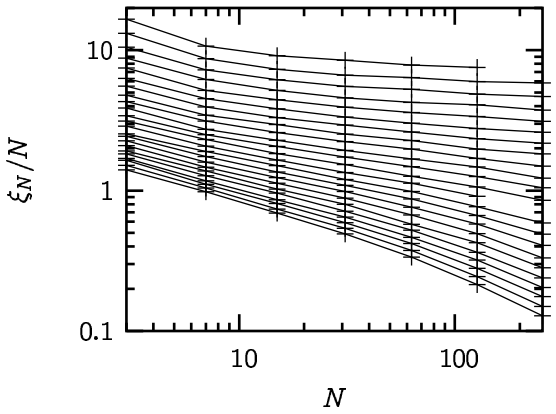

Figure 9.8: Localization length versus strip width. Each line refers to a fixed disorder strength. Disorder strength varies from 1.6 (top line) to 6.0 (lowest line) in steps of 0.2 and in units of the hopping. System size ranges from 4 to 256 in powers of two.

Using the transfer-matrix method, we have calculated the localization length for the four-node model as a function of strip-width and disorder strength with a box-distribution of the disorder. The raw results are shown in figure 9.8. We clearly find a localized state at zero energy for the strongest disorder (6.0) under investigation. At this strength of disorder we have $\xi_{128} = 27.2$ and $\xi_{256} = 32.7$. Even though the strip width is still not large enough to compute the localization length reliably, ξ is increasing much smaller than N and will eventually saturate. For the weakest disorder strength (1.6), $\xi_{128} = 958$ is much larger than the strip width. In order to decide weather a localization transition exists, we tried to derive a scaling law for the localization length. Unfortunately, the results were not conclusive. It is therefore not clear, whether a localization transition exists, or whether the system is localized for all disorder-strengths.

Chapter 10

Dirac Fermions with Chiral Disorder

In this chapter we will discuss Dirac-fermions with two kinds of nondiagonal disorder on the lattice: local chiral disorder and random-phase hopping. Even though these are both chiral disorder they exhibit very different behavior concerning DoS and localization properties. This is rather surprising, because at first glance their counterpart in the continuous theory is the random vector-potential in both cases.

Ludwig et al. applied bosonization to a random vector-potential [37] in the continuum model. For Gaussian disorder of strength g they derive a power law for the DoS: $\langle n(E)\rangle \propto E^{\alpha}$, with $\alpha = (\pi - g)/(\pi + g)$. This result has been questioned lately by Gurarie, who claims that $\alpha = 0$ for $g > \pi$ [68] and that the result of Ludwig et al. is incorrect due to convergence issues. Concerning the localization properties, it turns out, that for the $E = 0$ state, the vector-potential can be eliminated by some kind of gauge-transformation. The zero-energy state is therefore delocalized for all disorder strengths.

On the lattice, the π-flux model, which gives a realization of Dirac fermions with two nodes, has been studied with disorder in the hopping. Numerically, the DoS is singular at zero energy [69], and the system is believed to be delocalized [54]. Unlike the continuum model however, there is no proof known up to date. This is changed by our proof of delocalization for bond-disordered systems given in chapter 7, which applies to this model.

In this chapter, we will reconsider the π-flux model because no details of the type of the singularity have been given so far [70], and will characterize the singularity of the DoS. Additionally, we will study four-node Dirac-fermions with local disorder, that is nondiagonal in the Dirac structure. We will discuss the DoS in the strong disorder limit by means of a hopping expansion as well as localization properties.

10.1 Random Phase Hopping

Consider the π-flux model, where we introduce additional phases on the bonds. The model reads

$$(H\psi)_{i,j} = -\mathrm{i}\left(\mathrm{e}^{\mathrm{i}\phi_{i,j}}\psi_{i+1,j} - \mathrm{e}^{-\mathrm{i}\phi_{i-1,j}}\psi_{i-1,j}\right) - \mathrm{i}\left(\mathrm{e}^{\mathrm{i}\chi_{i,j}}\psi_{i,j+1} - \mathrm{e}^{-\mathrm{i}\chi_{i,j-1}}\psi_{i,j-1}\right) \qquad (10.1)$$

where we have chosen the gauge in such a way, that in the clean limit the hopping phases are given by $e^{\mathrm{i}\phi_{i,j}} = (-1)^i$. This is the analogue of the Landau-gauge on the lattice for a π-flux per plaquette. In the disordered model, the phases are box distributed, where w is the width of the box.

In figure 10.1 the DoS is shown for different disorder strengths. For weak disorder, the DoS vanishes. Unfortunately, it is not possible to test the dependence on the disorder strength given by of Ludwig et al. for power law of the DoS. We were not able to extract the dependence of the exponent α on the disorder strength w, because in the clean limit the DoS behaves like $\varepsilon \ln \varepsilon$. For the available numerical data with system sizes up to 256×256 ε, this is similar to a power law $\varepsilon^{0.8}$ i.e. $\alpha < 1$.

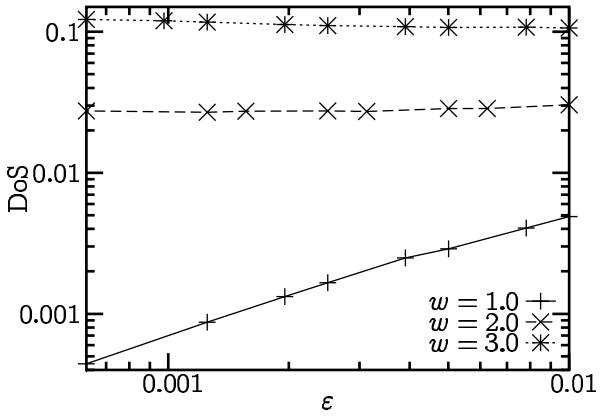

Figure 10.1: the DoS for different disorder strengths and system size 256×256.

For strong disorder the DoS diverges at zero energy. We have examined this divergence for $w = 2\pi$, when the phase of the hopping is fully random (see figure 10.2). We have fitted the divergence for a system size of 256×256 with two different functions, a logarithmic ($f_l(\varepsilon) = (a \ln \varepsilon + b)^2 + c$) and an algebraic one ($f_\alpha(\varepsilon) = \varepsilon^{-\alpha}(a + b\varepsilon)$). Reduced χ-squared is 0.56 for the logarithmic and 0.67 for the algebraic fit. Both of these fits have a considerably lower reduced χ-squared than the fit to the function $f(\varepsilon) = a\varepsilon^{-\alpha} + b$. The exponent corresponding to the algebraic fit is given by $\alpha = 0.049 \pm 0.0017$. Thus, the divergence is either algebraic with a very small exponent

or logarithmic. Note that a logarithmic divergence would agree with the prediction of Gurarie, that the DoS does not follow a scaling behavior for strong disorder.

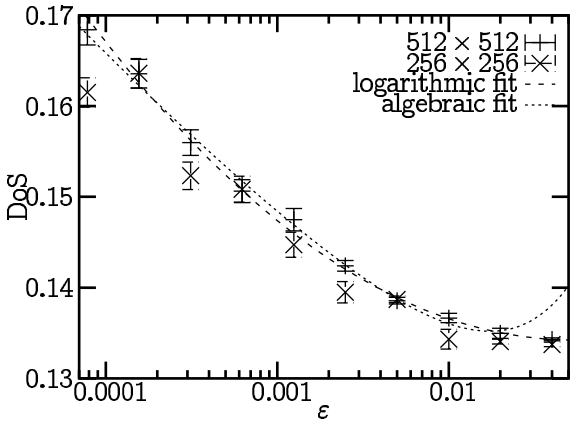

Figure 10.2: The average DoS for a completely random hopping phase ($w = 2\pi$), obtained by the iterative Greens-function method. The DoS is plotted for two different system sizes along with a logarithmic and an algebraic fit for the divergence as explained in the text. The relative error of each data point is about 1%. Up to 599 realizations of disorder were used for the averaging.

10.2 Local chiral Disorder

Next we want to discuss a model of Dirac-fermions with local disorder, that still has a chiral symmetry. We do so, by introducing two components of disorder, that are off-diagonal in the Dirac structure:

$$H = -\mathrm{i}\sigma_1\partial_1 - \mathrm{i}\sigma_2\partial_2 + a_1\sigma_1 + a_2\sigma_2 \tag{10.2}$$

One can convince oneself that there is a chiral symmetry $\sigma_3 H \sigma_3 = -H$. We will consider the DoS in the limit of strong disorder and localization properties. In the beginning we thought, that local chiral Disorder might have properties similar to the RPH model. This will turn out not to be true however.

In order to perform a hopping expansion, we decompose the Hamiltonian in two parts $H = H_0 + tH_1$ with the local part $H_0 = a_1\sigma_1 + a_2\sigma_2$ and the hopping part $H_1 = -\mathrm{i}(\sigma_1\partial_1 + \sigma_2\partial_2)$. At first we apply the Dyson-equation to the propagator $G(z) = (z - H)^{-1} = G_0 + tG_0TG$ with the local propagator $G_0 = (z - H_0)^{-1}$. We now want to discuss, which diagrams contribute to which order in $1/g$. To accomplish this, we consider a diagram with N visited sites, labeled 1 to N, each visited n_i times. The

power n of t is then given by $n+1=\sum_i n_i$. The diagram can be represented by some path on the lattice. Therefore this expansion will be an expansion in random paths. Only closed paths enter in the calculation of the DOS, therefore n is alway even. The contribution of this diagram is then given by

$$(*)=\frac{t^n}{g^N}\int\limits_{\mathbb{C}^N}\exp\left(-\sum_i a_i\overline{a}_i/2g\right)\frac{P(\{\sqrt{a_i\overline{a}_i}\},\varepsilon)}{\prod_i(\varepsilon^2+a_i\overline{a}_i)^{n_i}}\prod_i\frac{\mathrm{d}a_i\,d\overline{a}_i}{2\pi}\,. \tag{10.3}$$

P is some polynomial of order $n+1$. $\sqrt{a_i\overline{a}_i}$ enters P only in even powers and the order of P in $a_i\overline{a}_i$ is at most $n_i/2$. This means, that the propagator-part of the integrand falls off as $1/|a_i|^2$ or faster. By integrating out all complex phases we get

$$(*)=\frac{t^n\varepsilon^{2N-n-1}}{g^N}\int\limits_{\mathbb{R}_+^N}\mathrm{e}^{-\sum_i a_i^2/2g}\frac{P'(\{a_i^2/\varepsilon^2\})}{\prod_i(1+a_i^2/\varepsilon^2)^{n_i}}\prod_i\frac{a_i\mathrm{d}a_i}{\varepsilon^2}\,. \tag{10.4}$$

As the propagator-part of the integrand falls off at least as fast as $1/a_i^2$, the integral yields a logarithmic singularity, which is bounded by $const\times\ln^N(g/\varepsilon^2)$. An expansion in the number of visited sites is therefore an expansion in the small parameter $g^{-1}\ln g/\varepsilon^2$. Unfortunately, to each given power in $1/g$, there are contributions in all powers of $1/\varepsilon$. To get rid of this singularity, we have to sum up all diagrams that contribute to a given power in $1/g$. This is possible, because the series $G=G_0\sum_{n=0}^{\infty}(tH_1G_0)^n$ converges if $\varepsilon>2t$. We consider the limit $\varepsilon\ll t$ only after the summation. Note, that the logarithmic divergence of the integral is not removed by this summation.

The leading order of the DOS is now given by the one-site diagram, where no hopping occurs:

$$\rho_0=\frac{\varepsilon}{\pi g}\int a\mathrm{d}a\,\frac{\mathrm{e}^{-a^2/2g}}{\varepsilon^2+a^2}=\frac{\varepsilon}{2\pi g}\left(\log\frac{2g}{\varepsilon^2}-\gamma\right)+\mathcal{O}(\varepsilon^3)\,. \tag{10.5}$$

Here γ is Euler's Constant, $\gamma=0.577\ldots$

The two-site corrections to this result are given by $4(\rho_1-\rho_0)$, where ρ_1 is given by the diagrams

$\rho_1 =$ 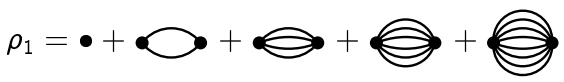 $+\ldots$

This leads to

$$\begin{aligned}\rho_1&=\frac{1}{2\pi}\,\mathrm{Im}\,\mathrm{tr}\left\langle G_{0,1}\sum_{k=0}^{\infty}\left(t^2G_{0,2}G_{0,1}\right)^k\right\rangle\\&=\frac{1}{2\pi}\,\mathrm{Im}\,\mathrm{tr}\left\langle G_0^1\left(\mathbb{1}-t^2G_{0,2}G_{0,1}\right)^{-1}\right\rangle\\&=\frac{\varepsilon}{\pi}\left\langle\frac{\varepsilon^2+a_2\overline{a}_2+t^2}{(\varepsilon^2+a_1\overline{a}_1)(\varepsilon^2+a_2\overline{2a}_2)+t^2(2\varepsilon^2-a^1\overline{a}^2-\overline{a}^1a^2)+t^4}\right\rangle\,.\end{aligned} \tag{10.6}$$

The factor four arises, because each site has four nearest neighbors and the two-site diagram is therefor four-fold degenerate. Writing a_1, a_2 in polar coordinates and integrating over the angular variables yields

$$\begin{aligned}\rho_1 &= \frac{\varepsilon}{\pi g^2}\int\limits_{\mathbb{R}_+^2}\mathrm{d}a_1\,\mathrm{d}a_2\,\frac{a_1a_2\mathrm{e}^{-(a_1^2+a_2^2)/2g}(\varepsilon^2+a_2^2+t^2)}{\prod_\pm\sqrt{(t^2\pm a_1a_2)^2+\varepsilon^2(\varepsilon^2+2t^2+a_1^2+a_2^2)}}\\ &\approx \frac{\varepsilon}{\pi g^2}\int\limits_0^\infty\mathrm{d}x\int\limits_0^1\mathrm{d}y\,\frac{x\mathrm{e}^{-x/g}(x+t^2)}{(t^2+x\sqrt{1-y^2})\sqrt{(t^2-x\sqrt{1-y^2})^2+2\varepsilon^2(t^2+x)}}\,.\end{aligned} \tag{10.7}$$

In the last equality we have employed a change of variables, $a_1 = \sqrt{x(1+y)}$, $a_2 = \sqrt{x(1-y)}$, and the approximation $\varepsilon \ll t$. The change of variables is possible here, because the integrand is symmetric with respect to a_1 and a_2. In order to evaluate this integral, we have to split the integration domain into the domains $x < t^2$, where no singularity occurs, and $x > t^2$, where the y-integration is divergent for $\varepsilon = 0$. The two contributions will be called ρ_1' and ρ_1'' respectively.

For $0 < x < t^2$ we can safely set $\varepsilon = 0$ within the integral, and get as contribution to the DOS

$$\begin{aligned}\rho_1' &= \frac{\varepsilon}{\pi g^2}\int\limits_0^{t^2}\mathrm{d}x\int\limits_0^1\mathrm{d}y\,\frac{x\mathrm{e}^{-x/g}(x+t^2)}{t^4-x^2+x^2y^2} = \frac{\varepsilon}{2\pi g^2}\int\limits_0^{t^2}\mathrm{d}x\,\mathrm{e}^{-x/g}\sqrt{\frac{t^2+x}{t^2-x}}\arcsin\frac{x}{t^2}\\ &= \frac{\varepsilon t^2}{\pi g^2}\int\limits_0^{\pi/2}\mathrm{d}z\,z\mathrm{e}^{-t^2/g\,\sin z}(1+\sin z)\,.\end{aligned} \tag{10.8}$$

In the limit $t^2 \ll g$ this evaluates to $\rho_1' = \frac{\varepsilon t^2}{\pi g^2}(1+\pi^2/8)$.

For $t^2 < x < \infty$ we approximate the y-integral around the near singular point $\sqrt{1-y_0^2} = t^2/x$ and consider the additional terms later on:

$$\begin{aligned}(1) &= \frac{\varepsilon}{\pi g^2}\int\limits_{t^2}^\infty\mathrm{d}x\int\limits_{-y_0}^{1-y_0}\mathrm{d}y\,\frac{x\mathrm{e}^{-x/g}(x+t^2)}{2t^2\sqrt{x^4y_0^2/t^4y^2+2\varepsilon^2(x+t^2)}}\\ &= \frac{\varepsilon}{2\pi g^2}\int\limits_{t^2}^\infty\mathrm{d}x\,\mathrm{e}^{-x/g}\sqrt{\frac{x+t^2}{x-t^2}}\left(\operatorname{asinh}\frac{x^2y_0(1-y_0)}{t^2\varepsilon\sqrt{2(x+t^2)}}+\operatorname{asinh}\frac{x^2y_0^2}{t^2\varepsilon\sqrt{2(x+t^2)}}\right)\\ &\approx \frac{\varepsilon}{2\pi g^2}\int\limits_{t^2}^\infty\mathrm{d}x\,\mathrm{e}^{-x/g}\sqrt{\frac{x+t^2}{x-t^2}}\ln\frac{2x^4y_0^3(1-y_0)}{t^4\varepsilon^2(x+t^2)}\,,\end{aligned} \tag{10.9}$$

where the result becomes exact in the limit $\varepsilon \ll t$.With this procedure we have captured the singular terms, and thus may set $\varepsilon = 0$ in the following. In this limit, the missing term $(2) = \rho_1'' - (1)$ is given by

$$\begin{aligned}(2) &= \frac{\varepsilon}{\pi g^2} \int_{t^2}^{\infty} \mathrm{d}x\, \mathrm{e}^{-x/g}(x+t^2) \int_0^1 \mathrm{d}y\, \left(\frac{1}{x^2|y^2-y_0^2|} - \frac{1}{2x^2 y_0 |y-y_0|} \right) \\ &= \frac{\varepsilon}{2\pi g^2} \int_{t^2}^{\infty} \mathrm{d}x\, \mathrm{e}^{-x/g} \sqrt{\frac{x+t^2}{x-t^2}} \int_0^1 \mathrm{d}y\, \frac{\operatorname{sgn}(y_0-y)}{y+y_0} \\ &= \frac{\varepsilon}{2\pi g^2} \int_{t^2}^{\infty} \mathrm{d}x\, \mathrm{e}^{-x/g} \sqrt{\frac{x+t^2}{x-t^2}} \ln \frac{4y_0}{1+y_0}\end{aligned} \tag{10.10}$$

and thus

$$\rho_1'' = \frac{\varepsilon}{2\pi g^2} \int_{t^2}^{\infty} \mathrm{d}x\, \mathrm{e}^{-x/g} \sqrt{\frac{x+t^2}{x-t^2}} \ln \frac{8(x^2-t^4)^2}{\varepsilon^2 (x+\sqrt{x^2-t^4})^2 (x+t^2)} + \mathcal{O}(\varepsilon^3)\,. \tag{10.11}$$

In the limit $t \to 0$ we get $\rho_1 \to \rho_0$, i. e. we recover the the limit of no hopping. Therefore $\rho_1 - \rho_0$ is indeed a $1/g^2$-correction to the single-site approximation. We have already said, that the two-site approximation is bounded by $(g^{-1} \ln g/\varepsilon^2)^2$. However in our result there appears no term $\propto \ln^2 g/\varepsilon^2$. The singularity in ε is $\propto \ln g/\varepsilon^2$.

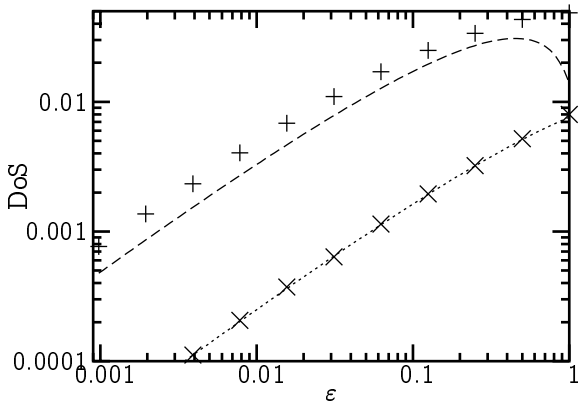

Figure 10.3: The DOS for system size 16×16 and Gaussian disorder. The dots give the numerical result with 1% accuracy and the lines the hopping expansion. The dashed line refers to $g/t^2 = 9$ and the dotted line to $g/t^2 = 100$ in units of the hopping. The numerical results were obtained by the iterative Greens-function method.

We have applied the iterative Greens function method to compare our result to numerical computations. Figure 10.3 shows, that the DoS vanishes for small ε and

large g and gives a comparison between the hopping expansion and the numerics. For $g/t^2 = 9$ the hopping-expansion and the numerical results deviate considerably, but the hopping-expansion is still qualitatively correct. Note that for $g/t^2 = 9$ the width of the disorder distribution is still of the order of the bandwidth of the clean system. Therefore this deviation is not that surprising. For $g/t^2 = 100$ both results agree very well.

Notice, that the iterative Greens-function method requires, that we apply open boundary conditions in one direction. This leads to a $1/L$-correction to the DoS for a $L \times L$-system. These corrections are still visible for the system sizes we have used for our numerical calculations. This finite size correction enters the hopping expansion by the fact, that right at the edge of the system there are only three next neighbors instead of four. The two-site contribution is therefore reduced by a factor of $1 - 1/2L$. The L-dependence of the DoS is shown for $g/t^2 = 9$ in figure 10.4. The DoS changes linearly in $1/L$, even though the correction to the thermodynamic limit is not given by $1 - 1/2L$. The latter is not surprising, as the contribution of higher orders in t^2/g are still significant at this disorder strength.

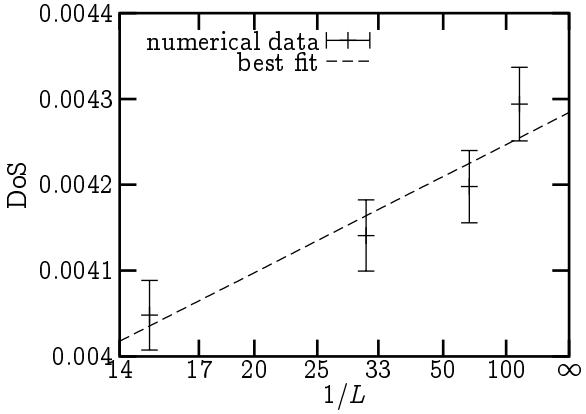

Figure 10.4: Size-dependence of the DoS. We have shown the DoS for $g = 9$, $\varepsilon = 2^{-7}$ and system sizes 15^2, 31^2, 63^2 and 127^2. The optimal fit is given by $\rho(L) = 0.00428 \cdot (1 - 0.871/L)$ for linear system size L.

We have also computed the localization-length as inverse Lyapunov-exponents. It turns out, that the localization-length obeys a scaling law and is exponentially large for small disorder strength, see figure 10.5. This behavior is similar to localization of the Anderson-model in two dimensions [71].

In conclusion, we find that local chiral disorder is very different to a RPH in that the strong disorder properties are very different. While RPH shows delocalization at zero energy for arbitrarily strong disorder and a diverging DoS, systems with local chiral disorder are localized for strong disorder and have a vanishing DoS, despite the

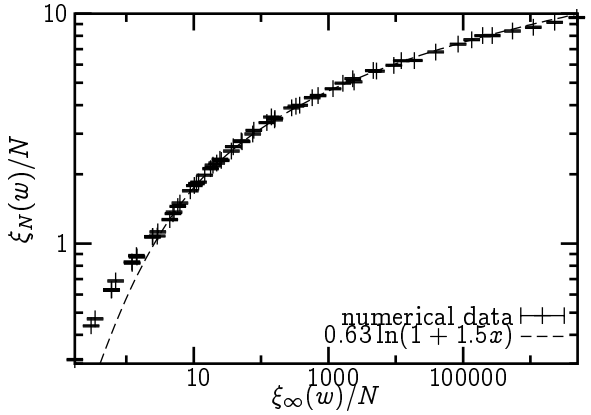

Figure 10.5: scaling-plot for the localization of local chiral disorder. We have used $\xi_\infty(w) = \mathrm{e}^{-34/w^2}$. The logarithmic behavior of the scaling function in the vicinity of the transition is indicated by the dashed line. The parameters involved were adjusted by hand rather by some automated fitting procedure, because the function to fit is too complicated.

fact, that they lead to the same system – Dirac fermions with random vector-potential – in the continuum limit.

Chapter 11

Conclusions

The results in the second part of this thesis were mostly obtained by the iterative Greens-function and transfer-matrix methods. These methods are most effective for systems with nearest neighbor hopping only. Nearest neighbor hopping allows us to calculate correlation functions by traversing quasi one-dimensional systems, where we consider only one slice of the system at a time.

Application of the transfer-matrix method to systems with bond-disorder only leads to a proof for delocalization for these systems at zero energy in the thermodynamic limit. For mesoscopic systems, where the lattice is finite in some directions (but not in all), boundary conditions become important and for open boundary conditions, we find an odd/even-effect for the localization.

This theorem can be applied to the Chalker-Coddington network model and yields a delocalized mode not only at the quantum-Hall transition but also far away from it. Further numerical studies confirm, that this mode corresponds to an edge-state and is therefore responsible for the Hall conductivity. At the transition this state extends through the whole system. Depending on the lateral size of the lattice, it is however still strongly anisotropic and is therefore not related to the longitudinal conductivity at the transition.

Dirac fermions were proposed as a model for the quantum-Hall effect. However, it is still under discussion whether a random Dirac mass alone is sufficient to drive the averaged DoS away from zero. We contribute to this discussion by computing numerically the DoS for different models of Dirac fermions with random-mass and up to four nodes in the dispersion. We have also considered the effect of the sublattice symmetry which is possible on the lattice but not in the continuum theory. We found that a larger number of nodes increases the DoS, as does introducing the sublattice symmetry.

The model with one node (for which no sublattice-symmetric exists) and the model

with two nodes and broken sublattice symmetry exhibits a vanishing DoS. This is not so for the other models, where the DoS is finite for finite system sizes. The four-node model with sublattice symmetry is known to have a nonvanishing DoS also in the thermodynamic limit. Even though the system sizes that we were able to treat numerically (up to 256×256) are still too small to capture a finite DoS, a scaling analysis reveals different scaling behavior for the two-node and the four-node models. The scaling of the DoS is captured by the scaling function $\rho(L, \varepsilon) \propto (\varepsilon + L_0/L)^\alpha$ in both cases. But while α is about 0.55 in both four-node models, we have $\alpha = 1$ in the two-node model with sublattice-symmetry. For application of Dirac fermions it is therefore absolutely necessary to specify exactly which model is to be considered.

We have also computed localization properties of the four-node model with sublattice symmetry and found that it is localized for strong disorder. We also tried to find scaling behavior in order to decide, whether there exists a delocalization transition for finite disorder strength. Unfortunately, the results were inconclusive. Further work is therefore needed in this direction. In conjunction with the results for the DoS mentioned above, it is highly desirable to consider localization properties for models with less nodes as well, in order to find out which model of Dirac fermions might be relevant for the quantum Hall transition.

Random vector potential is another type of disorder that is often considered for Dirac fermions. It is found to be delocalized at zero energy and exhibits multifractal behavior [37]. On the lattice there are two different types of chiral disorder. Random phase hopping and local chiral disorder.

Random phase hopping is delocalized at zero energy, because it is a bond-disordered system. This type of disorder has a divergent averaged DoS at zero energy. We found the divergence to be either $log^2 E$ or E^α with $\alpha \approx 0.05$. In contrast, local chiral disorder with box distributed disorder is localized at all disorder strengths with a localization length $\xi \propto e^{w_0^2/w^2}$, with $w_0 \approx 5.8$. For the latter, an expansion for strong disorder, which is equivalent to a random walk expansion gives a vanishing DoS. We compared the hopping expansion with numerical results and found good agreement for strong disorder. Concerning both DoS and localization properties these two models thus behave quite differently, although they both realize chiral disorder, and therefore both seem to be related to a random vector potential in the continuum limit at first sight.

All these results indicate that the concept of 'universality' at the phase transitions resp. localization transitions has to be changed profoundly when disorder is present and relevant at the transition. The strong dependence of the results on the UV-features (lattice regularization) of the system entails, that the physics is not determined by a simple continuum approximation alone. Although new 'universality' may arise, it is

no longer restricted to large scale properties.

Appendix A

Formulary

A.1 Integrals

In this section we present integrals that are needed in chapters 3, 4 and 10. In order to obtain the final results in said chapters, it may be necessary, to apply several of the formulas given here consecutively.

$$\begin{aligned}\int_{-\infty}^{\infty}\frac{\mathrm{d}p}{\sqrt{\pi}}\,(\mathrm{i}p-E)^n\mathrm{e}^{-p^2} &= \frac{1}{2^n}\,\frac{\partial^n}{\partial\alpha^n}\bigg|_{\alpha=0}\int_{-\infty}^{\infty}\frac{\mathrm{d}p}{\sqrt{\pi}}\,\mathrm{e}^{-p^2+2\alpha(\mathrm{i}p-E)}\\ &= \frac{1}{2^n}\,\frac{\partial^n}{\partial\alpha^n}\bigg|_{\alpha=0}\mathrm{e}^{-2\alpha E-E^2} = \frac{(-1)^n}{2^n}H_n(E)\end{aligned} \tag{A.1}$$

$$\begin{aligned}&\int_{-\infty}^{\infty}\frac{\mathrm{d}p}{\sqrt{\pi}}\,\left((\mathrm{i}p-E)^2\pm r\right)^n(\mathrm{i}p-E)^\nu\mathrm{e}^{-p^2-r}\\ &\qquad= \sum_{k=0}^{n}\binom{n}{k}(\pm1)^{n-k}\int_{-\infty}^{\infty}\frac{\mathrm{d}p}{\sqrt{\pi}}(\mathrm{i}p-E)^{k+\nu}\mathrm{e}^{-p^2}\int_0^\infty\mathrm{d}r\;\; r^{n-k}\mathrm{e}^{-r}\\ &\qquad= \frac{(\pm1)^n(-1)^\nu n!}{2^\nu}\sum_{k=0}^{n}\frac{(\pm1)^k H_{2k+\nu}(E)}{k!4^k}\end{aligned} \tag{A.2}$$

The following integrals contain singularities because they refer to the trace of some propagator. In order to fix the sign (and to ensure convergence in some cases), we

state that the integration path passes below the singularity.

$$\begin{aligned}\mathrm{Im}\int_{-\infty}^{\infty}\mathrm{d}q\ \frac{q\mathrm{e}^{-q^2}}{(q-E)^n} &= -\frac{\pi}{(n-1)!}\frac{\partial^{n-1}}{\partial q^{n-1}}\int_{-\infty}^{\infty}\mathrm{d}q\ \frac{q\mathrm{e}^{-q^2}}{q-E}\\ &= -\frac{\pi}{(n-1)!}\ \frac{\partial^{n-1}}{\partial q^{n-1}}\bigg|_{q=E} q\mathrm{e}^{-q^2} = \frac{-(-1)^n\pi}{2(n-1)!}H_n(E)\mathrm{e}^{-E^2}\end{aligned} \tag{A.3}$$

By help of the relation

$$\frac{\partial}{\partial r}\frac{(\mp 1)^n}{n!}\left(\sum_{k=1}^{n}\frac{(\mp 1)^k(k-1)!\mathrm{e}^{-r}}{(z\pm r)^k} - \mathrm{Ei}(\mp z - r)\right)\mathrm{e}^{\pm z} = \frac{\mathrm{e}^{-r}}{(z\pm r)^{n+1}}$$

we get

$$\int_0^{\infty}\mathrm{d}r\ \frac{\mathrm{e}^{-r}}{(z\pm r)^{n+1}} = -\frac{(\mp 1)^n}{n!}\left(\sum_{k=1}^{n}\frac{(\mp 1)^k(k-1)!}{z^k} - \mathrm{Ei}(\mp z)\mathrm{e}^{\pm z}\right) \tag{A.4}$$

$$\begin{aligned}\mathrm{Im}\int_{-\infty}^{\infty}\mathrm{d}q\ q\mathrm{e}^{-q^2-(q-E)^2}\,\mathrm{Ei}((q-E)^2) &= \pi\int_{-\infty}^{\infty}\mathrm{d}q\ q\mathrm{e}^{-q^2-(q-E)^2}\,\mathrm{sgn}(q-E)\\ &= -\frac{\pi}{4}\sqrt{2\pi}E\mathrm{e}^{-E^2/2}\,\mathrm{erf}(E/\sqrt{2}) + \frac{\pi}{2}\mathrm{e}^{-E^2}\end{aligned} \tag{A.5}$$

$$\begin{aligned}&\mathrm{Im}\int_{-\infty}^{\infty}\mathrm{d}q\ q(q-E)\mathrm{e}^{-q^2-(q-E)^2}\,\mathrm{Ei}(-(q-E)^2)\\ &\qquad= \pi\int_{-\infty}^{\infty}\mathrm{d}q\ q(q-E)\mathrm{e}^{-q^2-(q-E)^2}\,\mathrm{sgn}(q-E)\\ &\qquad= -\frac{\pi}{8}\sqrt{2\pi}\mathrm{e}^{-E^2/2}\,\mathrm{erf}(E/\sqrt{2})(1-E^2) + \frac{\pi}{4}\mathrm{e}^{-E^2}E\end{aligned} \tag{A.6}$$

$$\begin{aligned}\mathrm{Im}\int_{-\infty}^{\infty}\mathrm{d}q\ q\mathrm{e}^{-q^2+(q-E)^2}\,\mathrm{Ei}(-(q-E)^2) &= 2\pi\int_{E}^{\infty}\mathrm{d}q\ q\mathrm{e}^{-q^2+(q-E)^2}\\ &= \frac{\pi}{2}\mathrm{e}^{-E^2}\left(2+\frac{1}{E^2}\right)\end{aligned} \tag{A.7}$$

$$\begin{aligned}\operatorname{Im}\int_{-\infty}^{\infty}\mathrm{d}q\ q(q-E)\mathrm{e}^{-q^2+(q-E)^2}\operatorname{Ei}(-(q-E)^2) &= 2\pi\int_{E}^{\infty}\mathrm{d}q\ q(q-E)\mathrm{e}^{-q^2+(q-E)^2}\\ &= \frac{\pi}{2E}\mathrm{e}^{-E^2}\left(1+\frac{1}{E^2}\right)\end{aligned} \tag{A.8}$$

For the derivation of the last integral we have assumed that $E > 0$. The result however holds for any E. The derivation for $E < 0$ is analogous, but $\int_E^\infty \mathrm{d}q$ has to be replaced by $\int_{-\infty}^E \mathrm{d}q$.

For the following integral we require $a > b \geq 0$.

$$\int\frac{\mathrm{d}\phi}{a-b\cos\phi} = \frac{2}{\mathrm{i}}\oint_{|z|=1}\frac{\mathrm{d}z}{2az-bz^2-b} = \frac{2\pi}{\sqrt{a^2-b^2}} \tag{A.9}$$

A.2 Orthogonal Polynomials

We have made use of Laguerre- and Hermite-polynomials to calculate and write down the exact densities of states for the random matrix-ensembles. Therefore the used features of these polynomials will be presented in this section. For a more detailed overview see e. g. [72]

The Laguerre-polynomials $L_n^a(x)$ are orthogonal polynomials with respect to the weight function $w_a(x) = x^a\mathrm{e}^{-x}$ on the domain $\mathbb{R}^+$, i.e.

$$\int\mathrm{d}x\, w_a(x)L_i^a(x), L_j^a(x) = 0 \tag{A.10}$$

for $i \neq j$. They can be calculated by differentiation

$$n!L_n^a(x) = \mathrm{e}^x x^{-a}D^n(\mathrm{e}^{-x}x^{n+a})\,, \tag{A.11}$$

or by applying the recursion relation

$$(n+1)L_{n+1}^a(x) - (2n+a+1-x)L_n^a(x) + (n+a)L_{n-1}^a(x) = 0\,. \tag{A.12}$$

We need the finite sum

$$\sum_{m=0}^{n}L_m^a(x) = L_n^{a+1}(x)\,. \tag{A.13}$$

The Hermite-polynomials $H_n(x)$ are orthogonal polynomials with respect to the weight function $w(x) = \mathrm{e}^{-x^2}$ on the real axis as domain. They enter the integrals in the last section by means of the formula

$$H_n(x) = (-1)^n \mathrm{e}^{x^2} D^n \mathrm{e}^{-x^2} \,. \tag{A.14}$$

Alternatively they can be calculated via the recursion relation

$$H_{n+1}(x) - 2xH_n(x) + 2nH_{n-1}(x) = 0 \,, \tag{A.15}$$

and they can be expressed in terms of Laguerre-Polynomials:

$$\begin{aligned} H_{2n}(x) &= (-1)^n 2^{2n} n! L_n^{-1/2}(x^2) \,, \\ H_{2n+1}(x) &= (-1)^n 2^{2n+1} n! x L_n^{1/2}(x^2) \,. \end{aligned} \tag{A.16}$$

Bibliography

[1] T. Guhr, A. Müller-Groeling and H. A. Weidenmüller, Phys. Rep. **299**, 190 (1998) [cond-mat/9707301]

[2] E. P. Wigner: Proc. Cambridge Philos. Soc. **47**, 790 (1951)

[3] G. Akemann and G. Vernizzi, Nucl. Phys. B **631** (2002) 471 [hep-th/0201165]

[4] R. Delannay and G. Le Caer: J. Phys. A **33**, 2611 (2000)

[5] M. L. Mehta: *Random Matrices*. Academic Press, San Diego 1991

[6] T. Nagao and K. Slevin, J. Math. Phys. **34**, 2075 (1993)

[7] T. Nagao and K. Slevin, J. Math. Phys. **34**, 2317 (1993)

[8] K. Efetov: Adv. Phys. **32**, 53 (1983) see also *Supersymmetry in Disorder and Chaos*. Cambridge University Press, Cambridge 1997

[9] K. Ziegler: Z. Phys. B **48**, 293 (1982)

[10] M. Zirnbauer: J. Math. Phys. **37**, 4986 (1996) [math-ph/9808012]

[11] A. Altland and M. R. Zirnbauer: Phys. Rev. B **55**, 1142 (1997) [cond-mat/9602137]

[12] D. A. Ivanov: J. Math. Phys. **43**, 126 (2002) [cond-mat/0103137]

[13] J. J. M. Verbaarschot, H. A. Weidenmüller, M. R. Zirnbauer: Phys. Rep. **129**, 367 (1985)

[14] M. Scheunert: *The theory of Lie Superalgebras*. Springer, Heidelberg 1979

[15] L. Corwin, J. Neemann, S. Sternberg: Rev. Mod. Phys. **47**, 573 (1975)

[16] M. Bocquet, D. Serban, M. R. Zirnbauer: Nucl. Phys. B **578**, 628 (2000) [cond-mat/9910480]

[17] W. H. Press et al.: *Numerical Recipes in C* (2nd ed.). Cambridge University Press, Cambridge 1993

[18] F. Wegner: Z. Phys. B **36**, 209 (1980)

[19] J. W. Negele, H. Orland: *Quantum Many-Particle Systems*. Addison-Wesley, New York 1988

[20] K. v. Klitzing, G. Dorda, M. Pepper: Phys. Rev. Lett. **45**, 494 (1980)

[21] C. Kittel: *Introduction to Solid State Physics* 4^{th} ed., Wiley & Sons, New York 1971

[22] R. E. Prange, S. M. Girvin (ed.): *The Quantum Hall Effect* (2nd ed.). Springer, New York, 1990

[23] M. E. Cage, R. F. Dziuba, B. F. Field: IEEE Transactions on Instrumentation and Measurement **IM-34** 301 (1985)

[24] D. C. Tsui, H. L. Störmer, A. C. Gossard: Phys. Rev. Lett. **48** 1559 (1982)

[25] B. Huckestein: Rev. Mod. Phys. **67**, 357 (1995) [cond-mat/9501106]

[26] R. B. Laughlin: Phys. Rev. B **23** 5632 (1981)

[27] D. J. Thouless: J. Phys. C **17**, L325 (1984)

[28] M. Kohmoto: Ann. Phys. (NY) **160**, 343 (1985)

[29] H. Levine, S. B. Libby, A. M. M. Pruisken: Phys. Rev. Lett. **51**, 1915 (1983)

[30] A. M. M. Pruisken, M. A. Baranov, M. Voropaev [cond-mat/0101003]

[31] B. Huckestein, B. Kramer: Phys. Rev. Lett. **64**, 1437 (1990)

[32] Y. Huo, R. N. Bhatt: Phys. Rev. Lett. **68**, 1375 (1992)

[33] H. P. Wei, D. C. Tsui, M. Paalanen, M. M. Pruisken: Phys. Rev. Lett. **61**, 1294 (1988)

[34] S. Koch, R. Haug, K. von Klitzing, K. Ploog: Phys. Rev. Lett. **67**, 883 (1991)

[35] J. T. Chalker, P. D. Coddington: J. Phys. C **21**, 2665 (1988)

[36] G. V. Mil'nikov, I. M. Sokolov: JETP Lett. **48**, 536 (1988)

[37] A. W. W. Ludwig, M. P. A. Fisher, R. Shankar, and G. Grinstein: Phys. Rev. B **50**, 7526 (1994)

[38] V. S. Dotsenko, V. S. Dotsenko: Adv. Phys. **32**, 129 (1983)

[39] R. Shankar: Phys. Rev. Lett. **58**, 2466 (1987)

[40] A. W. W. Ludwig: Nucl. Phys. B **285**, 97 (1987)

[41] L. Schweitzer, B. Kramer, A. MacKinnon: J. Phys. C **17**, 4111 (1984)

[42] J. L. Pichard, G. Sarma: J. Phys. C **14**, L127 and L617 (1981)

[43] B. Kramer, A. MacKinnon: Rep. Prog. Phys. **56**, 1469 (1993)

[44] I. V. Oseledec: Moscow Math. Soc. **19**, 197 (1968)

[45] D. S. Fisher, P. Lee: Phys. Rev. B **59** 6851 (1981)

[46] K. A. Muttalib, J.- L. Pichard, A. D. Stone: Phys. Rev. Lett. **59** 2475 (1987)

[47] J.-P. Eckmann, D. Ruelle: Rev. Mod. Phys. **57**, 617 (1985)

[48] E. Abrahams, P. W. Anderson, D. C. Licciardello, T. V. Ramakrishnan: Phys. Rev. Lett. **42**, 673 (1979)

[49] S. Hikami, A. I. Larkin, Y. Nagaoka: Prog. Theor. Phys. **63**, 707 (1980)

[50] T. Ando: Phys. Rev. B **40**, 5325 (1989)

[51] Y. Asada, K. Slevin, T. Ohtsuki: Phys. Rev. Lett. **89**, 256601 (2002) [conad-mat/0204544]

[52] G. Theodorou, M. H. Cohen: Phys. Rev. B **13**, 4597 (1976)

[53] A. Eilmes, R. A. Römer, M. Schreiber: Physica B **296**, 46 (2001) [cond-mat/0007102]

[54] Y. Hatsugai, X.-G. Wen, M. Kohmoto: Phys. Rev. B **56**, 2061 (1997) [cond-mat/9603169]

[55] P. W. Brouwer, C. Mudry, B. D. Simons, A. Altland: Phys. Rev. Lett. **72**, 2628 (1994) [cond-mat/9807189]

[56] C. Mudry, P. W. Brouwer, A. Furusaki: Phys. Rev. B **62**, 8249 (2000) [cond-mat/0004042]

[57] P. Cain, R. A. Römer, M. Schreiber: Ann. Phys. (Leipzig) **8**, SI-33-36 (1999) [cond-mat/9908255]

[58] C. Barnes, B. L. Johnson, G. Kirczenow: Phys. Rev. Lett. **70** 1159 (1993)

[59] D. H Lee, Z Wang, S. Kivelson: Phys. Rev. Lett. **70**, 4130 (1993)

[60] B. Huckestein: Europhys. Lett. **20**, 451 (1992)

[61] P. Cain, M. E. Raikh, R. A. Römer, M. Schreiber: Phys. Rev. **B** 235326 (2001) [cond-mat/0209356]

[62] U. Eckern, K. Ziegler: J. Phys.: Condensed Matter **10**, 6749-6760 (1998) [cond-mat/9806283]

[63] A. A. Nersesyan, A. M. Tsvelik, F. Wenger: Phys. Rev. Lett. **72**, 2628 (1994)

[64] K. Ziegler, M. H. Hettler, P. J. Hirschfeld: Phys. Rev. B **57**, 10825 (1998) [cond-mat/9604176]

[65] P. J. Hirschfeld, W. A. Atkinson: Journal of Low Temperature Physics **126(3)**, 881-900 (2002) [cond-mat/0108487]

[66] K. Ziegler: Phys. Rev. B **55**, 10661 (1997) [cond-mat/9611088]

[67] Gnuplot can be found at `http://www.gnuplot.info`

[68] V. Gurarie: [cond-mat/9907502]

[69] S. Ryu, Y. Hatsugai: [cond-mat/0107516]

[70] A. Furusaki: Phys. Rev. Lett. **82**, 604 (1999) [cond-mat/9808059]

[71] A. MacKinnon, B. Kramer: Z. Phys. B **53**, 1 (1983)

[72] A. Erdélyi (ed.): *Higher transcendental functions* vol. II. McGraw-Hill, New York 1953

Acknowledgments

This thesis would not exist without help and influence of other people. I want to thank Prof. Klaus Ziegler that he gave me the opportunity to undertake this work. Daniel Braak and Peter Schwab gave help in numerous discussions and by proofreading the thesis. This work was supported by the *Graduiertenkolleg* "Nonlinear Problems in Analysis, Geometry and Physics" (GRK 283), financed by the German Science Foundation (DFG) and the State of Bavaria.

Last but not least I want to thank my wife Johanna for all patience she has shown and the support she has given me while I was working on this thesis.